4th semester – M.Sc.
Sohngårdsholmsvej 57
9000 Aalborg
+45 96 35 80 80
http://www.bsn.aau.dk

Title:
Strength and Deformation Properties of Tertiary Clay at Moesgaard Museum and FE Investigations on the Interaction between a Pile and Swelling Clay

Theme:
Master's Thesis

Made by:
Kristine Lee Kaufmann
Graduate Student
Master of Science in Civil Engineering
4th semester, 2010

Supervisors:
Anders Hust Augustesen, COWI A/S
Benjaminn Nordahl Nielsen, Aalborg University

Copies: 4

Number of pages: 61

Number of pages (appendix): 85

Completed: September 8, 2010

Kristine Lee Kaufmann

PREFACE

This thesis is the product of a short Master project period carried out in the period of February to September 2010 at the Faculties of Engineering, Science and Medicine, Aalborg University, Denmark.

The thesis consist of an introduction, two papers and eight related appendices. A list of references is situated after the introduction and each paper. Additionally, a complete list of references is situated after the last appendix. The appendices are numbered by letters. Figures, tables and equations are presented with consecutive numbers in each paper/appendix. If a figure is not a product of the work of the author, the caption is followed by a source reference. Cited references are marked with author specifications and year of publication.

A PDF-script of the thesis and the produced computational programs are included on the enclosed compact disc.

The papers are published at the Research Database of Aalborg University as DCE Technical Report Nos. 103 and 104. The database can be found online at `http://vbn.aau.dk`.

The author would like to thank the support and technical advice from Professor MSO Lars Bo Ibsen, Ph.D. Student Rikke Poulsen, M.Sc. Gitte Lyng Grønbech and Assistant Engineers Kurt Skjellerup Sørensen and Anette Næslund Pedersen. Additionally, COWI A/S is thanked for providing geotechnical borings, boring records and a proposition of testing programs for the laboratory tests of the tertiary clay at Moesgaard Museum.

Aalborg, September 8, 2010

List of Symbols

List of Symbols

A	Skempton's coefficient of pore pressure [-]
B	Outer width of soil mass [m], Skempton's coefficient of pore pressure [-]
C_{cu}	Compression index for the unloading path [%]
$C_{c\varepsilon}$	Compression index for the primary loading curve [%]
D	Diameter of specimen for consolidation and triaxial tests [mm], diameter of pile [m]
E_{50}	Secant modulus [MPa]
E_{oed}	Constrained modulus [MPa]
$E_{oed,0}$	Constrained modulus for zero effective stress [MPa]
E_{ur}	Unloading–reloading modulus [MPa]
ESP	Effective stress path
H	Height of specimen for consolidation and triaxial tests [mm], height of the soil model after excavation [m]
I_P	Plasticity index [%]
K_0	Coefficient of horizontal earth pressure at rest [-]
L	Length of pile [m]
OCR	Overconsolidation ratio [-]
POP	Pre-overburden pressure [kPa]
R_{inter}	Strength reduction factor [-]
TSP	Total stress path
a	Vertical displacement from (0,0) of failure criterion of triaxial test [kPa]
c'	Drained shear strength [kPa]
c'_{tr}	Drained shear strength determined by triaxial test [kPa]
c_i	Interface cohesion [kPa]
c_k	Coefficient of consolidation [m^2/s]
c_u	Undrained shear strength [kPa]
c_v	Vane shear strength [kPa]
f_{ck}	Compressive strength of concrete [MPa]
f_{ctk}	Tensile strength of concrete [MPa]

k_x	Coefficient of horizontal permeability [m/s]
k_y	Coefficient of vertical permeability [m/s]
m	Factor of material [-], power for stress–level dependency of stiffness [-]
n	Depth of swelling zone [m]
p	Unloading pressure [kPa], mean stress [kPa]
p'_O	Effective overburden pressure [kPa]
q	Deviatoric stress [kPa]
r	Factor of regeneration [-]
t_{max}	Surface resistance of pile [kPa]
u	Pore pressure [kPa]
u_x	Displacements in the x-direction
u_y	Displacements in the y-direction
w	Natural water content [%]
w_L	Liquid limit [%]
w_P	Plastic limit [%]
ΔE_{oed}	Addition to E_{oed} per stress unit [-]
Δu	Excess or negative pore pressure [kPa]
$\Delta\sigma$	Effective stress variation [kPa]
α	Inclination of failure criterion of triaxial test [° or rad], ratio of c_i to c_u [-]
γ_{sat}	Saturated unit weight [kN/m^3]
γ_{unsat}	Unsaturated unit weight [kN/m^3]
γ_w	Unit weight of water [kN/m^3]
δ	Heave [mm]
ε_0	Start value of consolidation strain [%]
ε_1	Axial strain [%]
ε_{100}	Strain at 100 % consolidation [%]
ε_S	Creep strain [%]
ε_v	Volumetric strain [%]
ν	Poisson's ratio [-]
σ'	Effective stress [kPa]
σ'_0	Effective vertical in situ stress [kPa]
σ_1	Total vertical stress [kPa]
σ_3	Total radial stress [kPa]
σ'_N	Effective normal stress at the failure line at the interface [kPa]
σ'_{pc}	Effective preconsolidation stress [kPa]
σ'_{red}	Lowest effective stress of the soil [kPa]
σ'_S	Swelling pressure [kPa]

σ'_u	Effective unloading stress [kPa]
σ'_{yy}	Internal vertical stresses in the pile [kPa]
σ'_κ	Reference stress [kPa]
τ_i	Shear stress at interface [kPa]
τ_{max}	Coulomb failure criterion [kPa]
φ'	Effective angle of internal friction [°]
φ'_i	Effective angle of internal friction of the interface [°]
φ'_{tr}	Effective angle of internal friction determined by triaxial test [°]
ψ	Angle of dilatancy [°], ratio of c_u to p'_O

SUMMARY

This thesis consists of two individual papers. In the first paper, the tertiary clay at Moesgaard Museum is geologically and geotechnically described. The second paper concerns finite element modelling of a single pile positioned in a swelling clay. The swelling is modelled as an unloading by an excavation.

The subjects of the two papers are summarised in the following.

Swelling soils are highly expansive in combination with water, which could lead to damaging of buildings due to heave of the soil. Thus, it is important to determine at which stress levels swelling is expected to occur. This is represented by the swelling pressure. Additionally, deformation and strength parameters of the clay are necessary for a detailed design of the foundation of new buildings.

The first paper evaluates the strength and deformation properties of the tertiary clay at Moesgaard Museum situated 10 km south of Aarhus. This includes analyses of two consolidation tests and a single triaxial test. The swelling pressure, the preconsolidation stress, the compression index and the constrained modulus are determined based on the consolidation tests. The drained and undrained strength are found by the triaxial test.

Pile foundations designed to resist compressive loads caused by settlements are occasionally situated in swelling soils. Due to the friction between pile and soil, the heave caused by swelling leads to an additional tensile loading. Analysis of this combination of tensile and compressive loading is complex, both theoretically and numerically.

In the second paper, the mechanisms of the combined tensile and compressive loading of a single pile caused by swelling are decoupled. Thus, the problem is simplified to a fixed pile which, because of an excavation, is exposed to tensile loading. This is modelled numerically, and the heave of the new ground surface, the shear stresses at the soil–pile interface and the internal vertical stresses are analysed based on a case study of Little Belt Clay. The analyses show that the presence of the pile creates a weak zone

within a radius of 3 pile diameters from the axis of symmetry of the pile. The maximum heave within this zone is polynomially decreasing with increasing interface strength. The swelling of the surrounding soil implies upward shear stresses at the soil–pile interface. This leads to tensile vertical stresses in the pile which in the current case exceed the tensile strength of concrete. The tensile vertical stresses peak after 35-50 years even though the heave of the soil continues for additional 300 years. It appears that the development of plastic interface implies the shrinkage of the pile because of the slip at the pile surface.

RESUMÉ (SUMMARY IN DANISH)

Denne afhandling består af to individuelle artikler. I den første artikel beskrives den tertiære ler ved Moesgård Museum geologisk og geoteknisk. Den anden artikel omhandler numerisk modellering af en enkeltpæl placeret i en svellende ler, hvor svelningen modelleres som en aflastning ved afgravning.

Problemstillingerne i de to artikler er resumeret nedenfor.

Svellende ler er særdeles ekspansivt, når det kommer i forbindelse med vand, hvilket kan medføre store skader af bygninger pga. hævning af jorden. Derfor er det af stor vigtighed at bestemme ved hvilket spændingsniveau, svelning kan forventes, i form af svelletrykket. Derudover er både deformations– og styrkeparametre nødvendige for at kunne dimensionere fundamenter for nye konstruktioner.

Den første artikel behandler de styrke– og deformationsmæssige egenskaber af den tertiære ler ved Moesgård Museum, som ligger 10 km syd for Århus. Dette indbefatter evaluering af to konsolideringsforsøg og et triaksialforsøg. Ud fra konsolideringsforsøgene er svelletrykket, forbelastningsspændingen, tøjningsindekset og konsolideringsmodulet fundet. Den drænede og udrænet styrke er bestemt ud fra triaksialforsøget.

Pælefundering, der er dimensioneret til at optage tryklaster pga. sætninger, benyttes sommetider i svellende ler. Grundet friktionen mellem pæl og jord fører hævningen, som følge af svelning, til en yderligere trækbelastning. Denne kombination af træk- og trykbelastning kan være kompleks at analysere, både teoretisk og numerisk.

I den anden artikel adskilles mekanismerne ved den kombinerede træk– og trykbelastning af en enkeltpæl som følge af svelning, hvormed problemet simplificeres til en indspændt pæl, der pga. en afgravning trækbelastes. Denne modelleres numerisk, hvorefter hævningen af jordoverflade, forskydningsspændingerne i jord–pæl interface og normalspændingerne i pælen baseret på et casestudie af Lillebæltsler er analyseret. Analyserne viser, at tilstedeværelsen af pælen skaber en svag zone inden for en radius af 3 pælediametre fra pælens centerlinie, hvor den maksimale hævning inden for denne radius aftager polynomisk med stigende styrke af grænseflade. Svelningen af jorden fører til opadrettede forskydningsspændinger i jord–pæl grænsefladen, hvilket medfører aksiale trækspændinger i pælen, som i det undersøgte tilfælde overstiger betonens trækstyrke. Trækspændingerne i pælen topper efter 35–50 år, på trods af at hævningerne i jorden forløber over yderligere 300 år. Det ser ud til, at udviklingen af plastisk grænseflade medfører en sammentrækning af pælen pga. brud langs pælens overflade.

TABLE OF CONTENTS

CHAPTER 1

INTRODUCTION

This chapter gives an introduction to some of the concepts of swelling and a brief description of pile foundations with emphasis on the surface resistance.

1.1 Swelling Soils

Swelling is a characteristic of clays with a moderate to high activity, i.e. the ratio of plasticity index to clay content, which happens when the clay is exposed to moisture changes. Clays containing the clay mineral montmorillonite are swelling clays. (Barnes, 2000)

Swelling of clay may occur by different reasons, e.g. slow unloading, leaving time for the pore pressure to dissipate, and fast unloading, where soils of low permeability respond in undrained manner resulting in negative pore water pressure. In clay, the time frame for the clay to respond in drained manner is very large, and thus, only undrained conditions are investigated in this thesis. (Barnes, 2000)

In undrained conditions, the unloading leads to a decrease in total stresses. At first, this change is only expressed by a decrease in pore water pressure, in the following names pore pressures, and the effective stresses are unchanged until the pore water starts to drain from the surrounding soil to the soil exposed to unloading establishing hydrostatic pressure. This leads to increased pore pressure. Since no further unloading or reloading is occurring, the total stresses are unchanged and the effective stresses must decrease to correspond the increase in pore water pressure. The stress variation can be seen in Figure 1.1.

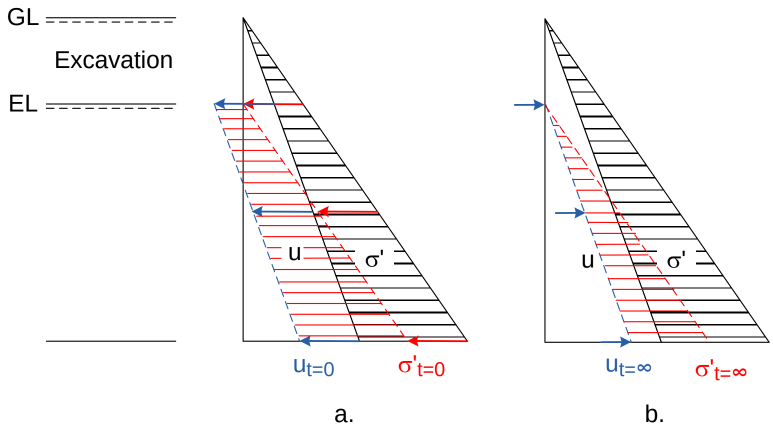

Figure 1.1: Stress variation for fast unloading by excavation. a. Total stresses σ as a result of pore pressures u and effective stresses σ' straight after unloading ($t = 0$). b. Total stresses, pore pressures and effective stresses straight after increase of pore water pressure to an equilibrium state ($t = \infty$). GL is ground level, and EL is excavation level.

The variation of stresses can be seen in Figure 1.2.

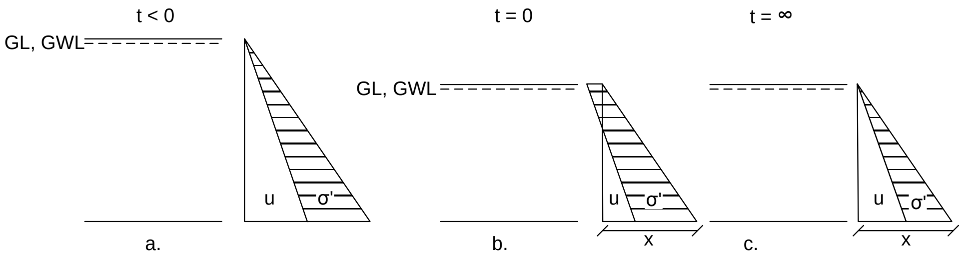

Figure 1.2: Stress variation for fast unloading by excavation. a. Total stresses σ as a result of pore pressures u and effective stresses σ' before unloading ($t < 0$). b. Total stresses, pore pressures and effective stresses straight after unloading ($t = 0$). c. Total stresses, pore pressures and effective stresses after increase of pore pressure to an equilibrium state ($t = \infty$). The lengths x are identical. GL is ground level, and GWL is ground water level.

Simultaneously, the soil particles move further apart resulting in increasing volume of voids, also known as swelling. In clay, the water molecules are placed in the voids between the clay minerals during swelling, cf. Figure 1.3. Since the effective stress is smaller than before the unloading, the shear strength is reduced, cf. the Coulomb expression $\tau = c' + \sigma' \tan \varphi'$. (Barnes, 2000; Sazhin, 1968)

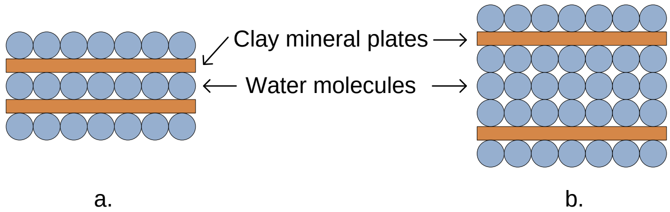

Figure 1.3: Clay minerals and water molecules in a swelling clay. a. Before swelling. b. After swelling.

In the United States it has been estimated that the cost of damaged buildings due to swelling and shrinkage of expansive soils exceeds the financial losses caused by earthquakes, tornadoes, hurricanes and floods combined (Holtz, 1983). In other words, swelling leads to very large forces on buildings and foundations. In this thesis, the focus is on the effect of swelling on a single pile of a pile group used for reducing settlements.

1.2 Pile Foundations

If a soil cannot sustain the loads from the superstructure by a shallow foundation implying inadequate bearing capacity or unacceptable settlements, a pile foundation can be a solution. Piles have the function of transferring load from the pile head to lower levels by shaft and toe resistances. Single piles often form part of a pile group. However, only single piles are described in the following. The description of piles is based on Augustesen (2006); Barnes (2000); Jardine et al. (2005); Krebs Ovesen et al. (2007).

Piles can be classified according to:

- Method of installation, i.e. driven, bored or jacked,
- Material, i.e concrete, steel or timber, full length or segmental,
- Size, i.e. length, diameter,
- Loading conditions, i.e. vertical or horizontal, in tension or in compression,
- The way the piles transfer load to the surrounding soil, i.e. end bearing or friction piles,
- Effects during installation, i.e displacement or replacement.

For further information about pile types, reference is made to Tomlinson and Woodward (2008).

In this thesis, main focus is on the shaft resistance of a circular concrete pile in a cohesive soil. Generally, the shaft resistance is determined by either an α-, β- or λ-method. In the α-method, the shaft friction is related to the undrained shear strength by the factor α. The β-method makes use of the Coulomb failure criterion excluding a cohesion. The λ-method is a combination of the α- and β-method.

In Denmark, the determination of the shaft resistance is based on the α-method where α is a function of the pile material and the remoulded shear strength of the soil, represented by the factors m and r, respectively. If r is not determined, the factor of regeneration may be taken as 0.4, cf. EN1997-1 DK NA:2008 (European Committee for Standardisation, 2008). It should be noted that time effects are not included in the Danish practice of determining the shaft resistance even though these have great influence on this parameter (Augustesen, 2006).

Further factors affecting the shaft resistance can be seen in Figure 1.4.

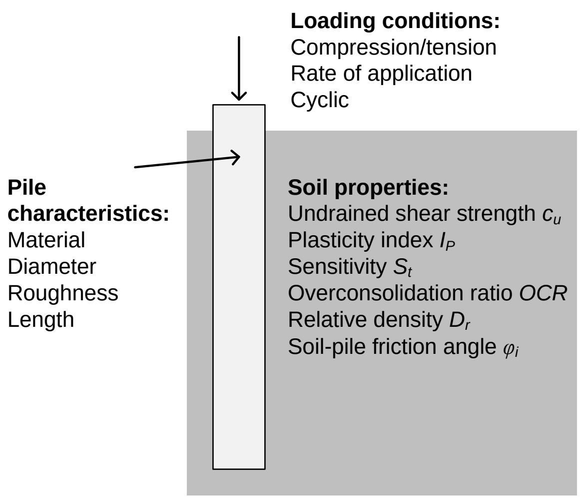

Figure 1.4: Influencing factors on the shaft resistance of a pile. According to Augustesen (2006).

1.3 Description of the Project

This thesis consists of three chapters and five appendices. The second and third chapter are individual papers with independent bibliographies. The bibliography enclosed in the end of this thesis includes all references.

Chapter 2 concerns the strength and deformation properties of the tertiary clay at Moesgaard Museum situated 10 km south of Aarhus. This includes analyses of two consolidation tests and a single triaxial test. The swelling pressure, the preconsolidation stress, the compression index and the constrained modulus are determined based on the consolidation tests. The drained and undrained strength are found by the triaxial test.

Chapter 3 concerns a fixed pile which, because of an excavation illustrating swelling, is exposed to tensile loading. This is modelled numerically, and the heave of the new ground surface, the shear stresses at the soil–pile interface and the internal vertical stresses are analysed based on a case study of Little Belt Clay.

The analyses show that the presence of the pile creates a weak zone within a radius of 3 pile diameters from the axis of symmetry of the pile. The maximum heave within this zone is polynomially decreasing with increasing interface strength. The swelling of the surrounding soil implies upward shear stresses at the soil–pile interface. This leads to tensile vertical stresses in the pile which in the current case exceed the tensile strength of concrete. The tensile vertical stresses peak after 35-50 years even though the heave of the soil continues for additional 300 years. It appears that the development of plastic interface implies the shrinkage of the pile because of the slip at the pile surface.

1.4 Project Limitations

The second consolidation test, i.e. the test with several un- and reloading paths, is solely used for determination of the constrained modulus. However, various parameters could have been determined by this test, e.g. the preconsolidation strain, the creep strain, the coefficient of permeability and the coefficient of consolidation.

The investigations in Chapter 3 concern a single pile where group effect is not taken into account.

The numerically modelled pile of Chapter 3 is assumed to be installed and, hence, effects of the installation are not accounted for.

Only the pile part situated within the swelling zone is considered in Chapter 3. The loading on the pile is assumed solely to originate from the swelling of the soil implying tensile stresses in the pile. Thus, the effects of an external compressive load is not covered by this thesis.

Strength and Deformation Properties of Tertiary Clay at Moesgaard Museum

K. L. Kaufmann
B. N. Nielsen
A. H. Augustesen

ISSN 1901-726X
DCE Technical Report No. 103

AALBORG UNIVERSITY
Department of Civil Engineering

Aalborg University
Department of Civil Engineering
Water & Soil

DCE Technical Report No. 103

Strength and Deformation Properties of Tertiary Clay at Moesgaard Museum

by

K. L. Kaufmann
B. N. Nielsen
A. H. Augustesen

September 2010

Scientific Publications at the Department of Civil Engineering

Technical Reports are published for timely dissemination of research results and scientific work carried out at the Department of Civil Engineering (DCE) at Aalborg University. This medium allows publication of more detailed explanations and results than typically allowed in scientific journals.

Technical Memoranda are produced to enable the preliminary dissemination of scientific work by the personnel of the DCE where such release is deemed to be appropriate. Documents of this kind may be incomplete or temporary versions of papers—or part of continuing work. This should be kept in mind when references are given to publications of this kind.

Contract Reports are produced to report scientific work carried out under contract. Publications of this kind contain confidential matter and are reserved for the sponsors and the DCE. Therefore, Contract Reports are generally not available for public circulation.

Lecture Notes contain material produced by the lecturers at the DCE for educational purposes. This may be scientific notes, lecture books, example problems or manuals for laboratory work, or computer programs developed at the DCE.

Theses are monograms or collections of papers published to report the scientific work carried out at the DCE to obtain a degree as either PhD or Doctor of Technology. The thesis is publicly available after the defence of the degree.

Latest News is published to enable rapid communication of information about scientific work carried out at the DCE. This includes the status of research projects, developments in the laboratories, information about collaborative work and recent research results.

Published 2010 by
Aalborg University
Department of Civil Engineering
Sohngaardsholmsvej 57,
DK-9000 Aalborg, Denmark

Printed in Aalborg at Aalborg University

ISSN 1901-726X
DCE Technical Report No. 103

Strength and Deformation Properties of Tertiary Clay at Moesgaard Museum

K. L. Kaufmann[1], B. N. Nielsen[2] and A. H. Augustesen[3]

Aalborg University, September 2010

Abstract

The tertiary clay at Moesgaard Museum near Aarhus in the eastern part of Jutland in Denmark is a highly plastic, glacially disturbed nappe of Viborg Clay. The clay is characterised as a swelling soil, which could lead to damaging of the building due to additional heave of the soil. To take this characteristic, as well as the strength and deformation properties, into account during the design phase, two consolidation tests and one triaxial test have been conducted. This paper evaluates the results of the laboratory tests leading to the preconsolidation stress, the deformation parameters consisting of the swelling pressure, the constrained modulus and the compression index, and the strength parameters comprising the undrained shear strength, the drained shear strength and the effective angle of internal friction.

Keywords: Tertiary clay, strength properties, deformation properties, Moesgaard Museum.

1 Introduction

10 km south of Aarhus, Moesgaard Museum is situated, cf. Fig. 1. The tertiary clay at Moesgaard Museum is a highly plastic, glacially disturbed nappe of Viborg Clay. A geotechnical boring near Viborg known as the Viborg-1-boring gives an overview of the stratigraphy of the tertiary deposits.

Figure 1: Location of Moesgaard Museum near Aarhus marked by a circle.

The tertiary clay at Moesgaard Museum is a swelling soil, i.e. highly ex-

[1]Graduate Student, Dept. of Civ. Eng., Aalborg University, Denmark.

[2]Assistant Professor, M.Sc., Dept. of Civ. Eng., Aalborg University, Denmark.

[3]Specialist in Geotechnical Engineering, Ph.D., M.Sc., COWI A/S. Part-time lecturer, Dept. of Civ. Eng., Aalborg University, Denmark.

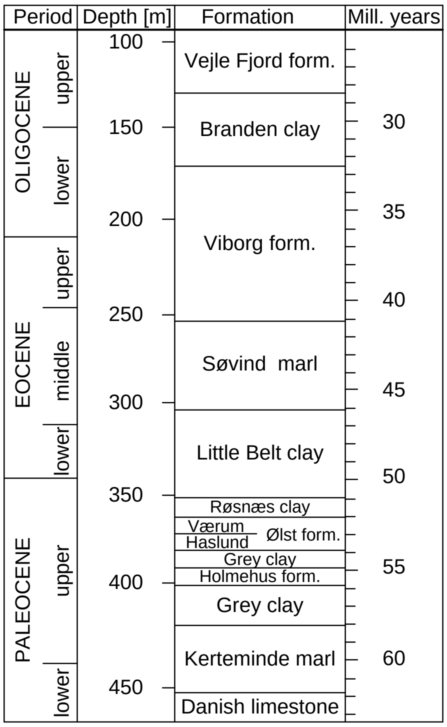

Figure 2: Profile of tertiary deposits based on the Viborg-1-boring near Viborg. According to (Thøgersen, 2001).

pansive in combination with water, which could lead to damaging of the building due to heave of the soil. Thus, it is important to determine at which stress levels swelling is expected to occur, represented by the swelling pressure.

Additionally, deformation and strength parameters of the clay are necessary for a detailed design of the foundation of new buildings. The parameters are, in addition to in situ tests, determined by two consolidation tests and one triaxial test. The results of the three laboratory tests are outlined in this paper.

2 Geological Description

The geological description of the area at Moesgaard Museum is based on two boring records and soil description in connection with the laboratory tests. Boring B106 is more sandy than boring B105. Segments of the boring records in the depths of the soil specimens can be seen in Fig. 4.

The tertiary clay at Moesgaard Museum is a highly plastic, glacially disturbed nappe of Viborg Clay from the Lower Oligocene period. The clay is a glacier deposit where the glacier has transported a large nappe of the Viborg Clay. Viborg Clay is a sea deposit which supersedes Søvind Marl and Little Belt Clay, cf. Fig. 2. The sea deposits are illustrated by the very homogeneous clay from about 12 to 26 m below ground surface. The sign of glacier deposits can be seen by the sand strias and gravel grains at 26–26.5 m and 28–29 m below ground surface. (COWI A/S, 2009)

The clay of the specimens from the two borings is characterised as highly plastic, greyish olive green and slightly micaous. Through the entire layer illustrated by the geotechnical borings, the clay is characterised as medium to very calcareous. This implies the greyish tone of the olive green colour. (COWI A/S, 2009)

Samples of the clay can be seen in Fig. 3. Both a homogenised, wet sample used for the classification tests and the dried, traversed soil specimen for the first consolidation test is shown.

Figure 3: Homogenised soil used for the classification tests (left) and traversed dried soil specimen used in the first consolidation test (right).

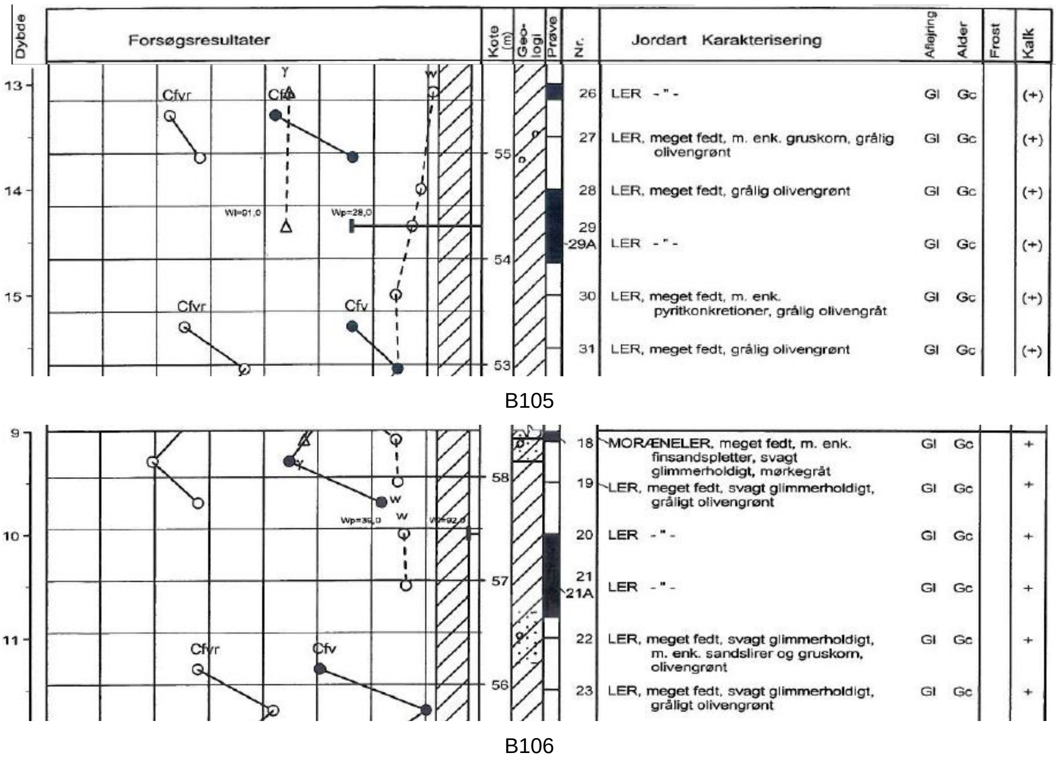

Figure 4: Segments of boring records B105 and B106 in depths of the soil specimens (29 and 21, respectively).

3 Classification

The tertiary clay at Moesgaard Museum is classified by the results of two geotechnical borings and the laboratory tests comprising the consolidation and triaxial tests. Following classification tests are conducted:

- Rolling out,
- The Casagrande method,
- The fall cone method.

The plastic limit is determined by rolling out, cf. Laboratoriehåndbogen (DGF's Laboratoriekomité, 2001). The liquid limit is determined by both the Casagrande method and the fall cone method, cf. Laboratoriehåndbogen (DGF's Laboratoriekomité, 2001). The classification parameters can be seen in Tab. 1.

Table 1: Classification parameters of the tertiary clay at Moesgaard Museum. The mean value is the arithmetic mean.

	w [%]	γ [kN/m^3]	w_P [%]	w_L [%]	I_P [%]
Results of boring records					
Min	19.0	18.8	28.0	91.0	53.0
Max	35.5	19.4	39.0	92.0	63.0
Mean	30.1	19.1	33.5	91.5	58.0
Results of laboratory test					
Min	32.8	18.1	34.5	95.0	60.0
Max	34.1	18.7	35.0	105.6	71.1
Mean	33.2	18.4	34.8	100.3	65.5

The results of the Casagrande method and the fall cone method differ about 2–9 %, cf. Fig. 5.

The liquid limit and the plasticity index determined by the two boring records and the mean values of the laboratory tests are plotted according to the Casagrande Chart, cf. Fig. 5.

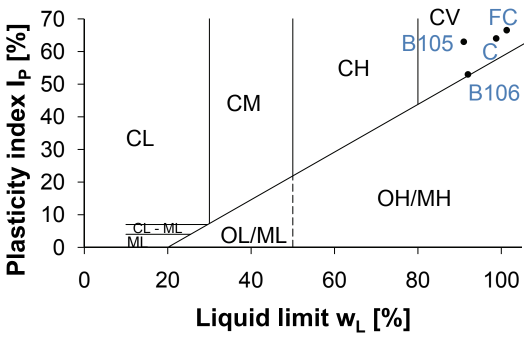

Figure 5: Classification of the tertiary clay at Moesgaard Museum according to the Casagrande Chart. *FC* is fall cone and *C* is Casagrande. According to Krebs Ovesen et al. (2007, Fig. 1.13).

Hence, the clay is characterised as very high plasticity clay marked by *CV* in the figure in accordance to the geological description of the boring records. For comparison, the classification of Søvind Marl and Little Belt Clay are plotted in Fig. 6 together with the tertiary clay at Moesgaard (Johannesen et al., 2008; Thøgersen, 2001).

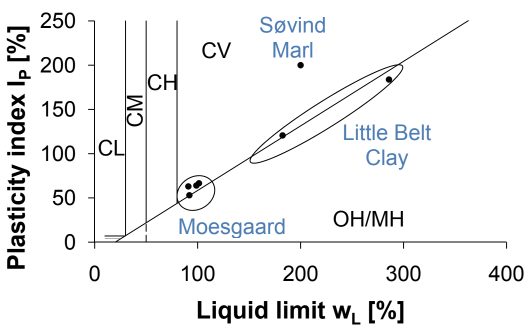

Figure 6: Classification of Søvind Marl, Little Belt Clay and the tertiary clay at Moesgaard Museum according to the Casagrande Chart. According to Krebs Ovesen et al. (2007, Fig. 1.13).

4 Consolidation Tests

The deformation properties of the tertiary clay at Moesgaard Museum are determined by two consolidation tests conducted according to the instructions in Laboratoriehåndbogen (DGF's Laboratoriekomité, 2001). The first consolidation test is conducted to determine the preconsolidation stress σ'_{pc} and the swelling pressure σ'_S. The second consolidation test is used to determine constrained modulus E_{oed}. However, various parameters can also be determined by the second consolidation test, e.g. σ'_{pc}, the creep strain ε_S, the coefficient of permeability k and the coefficient of consolidation c_k. Both consolidation tests are conducted by incremental loading.

In the first consolidation test, the initial dimensions of the specimen are $H = 2D = 60$ mm. The reason for the small dimensions are so that it is possible to apply stresses which are sufficiently large to observe a linear tendency of the primary path. The testing program consists of increasing loading to determine the virgin curve and one unloading step. Additionally, σ'_S is determined to be in the interval of the load step at which no swelling occurs and the step prior to this. The preconsolidation stress is preliminary estimated to 1120–1400 kPa corresponding to 4–5 times the vane shear strength c_v which is found to approximately 280 kPa at nearby depths (DGF's Laboratoriekomité, 2001).

To ensure that secondary consolidation has occurred, the duration of each load step is two–three days depending on the progress of the strain–time curve. For example, the strain–time curve for load step 6, which is an increase of the loading from 600 kPa to 1200 kPa, can be seen in Fig. 7. The duration of the load step is two days by which the progress of the secondary consolidation can be described by a linear regression line.

In the second consolidation test, the initial dimensions of the specimen are $H = 2D = 70$ mm. The testing program

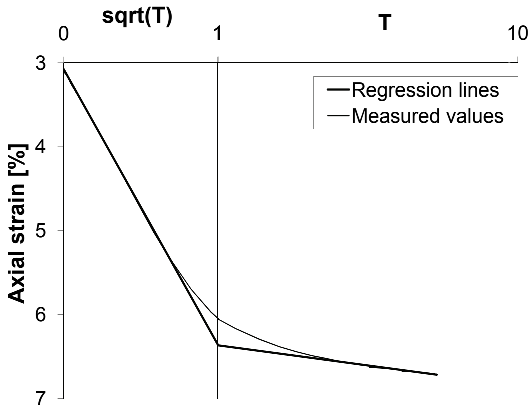

Figure 7: Strain–time curve for load step 6. $T = 1$ is after about 0.5 day and the final T is after two days.

consists of two times three unloading–reloading paths. The first three cycles include unloading to 650, 338 and 129 kPa, each followed by reloading to 1000 kPa. The next three cycles includes similar unloadings followed by reloading to 2000 kPa. After the last three cycles, the specimen is loaded to 4000 kPa and finally unloaded to zero loading.

The effective in situ stress is estimated to $\sigma'_0 = 200$ kPa (COWI A/S, 2010).

4.1 Deformation Properties

The swelling pressure, the preconsolidation stress and the compression index are determined on the basis of the first consolidation test.

The swelling pressure σ'_S is determined as the load interval at which swelling no longer occurs. It is found to be between 150.8 and 303.7 kPa.

The preconsolidation stress σ'_{pc} is estimated by the Terzaghi method (Moust Jacobsen, 1993; Thøgersen, 2001). In Terzaghi's method, the primary path, i.e. the curved line, of the primary loading curve is used to determine σ'_{pc}. According to Terzaghi, the primary path can be described by Eq. 1.

$$\varepsilon = C_{c\varepsilon} \cdot \log\left(1 + \frac{\sigma'}{\sigma'_\kappa}\right) + \varepsilon_0 \qquad (1)$$

Where $C_{c\varepsilon}$ is the compression index, σ'_κ is a reference stress and ε_0 is the start value of the consolidation strain (not equal to the initial strain ε_i). The reference stress σ'_κ is the addition to σ' by which the primary path gets linear in a semi-logarithmic depiction, named the virgin curve, cf. Fig. 8.

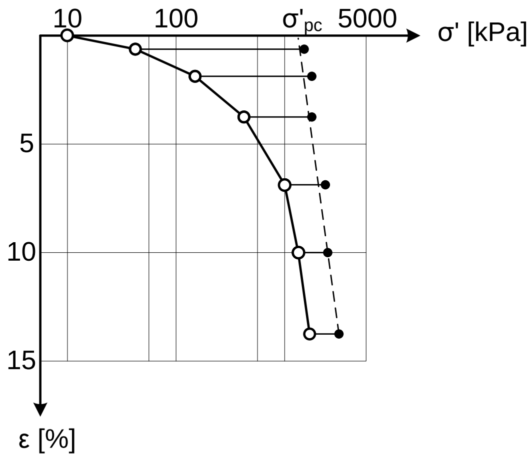

Figure 8: Determination of the virgin curve (the dashed line) used for Terzaghi's method.

σ'_{pc} is then estimated by Eq. 2.

$$\sigma'_{pc} \approx 2.0 \cdot \sigma'_\kappa \qquad (2)$$

The primary path and the virgin curve of the load-displacement curve can be seen in Fig. 9.

The preconsolidation stress is found to $\sigma'_{pc} = 1350$ kPa which implies an overconsolidation ratio of approximately $OCR = 6.8$. Additionally, estimations based on Akai's method, Janbu's method and the coefficient of consolidation, cf. Figs. 10–12, have been investigated leading to σ'_{pc} in the range $1200 - 1800$ kPa.

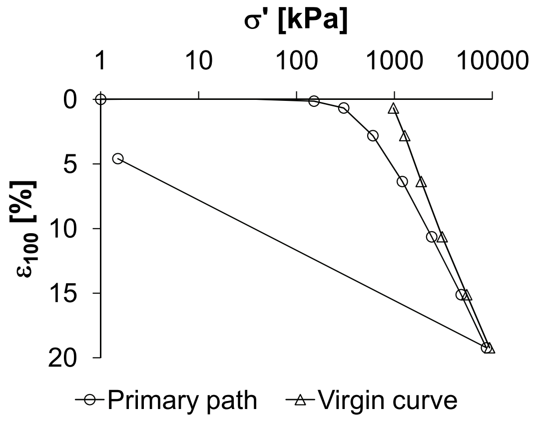

Figure 9: Primary path and virgin curve of the first consolidation test.

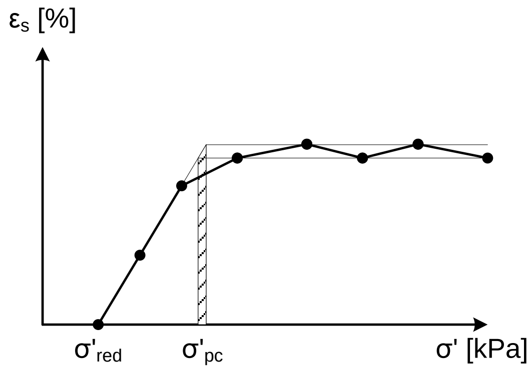

Figure 10: Akai's method of determining σ'_{pc}. σ'_{red} is the lowest effective stress of the soil. According to Moust Jacobsen (1993, Fig. 5.13).

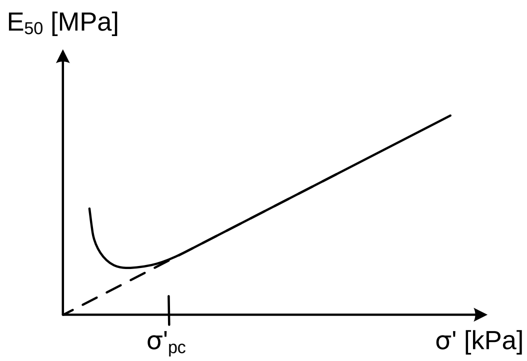

Figure 11: Janbu's method of determining σ'_{pc} based on the secant modulus E_{50}.

The compression index is determined as the slope of the linear part of the primary loading path as $C_{c\varepsilon} = 15.9$ %. For comparison, the compression index determined by the approximative approach in

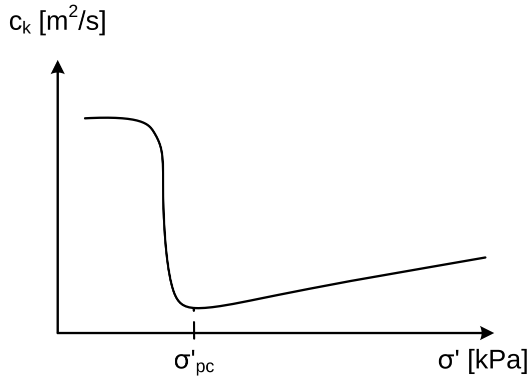

Figure 12: Determination of σ'_{pc} based on the coefficient of consolidation c_k. According to Thøgersen (2001, Fig. 5.9).

Eq. 3 for $w = 34.1$ % from the first consolidation test is found to $C_{c\varepsilon} = 12.3$ % (Steenfelt et al., 2007).

$$C_{c\varepsilon} = \frac{w - 25\ \%}{w + 40\ \%} \tag{3}$$

The primary path of the second consolidation test can be seen in Fig. 13.

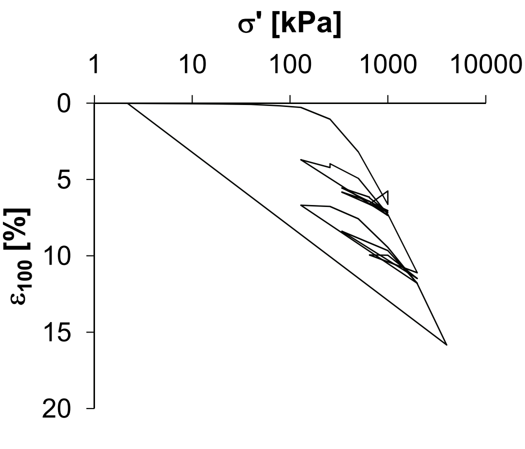

Figure 13: Primary path and unloading/reloading paths of the second consolidation test.

The constrained modulus is estimated based on the second consolidation test. It is determined by Eq. 4 according to Laboratoriehåndbogen (DGF's Laboratoriekomité, 2001).

$$E_{oed} = E_{oed,0} + \Delta E_{oed} \cdot \sigma'_{red} \tag{4}$$

Where $E_{oed,0}$ is the constrained modulus for zero effective stress, ΔE_{oed} the addition to E_{oed} per stress unit, and σ'_{red} the lowest effective stress of the soil. For each reloading path plotted in an (ε_{100}, σ')-diagram, the constrained modulus can be found as the reciprocal value of the initial slope. Plotting E_{oed} for each reloading path combined with σ'_{red} yields an estimate of Eq. 4.

The reloading paths can be seen in Fig. 15. As seen in the figure, the magnitude of E_{oed} for each reloading path depends on the choice of considered points. Choosing for example the first two points of the first reloading path for the second three cycles, i.e. (650 kPa, 9.9 %) and (999 kPa, 10.0 %), leads to E_{oed} = 1748 MPa, whereas the first and last point of this reloading path, i.e. i.e. (650 kPa, 9.9 %) and (1999 kPa, 11.5 %), leads to E_{oed} = 87 MPa. The constrained moduli for alle parts of the reloading paths are listed in Tab. 3.

As seen in Fig. 15 and Tab. 3, the constrained modulus depends significantly on the investigated stress level. Hence, multiple relations based on Eq. 4 for different stress levels could be a method of obtaining realistic values of E_{oed} in the future.

As an approximation of the constrained modulus, a linear regression between the first and last points of each reloading path is applied. This leads to the relation in Eq. 5 for the first three cycles and in Eq. 6 for the last three cycles, cf. Fig. 14.

$$E_{oed,1} = -3818 + 132 \cdot \sigma'_{red} \quad \text{[kPa]} \quad (5)$$
$$E_{oed,2} = 4560 + 128 \cdot \sigma'_{red} \quad \text{[kPa]} \quad (6)$$

In Eq. 5, the constrained modulus starts as a negative value. This is not realistic and Eq. 6 is used as an approximation of E_{oed}. For comparison, the constrained modulus of the tertiary Søvind Marl is approximately $E_{oed} = 10000 + 150 \cdot \sigma'_{red}$ (Johannesen et al., 2008).

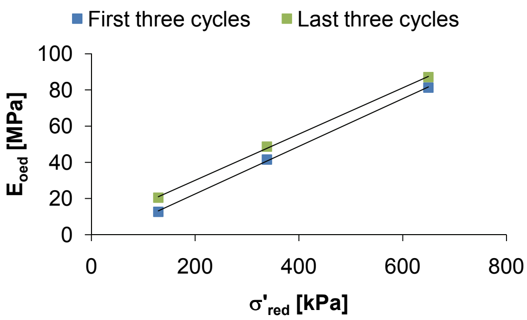

Figure 14: Initial slopes for the first three cycles and the last three cycles based on the first and last points of each reloading path.

The deformation parameters of the tertiary clay at Moesgaard Museum are listed in Tab. 2.

Table 2: Deformation parameters of the tertiary clay at Moesgaard Museum by the consolidation tests.

σ'_S	150.8-303.7 kPa
σ'_{pc}	1350 kPa
$C_{c\varepsilon}$	15.9 %
E_{oed}	$4560 + 128 \cdot \sigma'_{red}$ kPa

5 Triaxial Test

The strength properties of the tertiary clay at Moesgaard Museum are determined by a $CAU_{u=200}$ triaxial test with $H = D$ = 70 mm and smooth pressure cells. The test is conducted according to Laboratoriehåndbogen (DGF's Laboratoriekomité, 2001). The loading phase is conducted as an anisotropic loading controlled by the coefficient of horizontal earth pressure at rest K_0. The specimen is unloaded with constant K_0. The effective mean stress p' as a function of the deviatoric stress q can be seen in Fig. 16.

During the failure phase, the specimen is loaded to failure with a strain rate of 0.5 %/h.

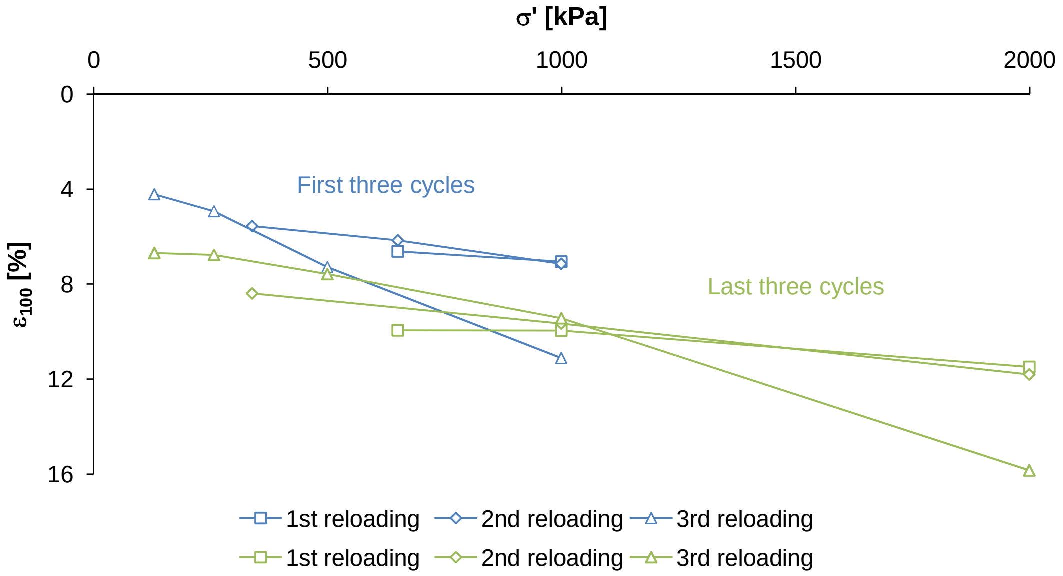

Figure 15: Reloading paths for the second consolidation test.

Table 3: Constrained moduli E_{oed} in MPa for all parts of the reloading paths.

	First three cycles			Last three cycles		
Points	1st reloading	2nd reloading	3rd reloading	1st reloading	2nd reloading	3rd reloading
1–2	81	52	18	1748	52	159
1–3		42	12	87	49	42
1–4			13			32
1–5						20
2–3		35	10	65	47	30
2–4			12			28
2–5						19
3–4			13			27
3–5						18
4–5						16

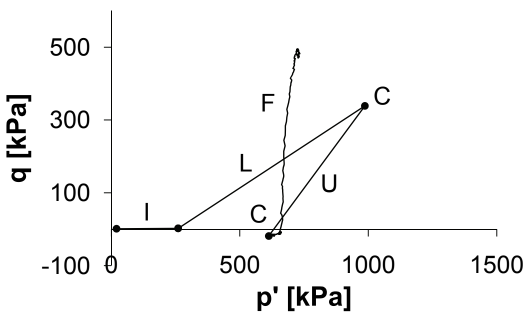

Figure 16: The effective mean stress p' as a function of the deviatoric stress q. I: Installation, L:Loading, C: Consolidation, U: Unloading, F: Failure.

The reader should be aware that the pore pressure was not measured during the test. This does, however, not have any significant consequence because the effective stress path and not the total stress path is followed during an undrained triaxial test, cf. Fig. 17. Problems appeared with the unloading equipment. This implied that the specimen was not unloaded to the desired stress level, cf. Fig. 18, and, thus, with a varying K_0.

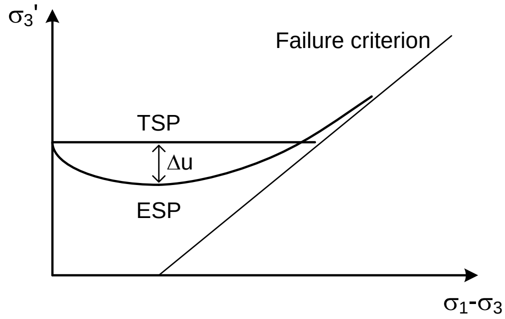

Figure 17: Total stress path (TSP), effective stress path (ESP) and failure criterion for undrained triaxial tests.

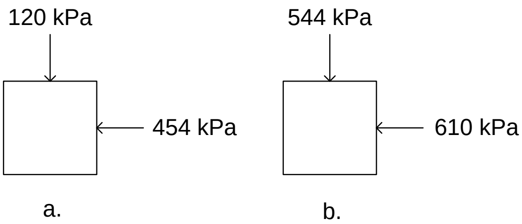

Figure 18: a. Desired stress levels after unloading. b. Actual stress levels after unloading.

5.1 Strength Properties

The axial strain ε_1 is plotted as a function of the effective deviatoric stress q' in Fig. 19.

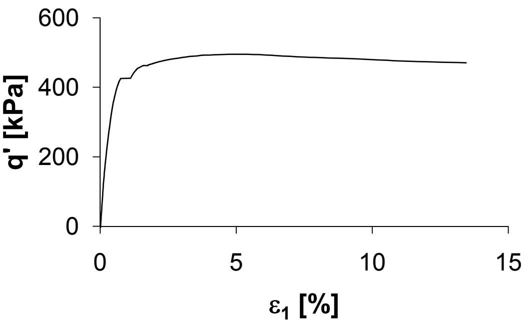

Figure 19: The axial strain as a function of the deviatoric stress.

The undrained shear strength c_u is determined as half the maximum deviatoric stress q, cf. Eq. 7.

$$c_u = \frac{q}{2} = \frac{\sigma_1 - \sigma_3}{2} \tag{7}$$

The maximum deviatoric stress for the failure criterion corresponding to 10 % additional strain is found to $q = 495$ kPa leading to $c_u = 247.5$ kPa. This corresponds well with the vane shear strength of $c_v = 280$ kPa which indicates a non-fissured clay.

For preconsolidated clays, the soil tends to dilate during loading. As seen in Fig. 20, this is not the case for the present triaxial test.

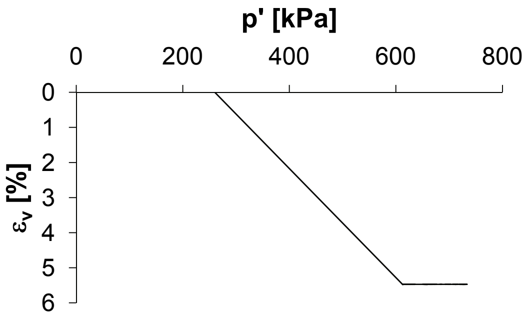

Figure 20: Volumetric strains ε_v as a functions of the effective mean stress p'.

The drained strength parameters c'_{tr} and φ'_{tr} are determined by Eqs. 8 and 9.

$$\sin\varphi'_{tr} = \frac{3}{1 + 6 \cdot \tan\alpha} \tag{8}$$

$$c'_{tr} = a \cdot \tan\alpha \cdot \tan\varphi'_{tr} \tag{9}$$

The parameters α and a are found by the failure criterion, cf. Fig. 21.

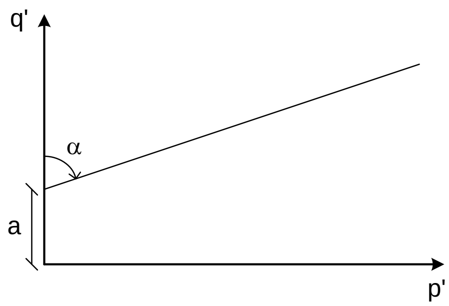

Figure 21: Failure criterion of triaxial test.

Because only a single failure point is found by the triaxial test, it is difficult to plot a unique failure criterion, cf. Fig. 21. Thus, both a solution including a cohesion defined by the parameter a

and a solution intersecting with (0, 0) are used. This leads to $(c'_{tr}, \varphi'_{tr}) = (0, 17.8°)$ and $(c'_{tr}, \varphi'_{tr}) = (47.1\text{ kPa}, 14.5°)$, respectively. It should be noted, though, that for the simple relation $c' = 0.1 \cdot c_u$, the value of $c'_{tr} = 47.1$ kPa implies $c_u = 471$ kPa. This value is almost twice the undrained shear strength determined earlier as $c_u = 247.5$ kPa. Hence, the second set of drained strength parameters including a cohesion is considered unrealistically high.

The strength parameters of the tertiary clay at Moesgaard Museum are listed in Tab. 4.

Table 4: Strength parameters of the tertiary clay at Moesgaard Museum by the triaxial test.

c_u	247.5 kPa
c'_{tr}	0 kPa/47.1 kPa
φ'_{tr}	17.8°/14.5°

6 Conclusions

The strength and deformation properties of the tertiary clay at Moesgaard Museum have been evaluated in this paper. The properties are found by means of two consolidation tests and one triaxial test.

The first consolidation test led to estimates on the swelling pressure, the preconsolidation stress and the compression index. The parameter were found to $\sigma'_S = 150.8 - 303.7$ kPa, $\sigma'_{pc} = 1350$ kPa and $C_{c\varepsilon} = 15.9$ %, respectively. The second consolidation test led to an estimate on the constrained modulus to $E_{oed} = 4560 + 128 \cdot \sigma'_{red}$ kPa.

The triaxial test provided the undrained shear strength and two sets of drained strength parameters: one set where the failure criterion intersects with (0, 0), i.e. excluding a cohesion, and a set where a cohesion is included. The undrained shear strength was found to $c_u = 247.5$ kPa. The first set of drained strength parameters was found to $(c'_{tr}, \varphi'_{tr}) = (0, 17.8°)$. The second set was found to $(c'_{tr}, \varphi'_{tr}) = (47.1\text{ kPa}, 14.5°)$. The drained shear strength of the second set is, however, considered high compared to the undrained shear strength when using the approximation $c' = 0.1 \cdot c_u$.

Bibliography

COWI A/S (2009). Case 71433-G-1 Moesgaard Museum, Moesgård Allé 20, Højbjerg. Boring records, COWI A/S.

COWI A/S (2010, 26 February). Moesgaard Museum, Moesgård Allé 20, Højbjerg - Forslag til program for udførelse af konsoliderings- og triaxialforsøg. Intern report. Document no. 71433.

DGF's Laboratoriekomité (2001). *DGF-Bulletin 15: Laboratoriehåndbogen*. Aalborg, Denmark: Dansk Geoteknisk Forening.

Johannesen, C. L., J. V. Madsen, and K. T. Vestergaard (2008, June). Geoteknikniske egenskaber for tertiært ler ved Light*house - forsøg med og numerisk modellering af søvindmergel. Aalborg University.

Krebs Ovesen, N., L. D. Fuglsang, and G. Bagge (2007). *Lærebog i Geoteknik* (1st ed.). Lyngby, Denmark: Polyteknisk Forlag.

Moust Jacobsen, H. (1993). *Lærebog i videregående geoteknik 2 - Sætninger i jord*. Aalborg, Denmark: Aalborg Universitet.

Steenfelt, J. S., C. S. Sørensen, and W. Bai (2007). *Teknisk Ståbi - Fundering*, Chapter 10. Nyt Teknisk Forlag.

Thøgersen, L. (2001). *Effects of Experimental Techniques and Osmotic Pressure on the Measured Behaviour of Tertiary Expansive Clay, Volume 1*. Ph. D. thesis, Soil Mechanics Laboratory, Aalborg University.

Recent publications in the DCE Technical Report Series

Kaufmann, K. L., Nielsen, B. N., & Augustesen, A. H. (2010). Finite Element Investigations on the Interaction between a Pile and Swelling Clay. *DCE Technical Report, 104*.

ISSN 1901-726X
DCE Technical Report No. 103

Finite Element Investigations on the Interaction between a Pile and Swelling Clay

K. L. Kaufmann
B. N. Nielsen
A. H. Augustesen

ISSN 1901-726X
DCE Technical Report No. 104

AALBORG UNIVERSITY
Department of Civil Engineering

Aalborg University
Department of Civil Engineering
Water & Soil

DCE Technical Report No. 104

Finite Element Investigations on the Interaction between a Pile and Swelling Clay

by

K. L. Kaufmann
B. N. Nielsen
A. H. Augustesen

September 2010

Scientific Publications at the Department of Civil Engineering

Technical Reports are published for timely dissemination of research results and scientific work carried out at the Department of Civil Engineering (DCE) at Aalborg University. This medium allows publication of more detailed explanations and results than typically allowed in scientific journals.

Technical Memoranda are produced to enable the preliminary dissemination of scientific work by the personnel of the DCE where such release is deemed to be appropriate. Documents of this kind may be incomplete or temporary versions of papers—or part of continuing work. This should be kept in mind when references are given to publications of this kind.

Contract Reports are produced to report scientific work carried out under contract. Publications of this kind contain confidential matter and are reserved for the sponsors and the DCE. Therefore, Contract Reports are generally not available for public circulation.

Lecture Notes contain material produced by the lecturers at the DCE for educational purposes. This may be scientific notes, lecture books, example problems or manuals for laboratory work, or computer programs developed at the DCE.

Theses are monograms or collections of papers published to report the scientific work carried out at the DCE to obtain a degree as either PhD or Doctor of Technology. The thesis is publicly available after the defence of the degree.

Latest News is published to enable rapid communication of information about scientific work carried out at the DCE. This includes the status of research projects, developments in the laboratories, information about collaborative work and recent research results.

Published 2010 by
Aalborg University
Department of Civil Engineering
Sohngaardsholmsvej 57,
DK-9000 Aalborg, Denmark

Printed in Aalborg at Aalborg University

ISSN 1901-726X
DCE Technical Report No. 104

Finite Element Investigations on the Interaction between a Pile and Swelling Clay

K. L. Kaufmann[1], B. N. Nielsen[2] and A. H. Augustesen[3]

Aalborg University, September 2010

Abstract

This paper aims to investigate the interaction between a pile and a swelling soil modelled as a cohesive soil subjected to unloading. The investigations include analyses of the heave of the excavation level, shear stresses at the soil–pile interface and internal pile forces based on a case study of Little Belt Clay. The case study involves a circular concrete pile installed in clay immediately after an excavation. The influence of the swelling soil on the soil–pile interaction and the internal pile forces are analysed by solely observing the upper pile part positioned in the swelling zone. For the investigated case study, the influence of the pile is observed in a radius of approximately 3 pile diameters from the pile centre creating a weak zone inside this radius. The maximum heave of the excavation level inside this radius decreases polynomially with increasing interface strength. The swelling of the surrounding soil implies upward shear stresses at the soil–pile interface leading to tensile vertical stresses in the pile. In the current case, they exceed the tensile strength of concrete. The tensile vertical stresses peak after 35-50 years. However, the heave of the soil continues for additional 300 years. It appears that the development of plastic interface implies the shrinkage of the pile.

Keywords: Swelling soil, single pile, soil–pile interaction, finite element modelling.

1 Introduction

When clay with a moderate to high activity is exposed to changes in moisture content, the increase in volume known as swelling occurs. The changes in moisture content may appear as an effect of unloading, e.g. an excavation, leading to an undrained response of soil.

Immediately after an unloading, a decrease in the pore pressures is observed. When drainage begins, the pore pressures increase resulting in decreasing effective stresses and, thus, increasing volume of voids, i.e. swelling. The stress variation during an unloading situation can be seen in Fig. 1. The depth to which swelling occurs is named the swelling zone.

[1] Graduate Student, Dept. of Civ. Eng., Aalborg University, Denmark.

[2] Assistant Professor, M.Sc., Dept. of Civ. Eng., Aalborg University, Denmark.

[3] Specialist in Geotechnical Engineering, Ph.D., M.Sc., COWI A/S. Part-time lecturer, Dept. of Civ. Eng., Aalborg University, Denmark.

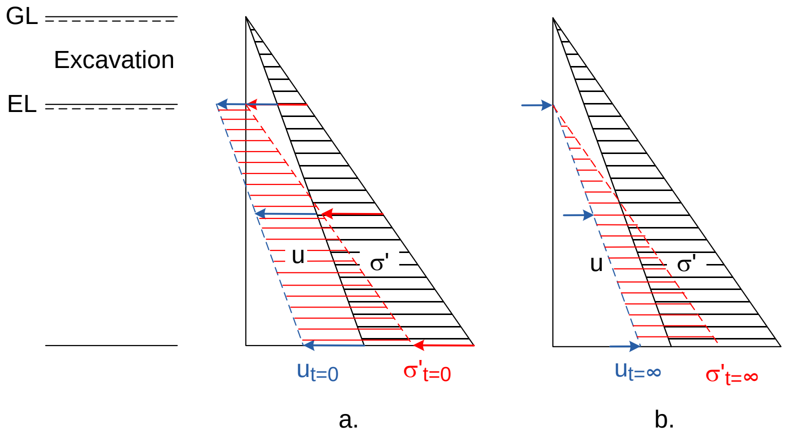

Figure 1: Stress variation for unloading by excavation. a. Total stresses σ, marked by the red dashed line, as a result of pore water pressures u, marked by the blue dashed line, and effective stresses σ', indicated by the hatched red area, immediately after unloading ($t = 0$). b. σ, u and σ' after increase of pore water pressure to an equilibrium state ($t = \infty$). The arrows show the change of stresses from the prior state to the current. GL is ground level and EL is excavation level.

Pile foundation is a common method of reducing settlements when buildings are situated on settlement-inducing soil layers. Due to the skin friction of the pile, the settlements imply downward movement and compressive loading of the pile.

Pile foundations designed to resist compressive loads are occasionally situated in swelling soils. Due to the friction between pile and soil, the heave caused by swelling leads to an additional tensile loading. The mechanisms are simplified in Fig. 3. In Fig. 3a, the pile is driven into the soil and axially loaded implying upward shear stresses at the soil–pile interface. Over time, the swelling implies heave of the ground surface leading to downward shear stresses at the interface inside the swelling zone, cf. Fig. 3b and Fig. 3c. Furthermore, the figures show that the height of the swelling zone n is increasing with time. Fig. 3c is divided into two parts, which can be analysed separately: Fig. 3d and Fig. 3e.

In this paper, focus is paid to the mechanisms of Fig. 3d by numerical analyses. This includes investigations on the heave of the ground surface, the shear stresses at the soil–pile interface and the internal forces in the pile. The analyses are based on a case study of a circular concrete pile installed in the swelling Little Belt Clay.

Initially, the geometrical model is validated by comparison of theoretical approaches and results of a model solely consisting of a swelling soil. Then, a single pile situated in the soil is modelled and the results comprising heave, shear stresses at the interface and internal normal stresses in the pile are analysed.

The positive stress directions used in this paper can be seen in Fig. 2. However, compressive stresses and pore pressures in the soil are defined positive in accordance with common geotechnical practice.

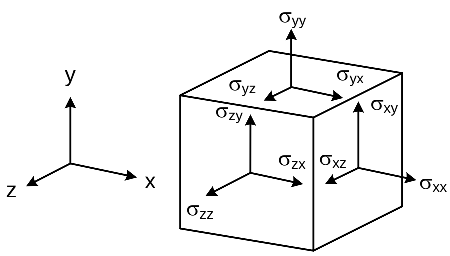

Figure 2: Coordinate system and sign convention of stresses.

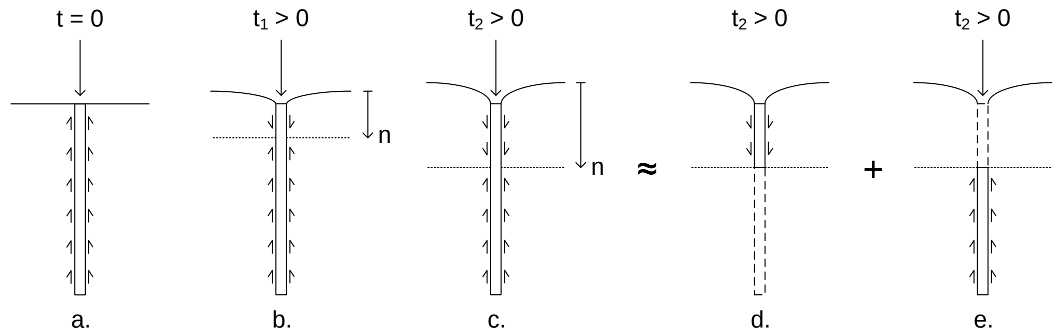

Figure 3: Simplification of the mechanisms for an axially loaded pile in a swelling soil. n is the height of the swelling zone. $t_1 < t_2$.

2 Review of Existing Literature

Swelling soils and piles situated in these soils have been analysed by several different methods in the existing literature. A review of three analysis methods are presented in the following to gain an insight to the difficulties of analysing swelling soils.

2.1 Okkels and Bødker, 2008

Okkels and Bødker (2008) aim to determine the height of the swelling zone n and the magnitude and time frame of the consequently heave by a simple first order theory. As an approximation, the one-sided drainage is assumed to be linearly distributed, cf. Fig. 4. The approximation is based on an expression of the height of the swelling zone n as a function of time. The approximation has shown to yield satisfactory results.

n is determined by equalising the incoming volume of water and the heave at a specific time calculated as consolidation settlements of preconsolidated clay. The progress of the n with time for a coefficient of consolidation of $c_k = 10^{-8}$ m^2/s can be seen in Fig. 5.

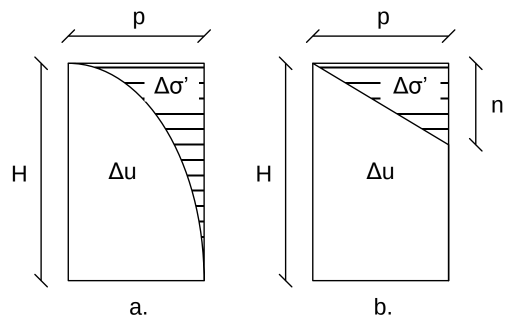

Figure 4: Stress variation for consolidation with one-sided drainage where H is the height of the layer, p the unloading pressure, Δu the excess pore pressure and $\Delta\sigma'$ the effective stress variation. a. One-sided drainage by Terzaghi's theory of consolidation. b. Linear approximation where n is the height of the swelling zone.

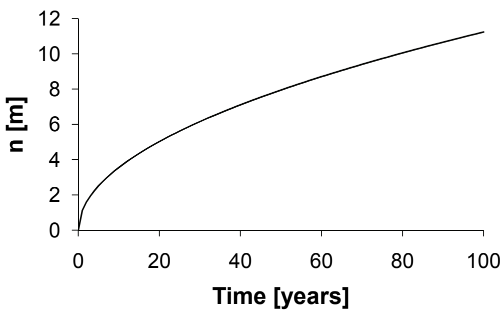

Figure 5: Progress of the height of the swelling zone with time for $c_k = 10^{-8}$ m^2/s.

The pore pressure is determined by the height of the swelling zone by which the total heave is calculated similar to settlements of a thin layer of normally consolidated clay by the conventional theory of consolidation. For this calculation, the compression index for the unloading path

C_{cu} is applied. Whether this index or the compression index for the primary path $C_{c\varepsilon}$ should be applied is debatable.

2.2 Moust Jacobsen and Gwizdala, 1992

The numerical approach in Moust Jacobsen and Gwizdala (1992) describes a method of determining the downward displacement through the pile and of the ground surface caused by settlements. The aim of the approach is to differentiate between the displacement of the pile shaft and the pile toe due to differences in load–displacement curves. The results are then combined to determine the total displacements. Even though the method is developed for loading situation, it is assumed to apply for unloading situations as well. Hereby, the upward displacements of the pile toe and the ground surface caused by heave can be determined.

2.3 Poulos and Davis, 1980

According to Poulos and Davis (1980), the heave of a pile in swelling soil can be determined by a reduction of the displacement at far field, i.e. of the soil without influence of the pile, due to the soil–pile interaction. According to the basic theory proposed by Poulos and Davis (1980), the pile displacements in a swelling soil are determined by elastic calculations.

The basic theory is modified to account for slip in the soil–pile interface, compressive and tensile failure of the pile, layered soil and variation in time. Slip is taken into account by introducing a limited shear stress at the interface τ_i. The limit, i.e. the strength of the interface, is equalised to the Coulomb failure criterion.

2.4 Overview of Existing Literature

An overview of the influencing parameters of the existing theory can be seen in Tab. 1. O&B is an abbreviation of Okkels and Bødker (2008), MJ&G is Moust Jacobsen and Gwizdala (1992) and P&D is Poulos and Davis (1980).

Table 1: Parameters of influence of the existing theory. Index s is for soil and i for interface. L is pile length and D is pile diameter.

O&B	MJ&G	P&D
n	n	n
γ_s	γ_s	Swelling profile
Surface load	Surface load	E_s
c_k	Factor of regeneration	ν_s
Time		Distribution of τ_i
C_{cu}	Pile diameter	Pile diameter
	Pile material	L/D
	c_u	Axial load on pile
		Tensile failure of pile
		If slip in interface: shear strength

The theory of Okkels and Bødker (2008) is used in the case study to determine the height of the swelling zone n. The remaining two theories of the literature are both based on floating piles. This differ from the concept of Fig. 3d, which is analysed in this paper, where the pile is fixed at the bottom of the model, cf. Sec. 3. Therefore, the latter two theories are not used further.

3 Case Study

The numerical modelling is conducted by the commercial FEM program PLAXIS 2D version 9.02. The case study involves a circular concrete pile with the dimensions $L = 20$ m and $D = 0.34$ m placed in clay immediately after a 10 m excavation of the overlying soil.

The outer width of the soil mass is chosen as $B = 20$ m. This complies with the recommendation by Abbas et al. (2008) of $B = 40D \approx 14$ m. It is assumed that the influence of the swelling soil on the soil–pile interaction and the internal forces in the pile can be analysed by solely observing the upper pile part positioned in the swelling zone. Thus, the height of the model is chosen equal to the height of the swelling zone n determined by Eq. 1 (Okkels and Bødker, 2008).

$$n = 2\sqrt{c_k \cdot t} \tag{1}$$

Where $c_k = \frac{k \cdot E_{oed}}{\gamma_w}$ is the coefficient of consolidation and t is the consolidation time. The soil parameters are listed in Tab. 2 and a life expectancy of $t = 100$ years is chosen. Hereby, the height of the model after the excavation is found to be 11 m.

Because of the circular pile, an axisymmetric model is chosen to study the problem, cf. Fig. 6.

The soil material is applied corresponding to the tertiary swelling clay, Little Belt Clay, and the pile is modelled as concrete. The material parameters of the clay are a combination of a sample with $w = 33.3$ %, $I_P = 183.8$ % and $\sigma'_{pc} = 550$ kPa defined by Thøgersen (2001) and the undrained and effective strength parameters defined by Harremoës et al. (1997). It should be noted, though, that

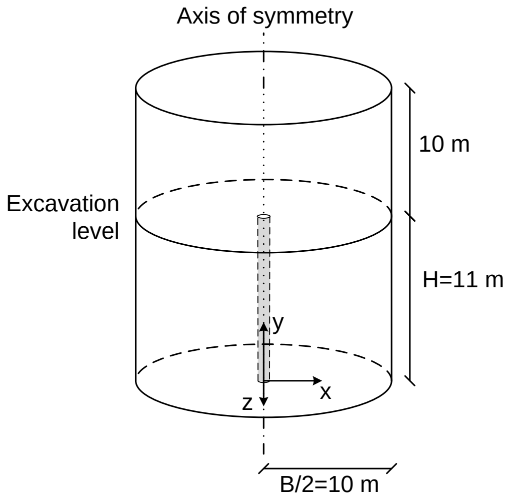

Figure 6: Dimensions of the soil model for the analysed case study. The diameter of the pile is $D = 0.34$ m.

the values of the coeficcients of permeability and the Young's moduli of elasticity are chosen. The moduli are estimated based on the relations $E_{50} = E_{oed}$ and $E_{ur} = 3 \cdot E_{oed}$ (Brinkgreve et al., 2008a). The material parameters for the materials are listed in Tab. 2.

Table 2: Material properties of the case study.

Parameter	Little Belt Clay	Concrete
w [%]	33.3	-
I_P [%]	183.8	-
σ'_{pc} [kPa]	550	-
γ_{sat} [kN/m^3]	18.49	-
γ_{unsat} [kN/m^3]	16.49	24
k_x [m/s]	10^{-11}	-
k_y [m/s]	10^{-11}	-
ν [-]	0.3	0.15
c'/c_u [kPa]	40/225	-
E_{oed} [MPa]	10	$34.8 \cdot 10^3$
E_{50} [MPa]	10	-
E_{ur} [MPa]	30	-
φ' [°]	16	-
ψ [°]	0	-

The soil is modelled as an undrained Hardening Soil (HS) material and the pile as a non-porous linear elastic material. The HS material model is chosen to account for the increase in stiffness appearing for unloading situations by use of the unloading–reloading modulus E_{ur} and the stress dependency of Young's moduli of elasticity. However, the power for stress–level dependency of stiffness m is chosen equal to zero for simplification. The model parameters for the materials are listed in Tab. 3.

Table 3: Model properties of the case study.

Parameter	Little Belt Clay	Concrete
Model type	Hardening-Soil	Linear elastic
Behaviour	Undrained	Non-porous
K_0 [-]	1	1
OCR [-]	1	-
POP [-]	0	-
R_{inter}	0.267	-
m	0	0

The strength reduction factor R_{inter} is determined as the ratio of the interface cohesion c_i to the undrained shear strength of the soil c_u. The interface cohesion is chosen as $c_i = 60$ kPa in accordance with Danish practice based on the assumption of an undrained failure at the interface, the undrained shear strength c_u and the factors of material and regeneration as $m = 1$ and $r = 0.4$. This leads to the strength reduction factor $R_{inter} = 0.267$. It should be noted that there has not been distinguished between a compressive or a tensile failure at the interface.

If the API Recommended Practice is applied instead of the Danish practice, R_{inter} can be equalised to the dimensionless factor α in Eq. 2 (API, 2000).

$$c_i = \alpha \cdot c_u \tag{2}$$

α is determined by Eqs. 3 and 4.

$$\alpha = 0.5 \cdot \psi^{-0.5} \quad \text{for } \psi \leq 1.0 \tag{3}$$
$$\alpha = 0.5 \cdot \psi^{-0.25} \quad \text{for } \psi > 1.0 \tag{4}$$

Where $\psi = c_u/p'_O$ and p'_O is the effective overburden pressure at the point in question. If a point at $y = 5.5$ m is used as representative point of the entire soil layer before the 10 m of excavation, the effective overburden pressure becomes $p'_O = (11 - 5.5) \cdot (\gamma_{sat} - \gamma_w) + 10 \cdot \gamma_{unsat} = 212$ kPa. This leads to $\psi = 1.1$ implying $\alpha = R_{inter} = 0.492$.

A parametric analysis shows that the maximum heave of the excavation level is polynomially decreasing with increasing R_{inter} as seen in Fig. 7. The maximum heave is found at distances 150–200 mm from the pile shaft. The maximum heave is found to be approaching the heave of the soil excluding the pile. This indicates that the horizontal extent of the model is adequately.

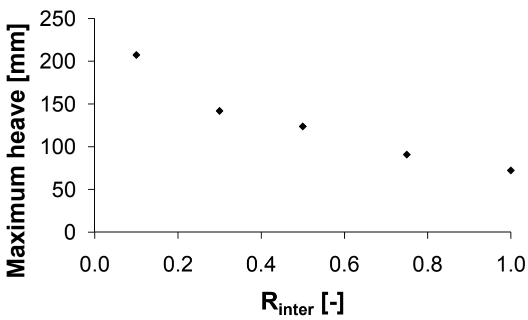

Figure 7: Maximum heave of the excavation level as a function of the strength reduction factor R_{inter}.

The analysed numerical models are listed in Tab. 4.

Table 4: Analysed models.

Model no.	Incl. pile	Pile load	Strength parameters
1	No	No	Undrained
2	No	No	Drained
3	Yes	No	Drained

Only the models excluding the pile make use of both the drained and the undrained strength parameters. The application of solely the drained strength parameters for the remaining model is the result of numerical problems experienced by the authors when applying undrained strength parameters.

4 Validation of the Geometrical Model of Soil

To validate the geometrical model of a swelling soil by use of PLAXIS, an axisymmetric model solely consisting of soil is constructed. In addition, the influence of the applied material model is also analysed by plotting the results when applying both the Mohr-Coulomb material model and the Hardening Soil. When applying the MC material model, the reference value of Young's modulus of elasticity is chosen equal to E_{oed}.

Additionally, both drained and undrained strength parameters are applied for both material models. This is chosen because both the drained and undrained parameters give rise to problems when implemented in undrained material models. When applying undrained strength parameters, the parameters are interpreted as drained strength parameters because undrained behaviour is analysed by the effective stresses in PLAXIS. When using the effective strength parameters combined with the undrained soil behaviour, the mean effective stress p' for a Mohr-Coulomb material is constant up to failure. In nature, the development of p' is somewhat different, cf. Fig. 8. Hence, both drained and undrained strength parameters are investigated for modelling undrained behaviour.

The outer dimensions and material properties are similar to the model described in Sec. 3 with the only exception

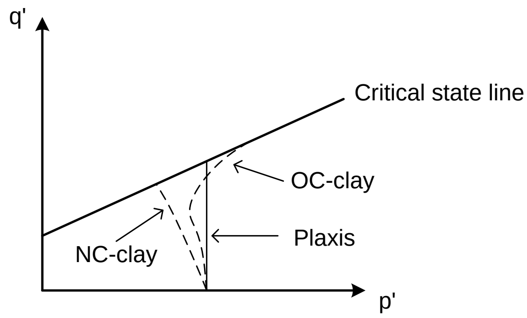

Figure 8: Effective stress paths for normally consolidated clay (NC-clay), overconsolidated clay (OC-clay) and for an undrained Mohr-Coulomb material with drained strength parameters defined in PLAXIS (Plaxis).

that the pile is not included. The model can be seen in Fig. 9.

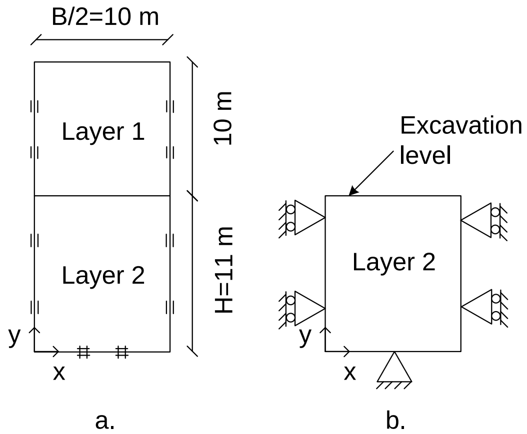

Figure 9: Model applied for numerical analysis of swelling soil in PLAXIS where the left vertical boundary is the axis of symmetry. a. Before excavation. b. After excavation.

The water level is located at the top of soil layer 2, i.e. at the excavation level. The mesh is constructed by 40 15-node elements with the global coarseness chosen as "Very Coarse" based on an analysis of convergence of the vertical displacement of the excavation level.

The boundary conditions of the soil mass are horizontal restraining $u_x = 0$ of the two vertical boundaries and horizontal and vertical restraining $u_x = u_y =$

0 of the lower boundary of the model, cf. Fig. 9. The vertical restraining of the lower boundary is chosen to ensure a reference line with zero vertical displacement. Hereby, the remaining vertical displacements of the soil body originate from displacements inside the model without influence of the subjacent soil layers. The horizontal restraining of both the lower boundary and the vertical boundaries are applied to ensure one-dimensional behaviour inside the soil body. This assumption agrees with the behaviour in nature where the surrounding soil of large horizontal extent functions as horizontal fixities.

The calculations consist of a plastic analysis of a staged construction simulating the excavation followed by a consolidation phase to model the swelling. During the calculations, the vertical boundaries and the horizontal lower boundary are modelled as *closed consolidation boundaries* to ensure no ground water flow through the boundaries.

4.1 Results of the Validation Analyses

A comparison between the effective stresses σ' immediately after the excavation determined by the submerged unit weight γ' and the depth and by PLAXIS revealed a satisfactory agreement between the two methods as seen in Fig. 10. The distributions of effective stresses through the soil are observed to be almost identical for both material models and for both drained and undrained strength parameters and are, thus, plotted combined as the "FEM" points in the figure. The maximum deviation is converged at a value of 2 %. The effective stress variation corresponds to the hatched red area in Fig. 1a. Skempton's

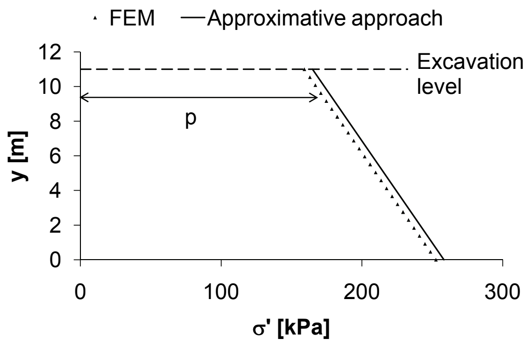

Figure 10: Effective stresses calculated by PLAXIS and the approximative approach of γ' and the depth through the axis of symmetry. $y = 0$ is the lower horizontal boundary of the model. $p = \gamma_{unsat} \cdot 10$ m is the unloading pressure.

coefficients of pore pressure are $A = 1/3$ and $B = 1$ for the determination of pore pressure u by the unit weight of water γ_w, the depth and the negative excess pore pressure Δu. The distribution of the pore pressures immediately after the excavation through the soil calculated by PLAXIS are plotted in Fig. 11.

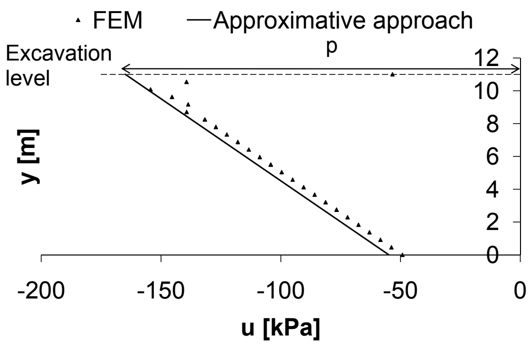

Figure 11: Pore pressures calculated by PLAXIS and the approximative approach of γ_w, Δu and the depth through the axis of symmetry. $y = 0$ is the lower horizontal boundary of the model. $p = \gamma_{unsat} \cdot 10$ m is the unloading pressure.

The distributions are observed to be almost identical for both material models and for both drained and undrained strength parameters. As seen in Fig. 11, there is a decrease in the absolute value of u near the excavation level which is not included in the approximative approach. Besides the values near the excavation level, the maximum deviation is found to be 10 %.

In PLAXIS, water is slightly compressible leading to a decrease in Δu in compare to a non-compressible fluid. Being determined by Eqs. 5 and 6, this leads to a decrease in Skempton's coefficients of pore pressure and, hence, a deviation from the coefficients applied to the conventional theory (Krebs Ovesen et al., 2007; Brinkgreve et al., 2008b). This deviation may be the reason for the slightly higher deviation between the method of determining u than for the method of determining σ'. This is, however, assumed negligible. Thus, the pressure distribution through the soil is modelled satisfactorily.

$$A = \frac{\Delta u - \Delta\sigma_3}{\Delta\sigma_1 - \Delta\sigma_3} \qquad (5)$$

$$B = \frac{\Delta u}{\Delta\sigma_3} \qquad (6)$$

The heave of the excavation level determined by PLAXIS is compared to heave of preconsolidated clay defined in Eq. 7 as a frame of reference. Because $\Delta\sigma'$ is negative for the unloading situation, δ becomes positive.

$$\delta = -\frac{\Delta\sigma'}{E_{oed}} \cdot H \qquad (7)$$

H is the thickness of the soil layer after excavation. The heave determined by Eq. 7 and by PLAXIS are plotted in Fig. 12.

As seen in Fig. 12, the choice of drained or undrained strength parameters does not influence the heave significantly. The material model, on the other hand, has great influence on the results. When applying the Mohr-Coulomb material models, the heave is close to the

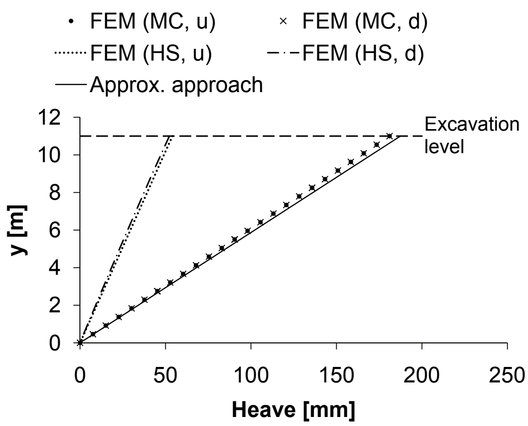

Figure 12: Heave calculated by PLAXIS (FEM) and the approximative approach of Eq. 7 through the axis of symmetry. $y = 0$ is the lower horizontal boundary of the model. u is for undrained and d for drained strength parameters.

approximative approach of Eq. 7. The deviation between the approximative approach and PLAXIS increases when applying the Hardening Soil material models. This could, however, be caused by the choice of Young's moduli of elasticity. Even though identical constrained moduli are applied for the two material models, the remaining moduli are chosen based on the relations $E_{50} = E_{oed}$ and $E_{ur} = 3 \cdot E_{oed}$ which influences the heave determined by the Hardening Soil material models. The heave determined by the Hardening Soil models are approximately 3.4 times smaller than by the Mohr-Coulomb models which indicates that the influencing parameter is the factor between E_{ur} and E_{oed}. This is substantiated by an analysis of the heave applying $E_{oed} = E_{ur} = 2 \cdot E_{50}$ where the heave of the HS-model is approximately 1.1 times smaller than of the MC-model.

The approximative approach of determining the heave by Eq. 7 leads to the largest results and is, thus, the most conservative of the applied methods based on the chosen Young's moduli of elasticity. This makes good sense because the approximative approach does not account for the increasing stiffness in unloading/reloading situations. Whether the Mohr-Coulomb or the Hardening Soil material model is closest to reality can only be evaluated by comparison with real observations of soil behaviour. This is, however, not covered by current analyses.

The maximum deviations between the results of PLAXIS and the approximative approaches are listed in Tab. 5. In addition to σ', u and the heave δ, the deviations of the negative excess pore pressures Δu calculated by PLAXIS compared to the theoretically determined values are also listed.

Table 5: Maximum deviation when applying the Hardening Soil and Mohr-Coulomb material models with undrained and drained strength parameters compared to the approximative approaches described above. δ is the heave.

Material model	σ'	Δu	u	δ
MC, undrained	2 %	3 %	10 %	6 %
MC, drained	2 %	3 %	10 %	6 %
HS, undrained	2 %	3 %	9 %	74 %
HS, drained	2 %	3 %	10 %	72 %

Overall, heave caused by an unloading to illustrate swelling is concluded to be modelled satisfactorily by the geometrical model.

5 Numerical Model of a Single Pile

A single pile is modelled in a cohesive soil exposed to unloading. Both model space, pile dimensions and material properties are based on the case study described in Sec. 3. The model can be seen in Fig. 13.

To illustrate the interaction between the soil and the pile, interfaces are applied

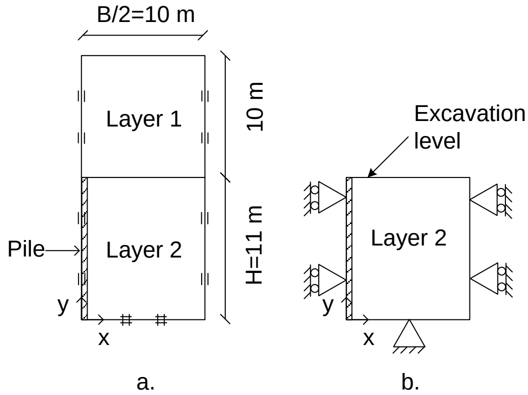

Figure 13: Model applied for numerical analyses of a single pile in swelling soil in PLAXIS where the left vertical boundary is the axis of symmetry. a. Before excavation. b. After excavation.

along the pile shaft. The interfaces are extended as seen in Fig. 14. This is implemented to avoid non-physical oscillations of stresses by enhancing the flexibility of the mesh and the number of nodes at the corners (Brinkgreve et al., 2008b).

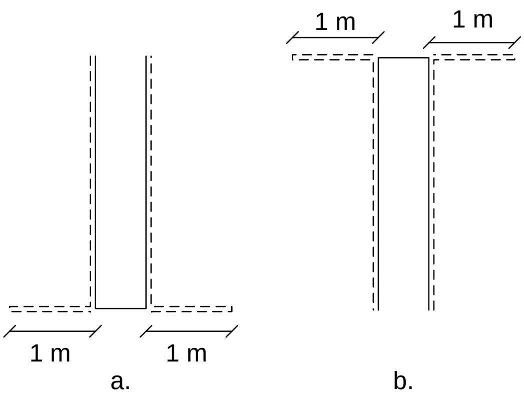

Figure 14: The applied interface between pile and soil. a. At $y = 0$. b. At $y = 11$ m.

The properties of the interface are connected to the surrounding soil materials by the strength reduction factor R_{inter} as described in Sec. 3. R_{inter} is determined by the cohesion of the soil materials and the desired cohesion of the interface of $c_i = 60$ kPa used for comparison to $R_{inter} = 0.267$.

The clay is modelled as an undrained Hardening Soil material with drained strength parameters. The pile material is modelled as a non-porous linear elastic material. The input parameters are defined in Tab. 2. The stiffness of the concrete is chosen significantly higher than the stiffness of the clay to ensure a visible effect of the soil–pile interaction.

The mesh is constructed by 1345 15-node elements with the global coarseness chosen as "Very Fine" based on an analysis of convergence of the heave of the excavation level.

The calculations consist of a plastic analysis of a staged construction simulating the excavation, a plastic analysis of a staged construction illustrating the installation of the pile and a consolidation phase to illustrate the swelling process. During the calculations, the vertical boundaries and the horizontal lower boundary are modelled as *closed consolidation boundaries*.

5.1 Results of the Numerical Model

The results are determined on the basis of nodal points A through N and cross-sections O-O through R-R defined in Fig. 15. It should be noted that the heave in the cross-sections is determined on the basis of interpolation between heave in nearby nodal points. In addition, stresses in the cross-sections as well as at the points are determined on the basis of extrapolation from nearby stress points. The approximations are assumed adequate. (Brinkgreve et al., 2008b)

The maximum values of the heave and shear stresses at points A through N are listed in Tab. 6. On the basis of the heave of points A and G, the pile is seen to

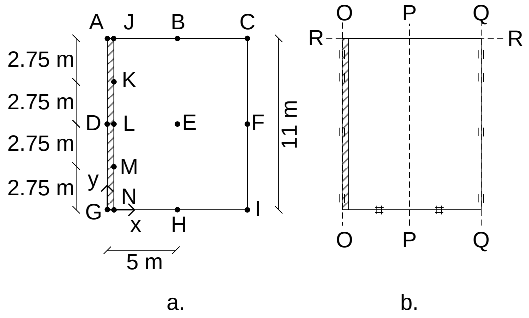

Figure 15: a. Definitions of points A through N. b. Definitions of cross-sections O-O through R-R.

be elongated 0.5 mm corresponding to 0.04 mm/m which seems realistic.

The heave through the cross-section O-O, i.e. through the pile, and through the cross-sections P-P and Q-Q, i.e. through the soil and at the right vertical boundary, can be seen in Fig. 16.

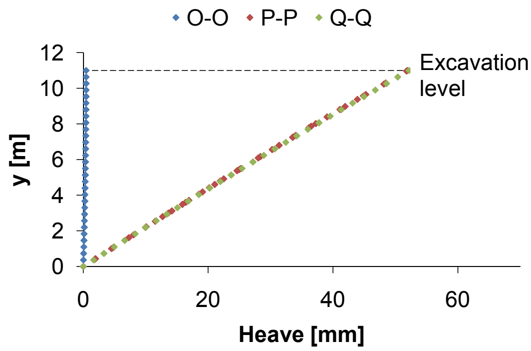

Figure 16: Vertical displacements through the cross-sections O-O through Q-Q. $y = 0$ m is the lower horizontal boundary of the model and $y = 11$ m is the level of the pile head, i.e. the excavation level.

As seen in the figure, the development of the heave is approximately identical for the cross-sections P-P and Q-Q indicating that the horizontal extent of the model is adequate. It also shows that neither the pile nor the mesh has any significant influence at these positions. This is substantiated by plotting the heave of the excavation level as seen in Fig. 17. From around $x = 1$ m, the heave is approximately constant. The deviation of the heave of the

Table 6: Maximum heave δ and shear stresses τ_i. Values separated by an oblique refer to displacements of pile and soil, respectively.

Point	A	B	C	D	E	F	G	H	I	J	K	L	M	N
x [m]	0	5	10	0	5	10	0	5	10	0.17	0.17	0.17	0.17	0.17
y [m]	11	11	11	5.5	5.5	5.5	0	0	0	11	8.25	5.5	2.75	0
δ [mm]	0.5	52	52	0.3	25	25	0	0	0	0.5/0.5	0.4/36	0.3/23	0.2/11	0/0.1
τ_i [kPa]	-	-	-	-	-	-	-	-	-	0.1	−20	−22	−24	−0.4

excavation level at 1 m$< x \leq$ 10 m from the heave of the excavation level for the model excluding the pile is less than 1 %. This implies a radius of influence of the pile of about 1 m corresponding to approximately 3 pile diameters.

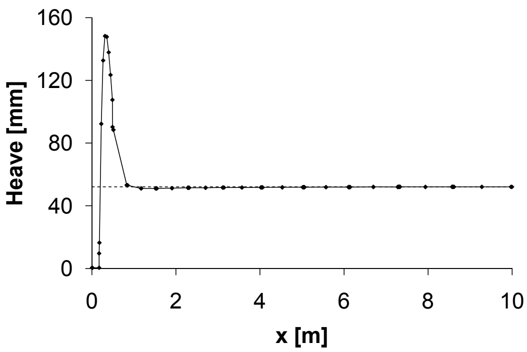

Figure 17: Heave through the cross-section Q-Q, i.e. at the excavation level. $x = 0$ m is the axis of symmetry and $x = 10$ m is the right vertical boundary of the model. The dashed line indicates the heave of the excavation level at the right vertical boundary.

As seen in Fig. 17, the soil close to the pile heaves significantly more than far from the pile. This is caused by the choice of the strength reduction factor R_{inter} = 0.267 which defines the strength of the interface as reduced strength parameters of the soil. This is substantiated by Fig. 18 where the heave of the excavation level is plotted as a function of R_{inter}. It can be seen in the figure that when R_{inter} approaches 1, i.e. the strength of the interface is equal to the strength of the soil, the heave close to the pile approaches the heave of the soil far from the pile.

Evidently, not only the soil at the in-

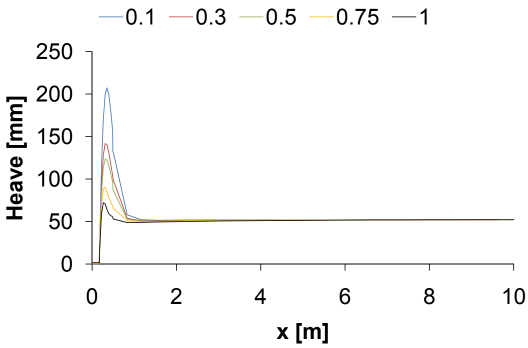

Figure 18: Heave of the excavation level as a function of R_{inter}.

terface but also the soil up to $3D$ from the centre line of the pile is affected by this "weakening". Thus, installation of unloaded piles with diameter D in swelling clays creates weak zones in a radius of $3D$ from the centre of the pile.

Since heave is a result of changes in stresses, the effective stresses close to the soil–pile interface ($x = 0.18$ m), inside the weak soil (x = 0.42 m) and in the unaffected soil (x = 2.0 m) are plotted, cf. Figs. 19–21.

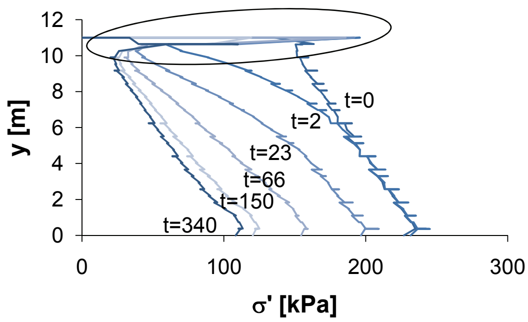

Figure 19: Effective stresses σ' through a vertical cross section at $x = 0.18$ m at different times. t is in years.

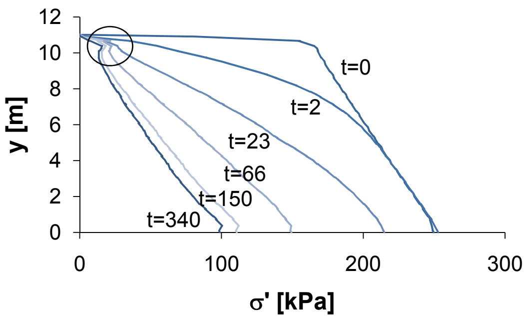

Figure 20: Effective stresses σ' through a vertical cross section at $x = 0.42$ m at different times. t is in years.

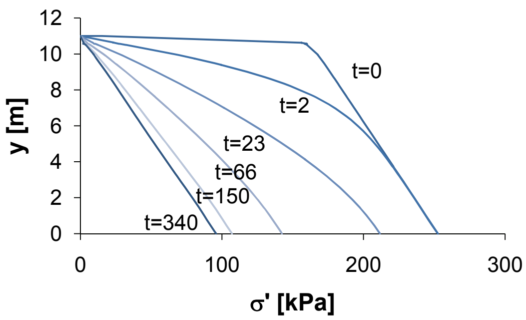

Figure 21: Effective stresses σ' through a vertical cross section at $x = 2.0$ m at different times. t is in years.

As seen in Fig. 19, significant increases in σ' are observed at $y = 10 - 11$ m. A slight increase in σ' can also be seen in Fig. 20 but clearly not as large as close to the soil–pile interface. As seen in Fig. 21, the effect of the pile cannot be observed in the development of σ' with time and depth. This indicates a connection between the local heave and the effective stresses at the upper 1 m of the soil in a radius of approximately $3D$ from the pile centre.

In Fig. 22, the heave at the points J through N at the soil–pile interface are plotted. When applying 15-node soil elements, the interface elements are defined by five pairs of nodes (Brinkgreve et al., 2008b). Hereby, the heave at the interface is determined both for the node connected to the pile and for the node connected to the soil leading to the two curves in Fig. 22. Since the interface elements have zero thickness, the coordinates of each node pair are identical.

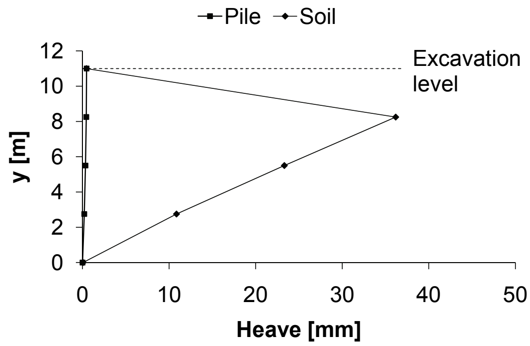

Figure 22: Heave at the points J through N at the interface.

As seen in the plot, the heave of the soil nodes at the interface are approximately equal to the heave of the pile nodes of the interface at the lower boundary of the model and at the pile head. At the remaining depths, the soil is exposed to up to 80 times the heave of the pile which implies shear stresses at the interface.

In Fig. 23, the shear stresses at the interface τ_i between the pile shaft and the soil are plotted. As seen in the figure, the interface is partly plastic indicated by the red dots. The Coulomb failure criterion for the interface is given in Eq. 8 for $\tan\varphi_i' = R_{inter} \cdot \tan\varphi' = \tan(4.4°)$ and $c_i' = R_{inter} \cdot c' = 10.7$ kPa.

$$\begin{aligned} \tau_{max} &= \sigma_N' \cdot \tan\varphi_i' + c_i' \\ \tau_{max} &= \sigma_N' \cdot \tan(4.4°) + 10.7\ kPa \end{aligned} \qquad (8)$$

σ_N' is the effective normal stress at the failure line at the interface. As seen in Fig. 23, the shear stresses are negative along the entire soil–pile interface. Since shear stresses are defined positive in the upward direction, cf. Brinkgreve et al. (2008b), the distribution indicates larger heave for the soil than for the pile. This was also observed by the heave shown in Fig. 22.

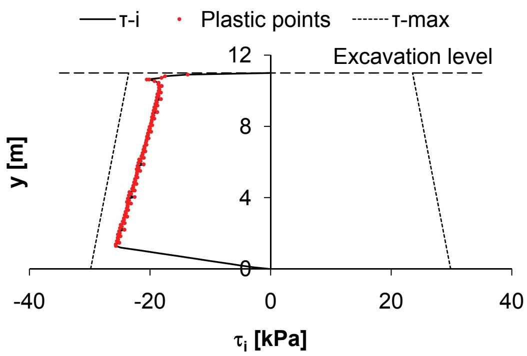

Figure 23: Shear stresses at the interface between pile shaft and soil. τ_{max} is the Coulomb failure criterion.

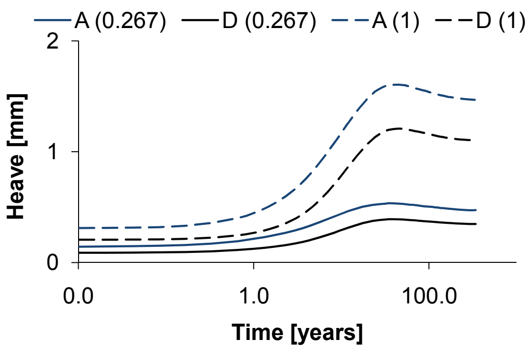

Figure 25: Heave at the points A and D as functions of time with $R_{inter} = 0.267$ and $R_{inter} = 1$.

In Fig. 24, the heave at the points A and D are plotted as functions of time. As seen in Fig. 24, the heave at point A is larger than at point D. This is expected because point A is situated further from the line of zero displacement at $y = 0$ than point D and is, thus, exposed to additional upward displacements. Additionally, it can be seen in the figure that the maximum heave is not at the end of the swelling phase, i.e. 340 years, but after about 40 years. From 40–340 years the pile is no longer elongating but shrinking.

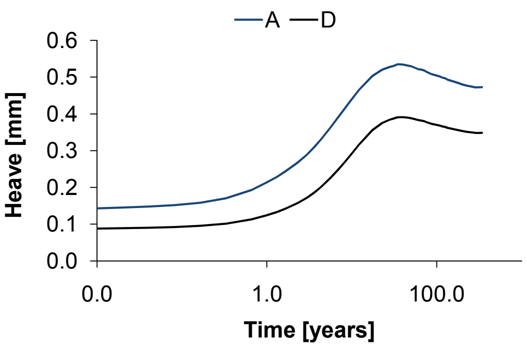

Figure 24: Heave at the points A and D as functions of time.

As seen in Fig. 25, the strength reduction factor R_{inter} does not influence this development of heave over time.

In Fig. 26, the percentage of the pile shaft where the soil–pile interface is plastic is plotted as a function of time. As seen in the figure, the percentage of plastic interface approaches an asymptotic value of 90 % corresponding to a plastic interface at 1.2 m $< y <$ 11 m. After 40 years, i.e. the time at which the heave in the pile starts to decrease, the interface is 74 % plastic corresponding to a plastic interface at 2.8 m $< y <$ 11 m. This indicates that the development of plastic interface implies the shrinkage of the pile because of the slip at the pile surface.

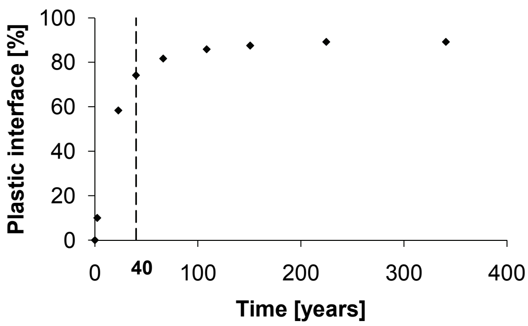

Figure 26: Percentage of the pile shaft which is plastic.

In Fig. 27, the heave at the points B, C, E and F are plotted as functions of time. It can be seen that the progress of the heave is identical for points in similar depths. Additionally, the heave at points B and C are larger than at points E and F as expected. The soil is fully swelled after 340 years.

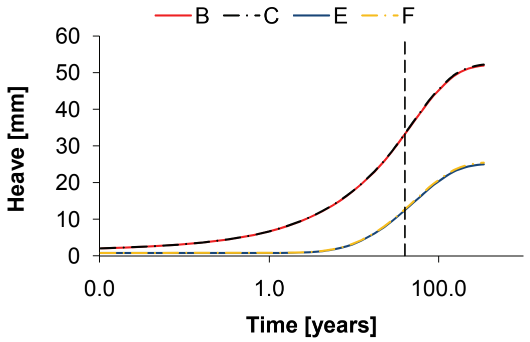

Figure 27: Heave at the points B, D, E and F as a function of time. The dashed line indicates 40 years, i.e. the time at which the heave in the pile starts to decrease.

The internal vertical stresses in the pile are determined in stress points through the pile from $y = 0$ to $y = 11$ m. The maximum value is found to $\sigma_{yy} = 2600$ kPa at the lowermost stress point after 50 years. It should be noted, though, that the maximum sum of internal vertical stresses through the pile is found to appear after approximately 35 years. This indicates a connection with the time at which the heave in the pile starts to decrease, cf. Fig. 24. The internal stresses through the pile after 50 years can be seen in Fig. 28.

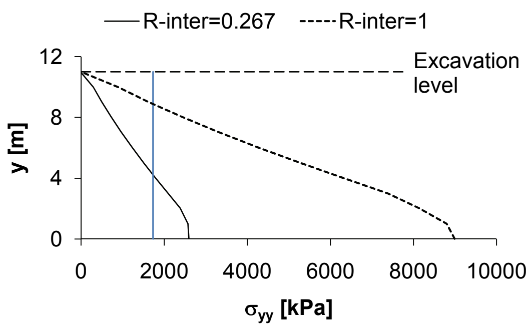

Figure 28: Internal vertical stresses through the pile after 50 years. The vertical blue line indicates the tensile strength of concrete with compressive strength of 30 MPa.

If, for example, the pile material is concrete with the compressive strength of $f_{ck} = 30$ MPa, the tensile strength can be approximated as $f_{ctk} = 1.7$ MPa by Eq. 9 (Jensen, 2007). Hence, tensile reinforcement is necessary to avoid failure of the pile.

$$f_{ctk} = \sqrt{0.1 \cdot f_{ck}} \tag{9}$$

In Fig. 28, the internal vertical stresses are also plotted for $R_{inter} = 1$. As seen in the figure, the stresses increase with increasing R_{inter} as expected.

6 Conclusions

For the investigated case study, the presence of the pile is observed to influence the heave in a radius of approximately 1 m, corresponding to 3 pile diameters D, from the axis of symmetry of the pile. The heave outside this radius is almost completely undisturbed by the pile with deviations from a model solely consisting of a swelling soil smaller than 1 %.

The heave inside the radius of influence is dependent on the strength reduction factor R_{inter}. The parametric analysis shows that the maximum heave of the excavation level is polynomially decreasing with increasing R_{inter}. However, for all investigated values of R_{inter}, the heave inside the radius of influence has shown to be larger than outside this radius. This indicates a weakening of the soil not only directly at the interface but up to $3D$ from the centre of the pile which should be further investigated. To minimise this effect, it is recommended to use piles with as rough surfaces as possible.

The choice of material model is seen to affect the heave significantly. Especially, the relation between the unloading–reloading modulus E_{ur} and the constrained modulus E_{oed} has great influence on the results and should be chosen carefully.

The swelling of the surrounding soil has shown to imply upward shear stresses at the soil–pile interface. This leads to tensile vertical stresses in the pile which in the current case exceed the tensile strength of concrete. Hence, it is necessary to take tensile reinforcement into account in design situations. The strength reduction factor R_{inter} influences significantly both the shear stresses at the interface and, hence, the internal vertical stresses in the pile. This factor should consequently be chosen with care.

During the swelling process modelled as a consolidation phase in PLAXIS, the pile has shown to be elongated to a maximum value after 35-40 years followed by some shrinkage up to the end of the swelling period of 340 years. It appears that the development of plastic interface implies the shrinkage of the pile because of the slip at the pile surface. This affects the internal stresses in the pile where the maximum values are observed after 35-50 years. Hence, when designing unloaded piles with a life expectancy of 100 years, the tensile stresses in the pile can be evaluated after the first 33–50 % of the design period.

Bibliography

Abbas, J. M., Z. H. Chika, and M. R. Taha (2008). Single pile simulation and analysis subjected to lateral load. *Electronic Journal of Geotechnical Engineering 13*(E), 1–15.

API (2000). *Recommended Practice for Planning, Designing and Constructing Fixed Offshore Platforms - Working Stress Design*. American Petroleum Institute.

Brinkgreve, R. B. J., W. Broere, and D. Waterman (2008a). *PLAXIS 2D Material Models Manual - Version 9.0*. PLAXIS bv.

Brinkgreve, R. B. J., W. Broere, and D. Waterman (2008b). *PLAXIS 2D Reference Manual - Version 9.0*. PLAXIS bv.

Harremoës, P., H. Moust Jacobsen, and N. Krebs Ovesen (1997). *Lærebog i GEOTEKNIK 1* (5th ed.). Århus, Denmark: Polyteknisk Forlag.

Jensen, B. C. (2007). *Betonkonstruktioner efter DS 411* (3rd ed.). Nyt Teknisk Forlag.

Krebs Ovesen, N., L. D. Fuglsang, and G. Bagge (2007). *Lærebog i Geoteknik* (1st ed.). Lyngby, Denmark: Polyteknisk Forlag.

Moust Jacobsen, H. and K. Gwizdala (1992). *Bearing capacity and settlements of piles*. Aalborg, Denmark: Centertrykkeriet, Aalborg University.

Okkels, N. and K. Bødker (2008). Beregning af hævninger under antagelse af retlinjet dræning. In *Nordisk Geoteknikermøde no. 15*, Sandefjord, Norway, pp. 383–389.

Poulos, H. G. and E. H. Davis (1980). *Pile foundation analysis and design* (1st ed.). John Wiley and sons.

Thøgersen, L. (2001). *Effects of Experimental Techniques and Osmotic Pressure on the Measured Behaviour of Tertiary Expansive Clay, Volume 1*. Ph. D. thesis, Soil Mechanics Laboratory, Aalborg University.

Recent publications in the DCE Technical Report Series

Kaufmann, K. L., Nielsen, B. N., & Augustesen, A. H. (2010). Strength and Deformation Properties of Tertiary Clay at Moesgaard Museum. *DCE Technical Report, 103*.

ISSN 1901-726X
DCE Technical Report No. 104

Part II

Appendices

APPENDIX A

BORING RECORDS FROM MOESGAARD MUSEUM

This appendix contains boring records from boring B105 and B105 at Moesgaard Museum provided by COWI A/S. In addition, a legend with English designations is enclosed after the last boring record.

Dybde | Forsøgsresultater | Kote (m) | Geo-logi | Prøve

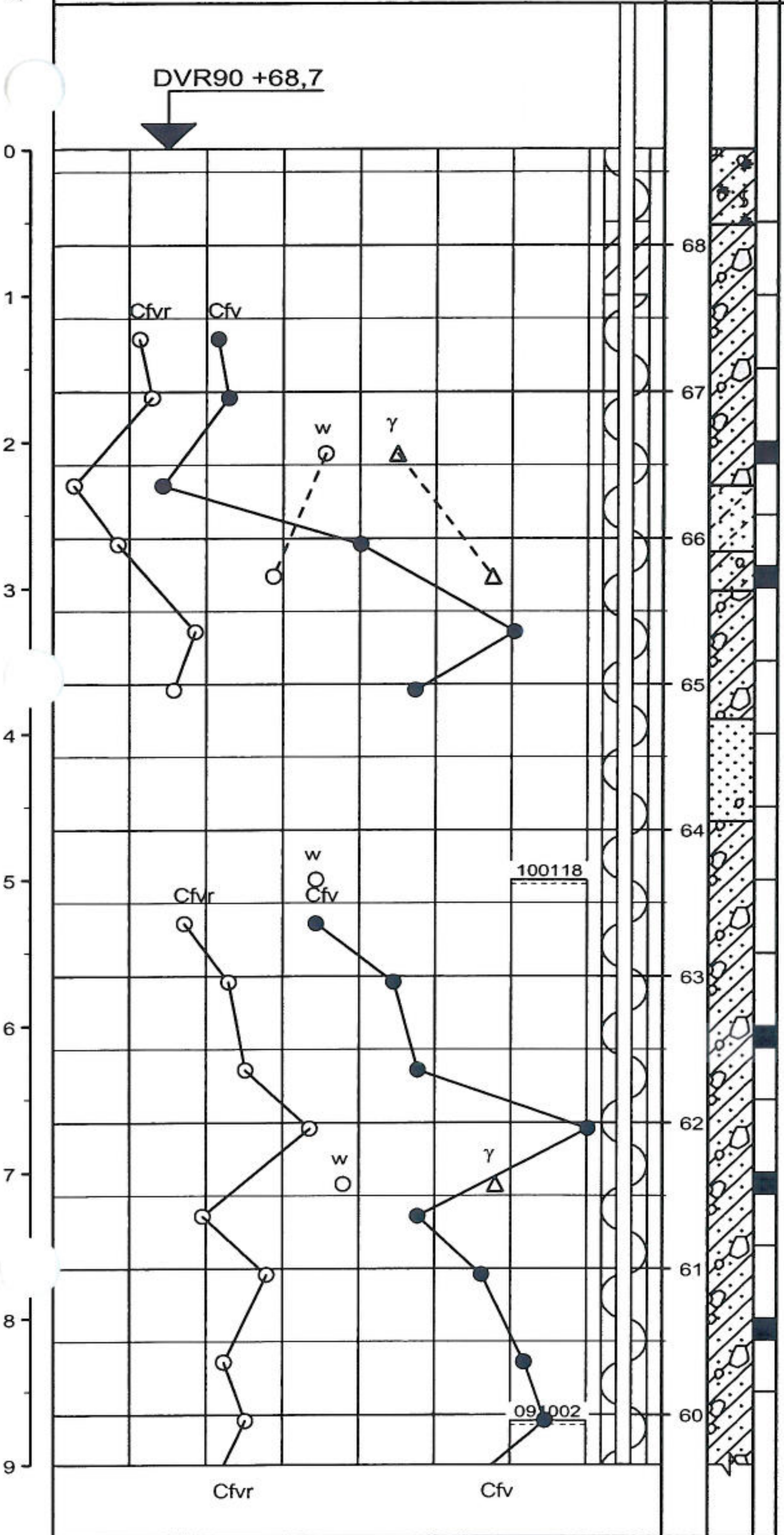

Nr.	Jordart Karakterisering	Aflejring	Alder	Frost	Kalk
1	LER, sandet, sv. humusbl., m. enk. gruskorn og planterødder, mørkt gråbrunt	Fl	Sg		-
2	MORÆNELER, sandet, gråbrunt	Gl	Gc		-
3	MORÆNELER - " -	Gl	Gc		-
4	MORÆNELER, sandet, m. store sandpartier, gråbrunt	Gl	Gc		-
5	SILT, sandet, brungråt	Sm	Gc		(+)
6	LER, siltet, stedvis stærkt sandet, m. enk. gruskorn, brungråt	Sm	Gc		(+)
7	MORÆNELER, svagt sandet, brungråt	Gl	Gc		(+)
8	SAND, fint - mellem, lyst brungråt	Sm	Gc		-
9	SAND, fint - mellem, m. enk. gruskorn, lyst brungråt	Sm	Gc		-
10	MORÆNELER, svagt sandet, m. enk. sandslirer, lyst brungråt	Gl	Gc		+
11	MORÆNELER, sandet, mørkegråt	Gl	Gc		+
12	MORÆNELER - " -	Gl	Gc		+
13	MORÆNELER, svagt sandet, m. enk. grønlige lerpletter, mørkegråt	Gl	Gc		+
14	MORÆNELER - " -	Gl	Gc		+
15	MORÆNELER, svagt sandet, m. enk. brunsorte lerslirer, gråt	Gl	Gc		+
16	MORÆNELER - " -	Gl	Gc		+
17	MORÆNELER, svagt sandet, m. enk. brunkulsstk., mørkegråt	Gl	Gc		+

Fortsættes

○	10	20	30	w (%)
△	14	18	22	γ (kN/m³)
●	100	200	300	Cfv,Cfvr (kN/m²)

P. 5-6: Lagdelt. P. 13-22: Tertiært præget. P. 24: Glacialt oppr. tertiær flage, Miocæn. P. 27, 49, 52, 53 og 57-59: Glacialt præget. P. 25-61: Glacialt forstyrret tertiær flage af Viborg Ler. N.Oligocæn og Eocæn Røsnæs Ler.

Boremetode : Tørboring med foring

Koordinat system : U32EUREF89

X : 576138 (m) Y : 6216692 (m) Plan :

Sag : 71433-G-1 Moesgård Museum, Moesgård Allè 20, Højbjerg

Geolog : LCX | Boret af : SNC | Dato : 20090925 | DGU-nr.: | Boring : B105

Udarb. af : ELPE | Kontrol : ALSC | Godkendt : ALSC | Dato : 22 feb 2010 | Bilag : 1.06 | S. 1 / 4

COWI

Boreprofil

Dybde	Forsøgsresultater	Kote (m)	Geo-logi	Prøve	Nr.	Jordart Karakterisering	Aflejring	Alder	Frost	Kalk

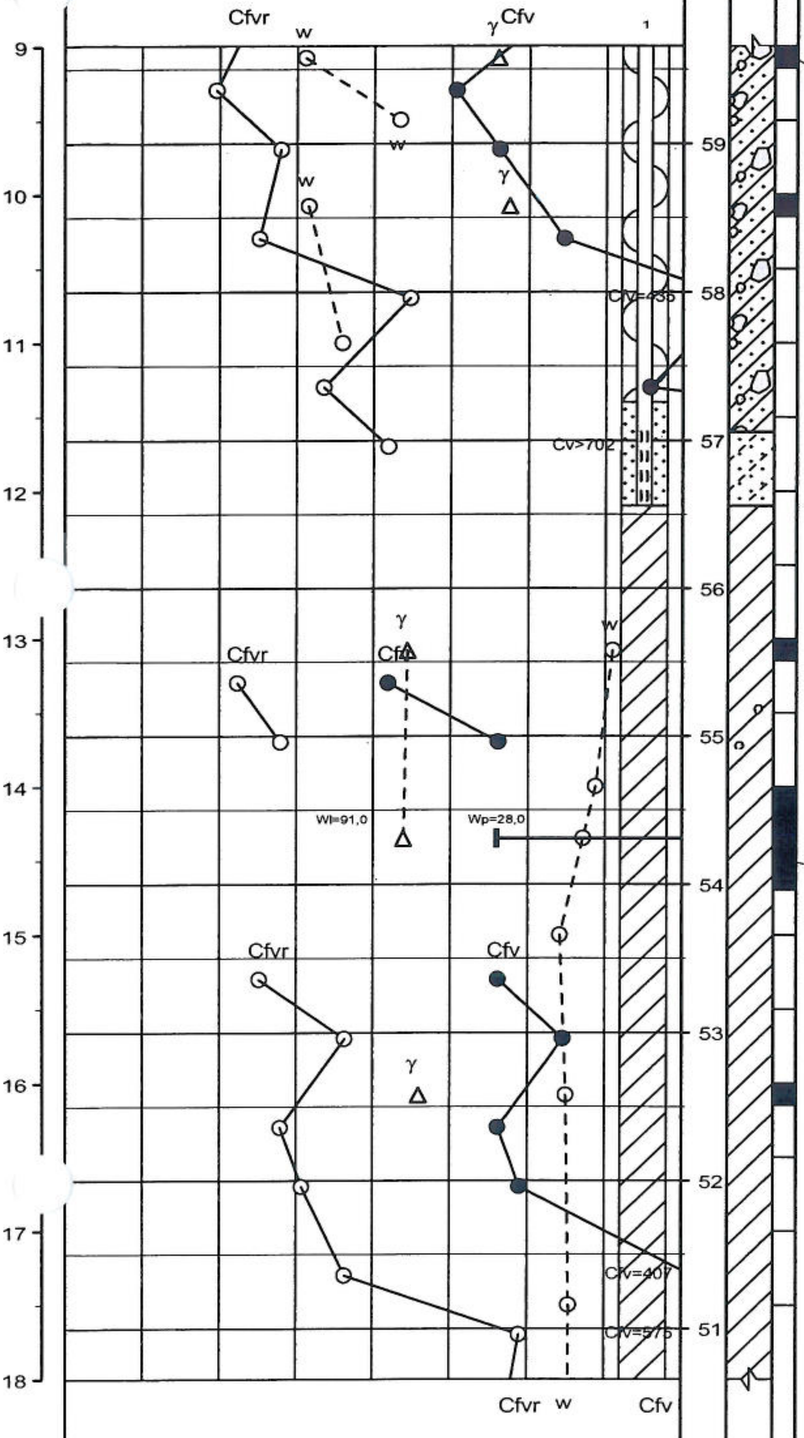

Fortsat

Nr.	Jordart Karakterisering	Aflejring	Alder	Frost	Kalk
18	MORÆNELER, sandet, m. enk. brunsorte lerpletter, mørkegråt	Gl	Gc		+
19	MORÆNELER, ret fedt, m. st. partier af søvind mergel, gråt	Gl	Gc		+
20	MORÆNELER, sandet, m. brunsorte lerslirer, mørkegråt	Gl	Gc		+
21	MORÆNELER, svagt sandet, m. brunsorte lerslirer, mørkegråt	Gl	Gc		+
22	MORÆNELER - " -	Gl	Gc		+
23	MORÆNELER, svagt sandet, mørkegråt	Gl	Gc		+
24	SILT, stærkt sandet, glimmerholdigt, gråsort	Gl	Gc		-
25	LER, meget fedt, grålig olivengrønt	Gl	Gc		(+)
26	LER - " -	Gl	Gc		(+)
27	LER, meget fedt, m. enk. gruskorn, grålig olivengrønt	Gl	Gc		(+)
28	LER, meget fedt, grålig olivengrønt	Gl	Gc		(+)
29 / 29A	LER - " -	Gl	Gc		(+)
30	LER, meget fedt, m. enk. pyritkonkretioner, grålig olivengråt	Gl	Gc		(+)
31	LER, meget fedt, grålig olivengrønt	Gl	Gc		(+)
32	LER - " -	Gl	Gc		(+)
33	LER - " -	Gl	Gc		(+)
34	LER, meget fedt, m. rødbrune lerslirer, grålig olivengrønt	Gl	Gc		(+)
35	LER, meget fedt, grålig olivengrønt	Gl	Gc		(+)

Fortsættes

○	10	20	30	w (%)
△	14	18	22	γ (kN/m³)
●	100	200	300	Cfv,Cfvr (kN/m²)

P. 5-6: Lagdelt. P. 13-22: Tertiært præget. P. 24: Glacialt oppr. tertiær flage, Miocæn. P. 27, 49, 52, 53 og 57-59: Glacialt præget. P. 25-61: Glacialt forstyrret tertiær flage af Viborg Ler. N.Oligocæn og Eocæn Røsnæs Ler.

Boremetode : Tørboring med foring

Koordinat system : U32EUREF89

X : 576138 (m) Y : 6216692 (m) Plan :

Sag : 71433-G-1 Moesgård Museum, Moesgård Allè 20, Højbjerg

Geolog : LCX	Boret af : SNC	Dato : 20090925	DGU-nr.:	Boring : B105	
Udarb. af : ELPE	Kontrol : ALSC	Godkendt : ALSC	Dato : 22 feb 2010	Bilag : 1.06	S. 2 / 4

COWI

Boreprofil

Dybde	Forsøgsresultater	Kote (m)	Geo-logi	Prøve	Nr.	Jordart Karakterisering	Aflejring	Alder	Frost	Kalk

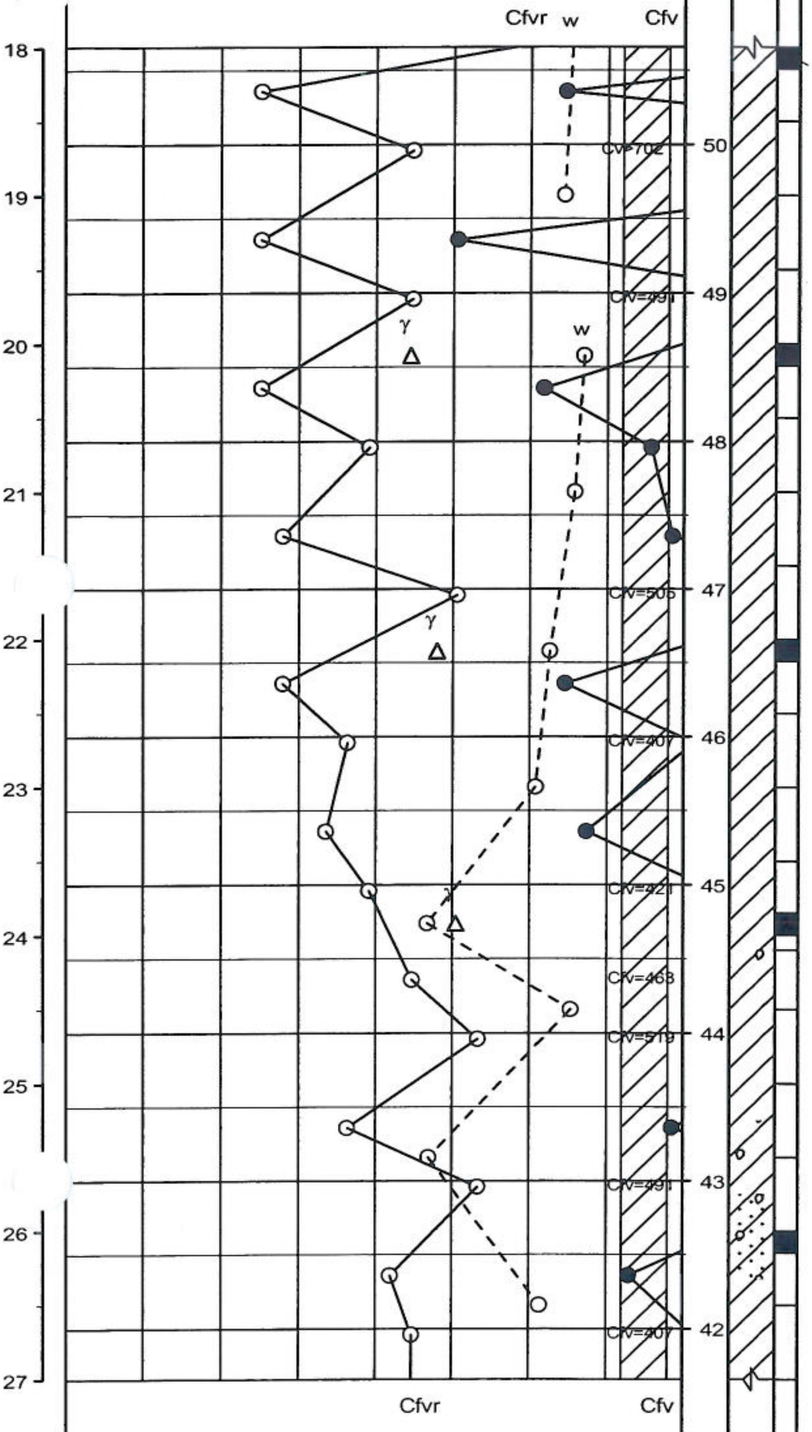

Fortsat

Nr.	Jordart Karakterisering	Aflejring	Alder	Frost	Kalk
36	LER, meget fedt, grålig olivengrønt	Gl	Gc		(+)
37	LER - " -	Gl	Gc		(+)
38	LER - " -	Gl	Gc		(+)
39	LER - " -	Gl	Gc		(+)
40	LER - " -	Gl	Gc		(+)
41	LER, meget fedt, m. enk. pyritkonkretioner, grålig olivengrønt	Gl	Gc		(+)
42	LER, meget fedt, grålig olivengrønt	Gl	Gc		(+)
43	LER - " -	Gl	Gc		(+)
44	LER - " -	Gl	Gc		(+)
45	LER - " -	Gl	Gc		(+)
46	LER - " -	Gl	Gc		(+)
47	LER, meget fedt, m. enk. pyritkonkretioner, grålig olivengrønt	Gl	Gc		(+)
48	LER, fedt, grålig olivengrønt	Gl	Gc		(+)
49	LER, fedt, m. enk. gruskorn, grålig olivengrønt	Gl	Gc		(+)
50	LER, meget fedt, grålig olivengrønt	Gl	Gc		(+)
51	LER, meget fedt, sv. glimmerholdigt, grålig olivengrønt	Gl	Gc		(+)
52	LER, fedt, sv. glimmerholdigt, m. enk. gruskorn, grålig olivengrønt	Gl	Gc		(+)
53	LER, meget fedt, sv. glimmerholdigt, m. enk. sandslirer, m. enk. gruskorn, grålig olivengrønt	Gl	Gc		(+)
54	LER, meget fedt, m. enk. rødbrune lerslirer, grålig olivengrønt	Gl	Gc		(+)
55	LER - " -	Gl	Gc		(+)

Fortsættes

○	10	20	30	w (%)
Δ	14	18	22	γ (kN/m³)
●	100	200	300	Cfv,Cfvr (kN/m²)

P. 5-6: Lagdelt. P. 13-22: Tertiært præget. P. 24: Glacialt oppr. tertiær flage, Miocæn. P. 27, 49, 52, 53 og 57-59: Glacialt præget. P. 25-61: Glacialt forstyrret tertiær flage af Viborg Ler. N.Oligocæn og Eocæn Røsnæs Ler.

Boremetode : Tørboring med foring

Koordinat system : U32EUREF89

X : 576138 (m) Y : 6216692 (m) Plan :

K 2.0 - 20/01/2010 14:46:49

Sag : 71433-G-1 Moesgård Museum, Moesgård Allè 20, Højbjerg

Geolog : LCX	Boret af : SNC	Dato : 20090925	DGU-nr.:
Udarb. af : ELPE	Kontrol : ALSC	Godkendt : ALSC	Dato : 22 feb 2010

Boring : B105

Bilag : 1.06 S. 3 / 4

BRegister - P

COWI

Boreprofil

Dybde	Forsøgsresultater	Kote (m)	Geo-logi	Prøve	Nr.	Jordart Karakterisering	Aflejring	Alder	Frost	Kalk
						Fortsat				

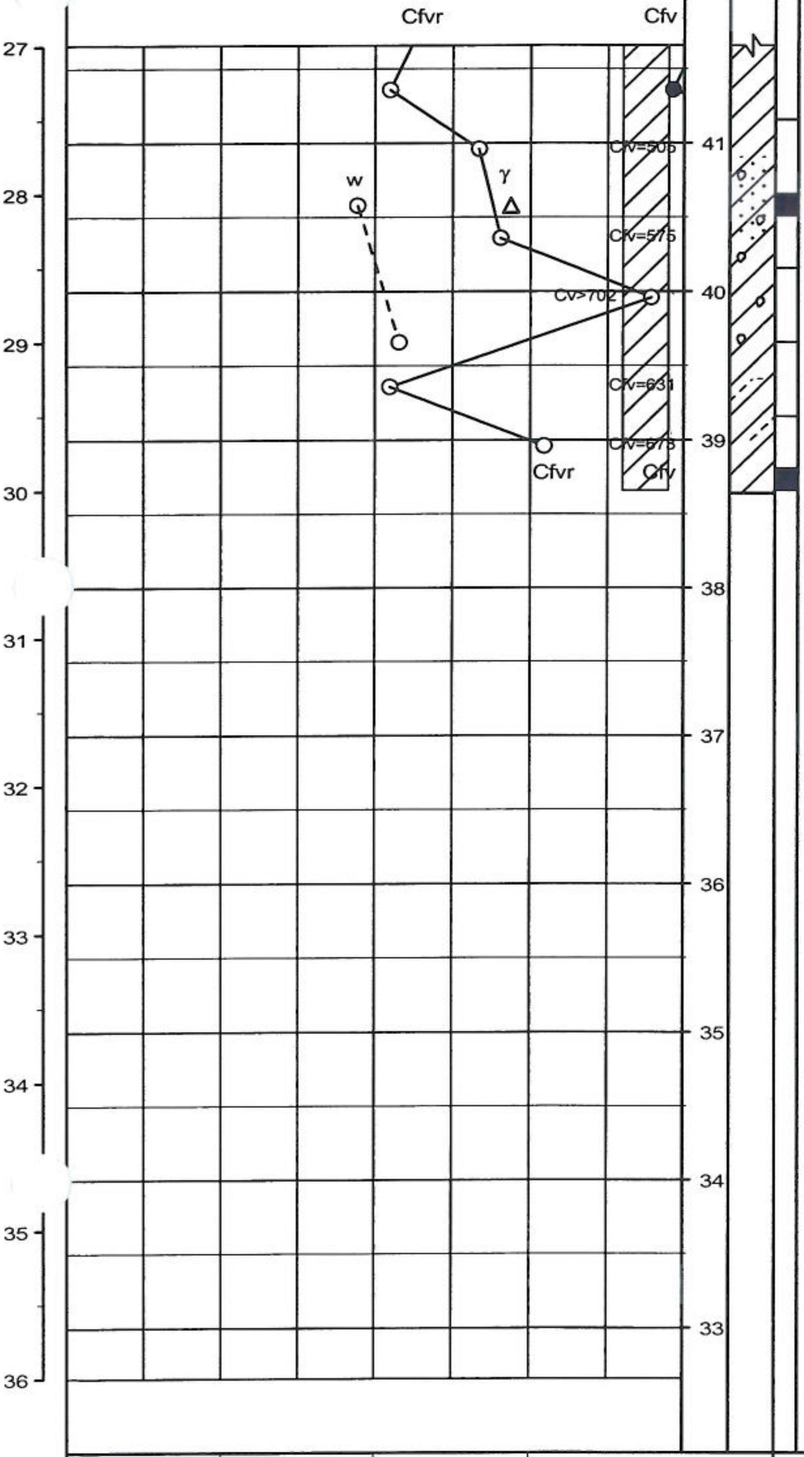

Nr.	Jordart Karakterisering	Aflejring	Alder	Frost	Kalk
56	LER, meget fedt, m. enk. rødbrune lerslirer, grålig olivengrønt	Gl	Gc		(+)
57	LER, meget fedt, m. enk. sandslirer, m. enk. gruskorn, grålig olivengrønt	Gl	Gc		+
58	LER, meget fedt, m. enk. gruskorn, olivensort	Gl	Gc		+
59	LER - " -	Gl	Gc		+
60	LER, meget fedt, m. enk. siltslirer, sv. glimmerholdigt, grålig olivengråt	Gl	Gc		+
61	LER, meget fedt, m. siltslirer, sv. glimmerholdigt, grålig olivengråt	Gl	Gc		+

○	10	20	30	w (%)
△	14	18	22	γ (kN/m³)
●	100	200	300	Cfv,Cfvr (kN/m²)

P. 5-6: Lagdelt. P. 13-22: Tertiært præget. P. 24: Glacialt oppr. tertiær flage, Miocæn. P. 27, 49, 52, 53 og 57-59: Glacialt præget. P. 25-61: Glacialt forstyrret tertiær flage af Viborg Ler. N.Oligocæn og Eocæn Røsnæs Ler.

Boremetode : Tørboring med foring

Koordinat system : U32EUREF89

X : 576138 (m) Y : 6216692 (m) Plan :

Sag : 71433-G-1 Moesgård Museum, Moesgård Allè 20, Højbjerg

Geolog : LCX	Boret af : SNC	Dato :	20090925	DGU-nr.:		Boring : B105
Udarb. af : ELPE	Kontrol : ALSC	Godkendt :	ALSC	Dato :	22 feb 2010	Bilag : 1.06 S. 4 / 4

COWI

Boreprofil

Dybde | Forsøgsresultater | Kote (m) | Geo-logi | Prøve

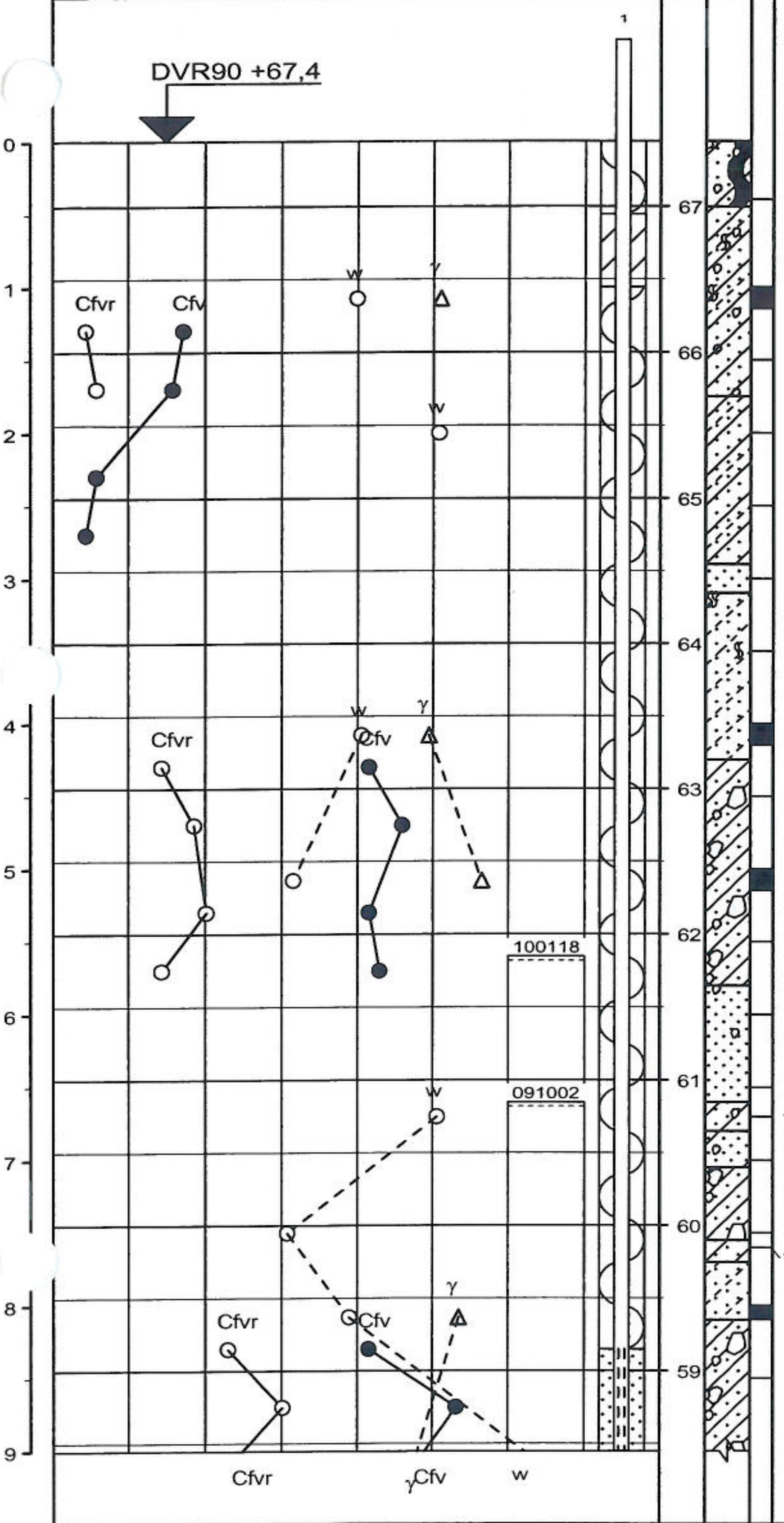

Nr.	Jordart Karakterisering	Aflejring	Alder	Frost	Kalk
1	MULD, leret, sandet, m. enk. gruskorn og planterester, mørkebrunt	Ov	Re		-
2	LER, sandet, svagt siltet, m. enk. gruskorn og små planterødder, brungråt	Fl	Sg		-
3	LER, stedvis stærkt sandet, m. enk. gruskorn, brungråt	Fl	Sg		-
4	LER, siltet, sandet, brungråt	Ne	Sg		-
5	LER - " -	Ne	Sg		-
6	SAND, finkornet, m. enk. planterødder, lyst brungråt	Sm	Sg		-
7	SILT, sandet, m. enk. planterødder, brungråt	Ne	Sg		-
8	SILT, sandet, brungråt	Ne	Sg		(+)
9	MORÆNELER, svagt sandet, brungråt	Gl	Gc		+
10	MORÆNELER, svagt sandet, m. enk. sandslirer, brungråt	Gl	Gc		+
11	MORÆNELER, sandet, brungråt	Gl	Gc		+
12	SAND, fin - mellemkornet, m. enk. gruskorn, brungråt	Sm	Gc		-
13	SAND, finkornet, svagt glimmerholdigt, lyst brungråt	Sm	Gc		-
13A	LER, fedt, m. sandpartier og enk. gruskorn, olivenbrunt	Gl	Gc		+
14	SAND, finkornet, m. enk. lerpletter og gruskorn, lyst brungråt	Sm	Gc		-
15	MORÆNELER, svagt sandet, m. grønliggrå sandpletter, mørkegråt	Gl	Gc		+
15A	LER, m. store sandpartier, glimmerholdigt, mørkebrunt	Gl	Gc		-
16	SILT, sandet, glimmerholdigt, mørkebrunt	Gl	Gc		-
17	MORÆNELER, sandet, m. enk. finsandspletter, mørkegråt	Gl	Gc		+

Fortsættes

Signatur				
○	10	20	30	w (%)
△	14	18	22	γ (kN/m³)
●	100	200	300	Cfv,Cfvr (kN/m²)

P. 2-5, 7 og 8: Sv. lagdelt, P.13,15,17 og 18: Tertiært præget. P.13A, 15A,16: Glacialt oppr., tertiær flage, P.22: Glacialt præget. P.15A,16; Miocæn-aflejring, P.19-28: Glacialt forstyrret tertiær flage af Viborg Ler, N. Oligocæn.

Boremetode : Tørboring med foring

Koordinat system : U32EUREF89

X : 576160 (m) Y : 6216697 (m) Plan :

Sag : 71433-G-1 Moesgård Museum, Moesgård Allè 20, Højbjerg

Geolog : LCX | Boret af : MGS | Dato : 20090829 | DGU-nr.: | Boring : B106

Udarb. af : ELPE | Kontrol : ALSC | Godkendt : ALSC | Dato : 22 feb 2010 | Bilag : 1.07 | S. 1 / 2

COWI

Boreprofil

Dybde	Forsøgsresultater	Kote (m)	Geo-logi	Prøve	Nr.	Jordart Karakterisering	Aflejring	Alder	Frost	Kalk
						Fortsat				

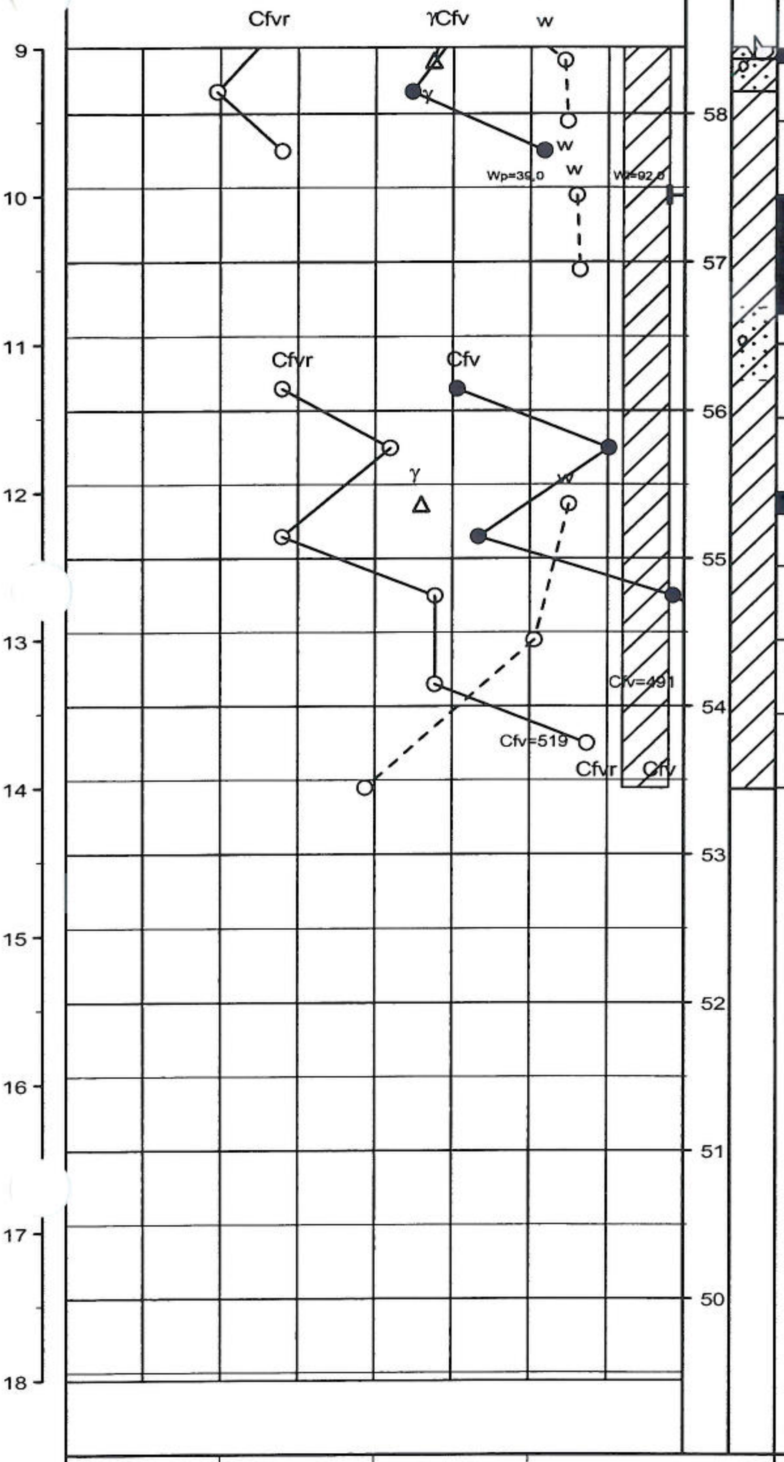

Nr.	Jordart Karakterisering	Aflejring	Alder	Frost	Kalk
18	MORÆNELER, meget fedt, m. enk. finsandspletter, svagt glimmerholdigt, mørkegråt	Gl	Gc		+
19	LER, meget fedt, svagt glimmerholdigt, gråligt olivengrønt	Gl	Gc		+
20	LER - " -	Gl	Gc		+
21, 21A	LER - " -	Gl	Gc		+
22	LER, meget fedt, svagt glimmerholdigt, m. enk. sandslirer og gruskorn, olivengrønt	Gl	Gc		+
23	LER, meget fedt, svagt glimmerholdigt, gråligt olivengrønt	Gl	Gc		+
24	LER, meget fedt, svagt glimmerholdigt, olivengrønt	Gl	Gc		+
25	LER - " -	Gl	Gc		(+)
26	LER - " -	Gl	Gc		+
27	LER, meget fedt, m. lyse siltslirer, svagt glimmerholdigt, brunsort	Gl	Gc		(+)
28	LER - " -	Gl	Gc		-

○	10	20	30	w (%)
Δ	14	18	22	γ (kN/m³)
●	100	200	300	Cfv,Cfvr (kN/m²)

P. 2-5, 7 og 8: Sv. lagdelt, P.13,15,17 og 18: Tertiært præget. P.13A, 15A,16: Glacialt oppr., tertiær flage, P.22: Glacialt præget. P.15A,16: Miocæn-aflejring, P.19-28: Glacialt forstyrret tertiær flage af Viborg Ler, N. Oligocæn.

Boremetode : Tørboring med foring

Koordinat system : U32EUREF89

X : 576160 (m) Y : 6216697 (m) Plan :

Sag : 71433-G-1 Moesgård Museum, Moesgård Allè 20, Højbjerg

Geolog : LCX Boret af : MGS Dato : 20090829 DGU-nr.: **Boring : B106**

Udarb. af : ELPE Kontrol : ALSC Godkendt : ALSC Dato : 22 feb 2010 Bilag : 1.07 S. 2/2

COWI **Boreprofil**

LEGEND FOR BOREHOLE LOGS

Soil Signature

Fill, Cobbles, Limestone

Mull, Gravel, Flint

Peat, Sand, Clay till

Gyttja, Silt, Silt till

Shells, Clay, Sand till

Plant remains, Rock, Gravel till

Till deposits can be expected to contain cobbles and boulders (not apparent in borings).

Location Plan

- LB 10
- Pump Boring
- Environmental Boring
- Simple Boring
- Stratigraphic Boring
- Geotechnical in situ boring and laboratory tests
- Sounding, dynamic penetration test

Borehole log

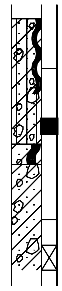

Geological abbreviations

Environment :

Fw	Freshwater deposit
Ss	Solifluction soil
Fi	Fill
Gl	Glacier deposit
Ma	Marine deposit
Wd	Washdown deposit
Ts	Top soil
Ls	Landslide deposit
Mw	Meltwater deposit
Ae	Aeolian (wind) deposit

Age :

Re	Recent
Pg	Postglacial
Lg	Late Glacial
Gc	Glacial
Ig	Interglacial
Te	Tertiary
Ct	Cretaceous
Da	Danian

Stand pipe

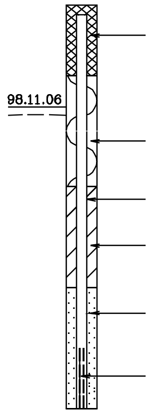

Definitions

Signature	Parameter	Sym.	Unit	Definition
	Water content	w	%	Weight of water in percent of solid matter
	Liquid limit	w_L	%	Water content at yield point
	Plastic limit	w_P	%	Water content at plastic limit
	Plastic index	I_P	%	$w_L - w_P$
	Volume weight	γ	kN/m³	Ratio between total weight and total volume
	Loss by combustion	gl	%	Weight loss of combustion in percent of solid matter
	Reduced loss by combustion	gl_{red}	%	gl − ka
	Lime content	ka	%	Weight of $CaCo^3$ in percent of solid matter
−/(+)/+/++	Lime sample	kp	−	Reaction w. hydrochoric acid: − = no lime; (+) = low content of lime; + = limy; ++ = high content of lime
	Shear strength	c_v	kN/m²	Shear strength measured with a vane test in undisturbed soil
	Shear strength, remoulded	c_{vr}	kN/m²	Shear strength measured with a vane test in disturbed soil
	Drilling resistance Loaded flat drill	R_{SP}	N_{200}	No. of ½-rotations pr. 200 mm penetration
	Sounding resistance Swedish penetration test	R_{RS}	N_{200}	No. of strokes pr. 200 mm penetration
	Sounding resistance Light penetration test	R_{LSD}	N_{200}	No. of strokes pr. 200 mm penetration
	Sounding resistance SPT-probe, closed/open	SPT	N_{300}	No. of strokes pr. 300 mm penetration

Date	Designed	Controlled	Approved	Dokument no.	Page
06.09.2002	VKJ	CTL	TBA	9003G-A4-01	1 of 1

COWI

LEGEND FOR BOREHOLE LOGS

Data sheet A−1

n:\I703\STD-Business Development\Geoteknik\DATABLAD, GEO\A-I\Datablad_AI_eng.dgn

APPENDIX B

STRAIN–TIME CURVES FOR THE FIRST CONSOLIDATION TEST

In this appendix, the strain–time curves for each load step of the first consolidation test are presented.

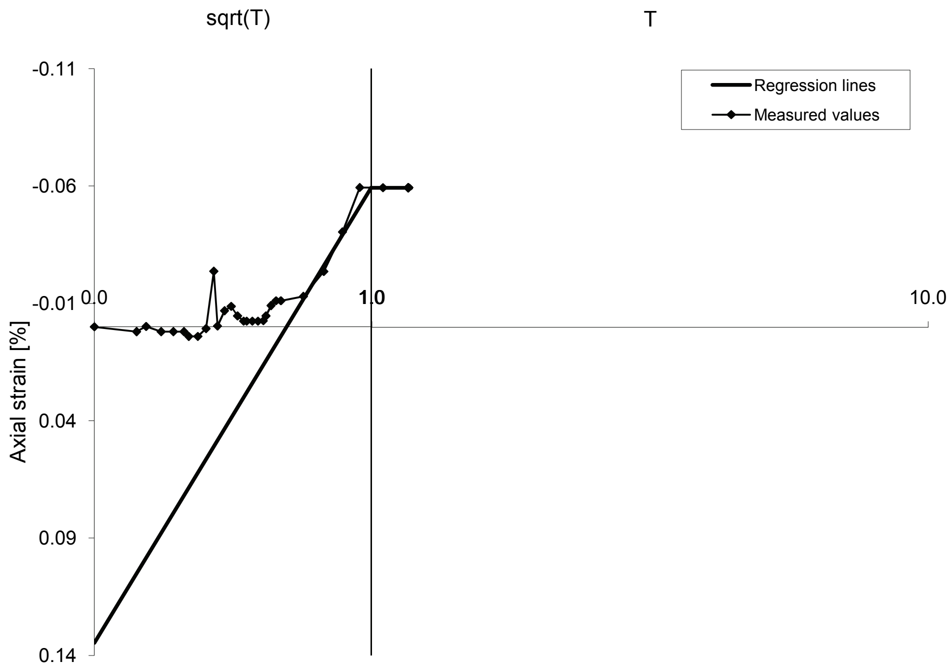

Figure B.1: Load step 1.

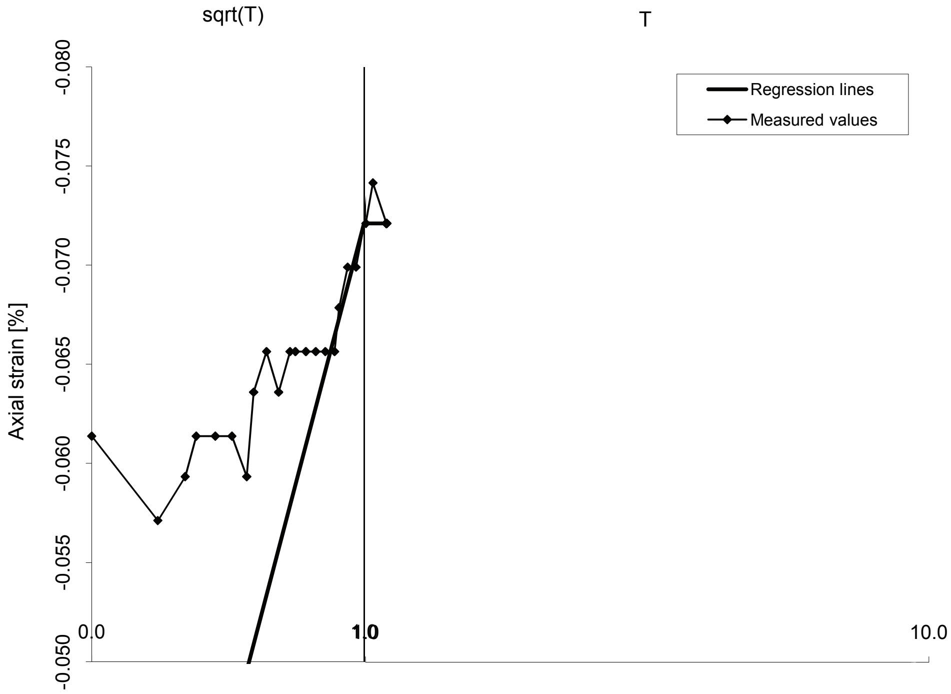

Figure B.2: Load step 2.

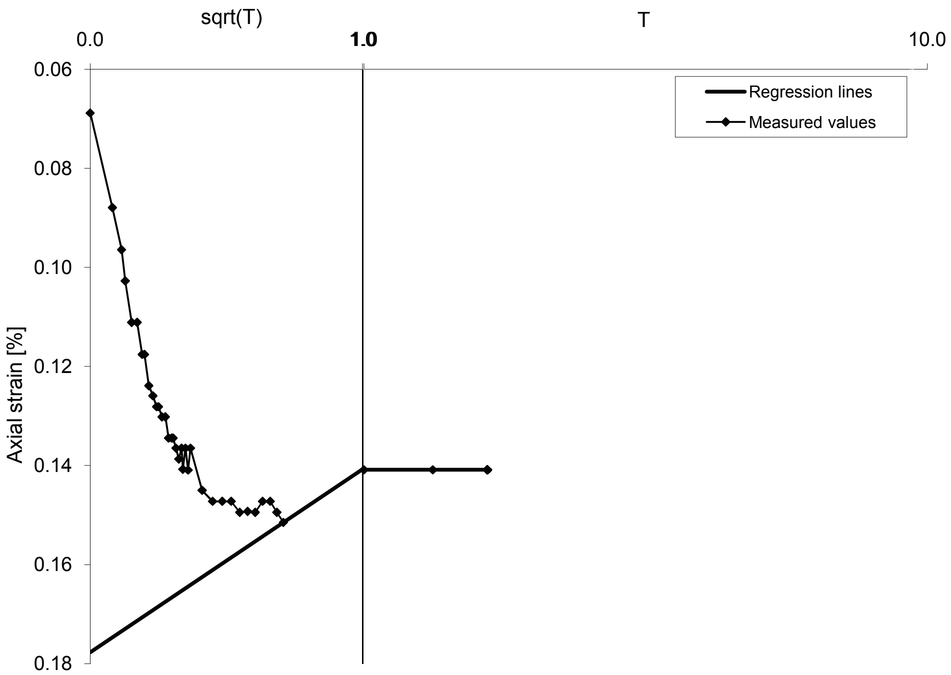

Figure B.3: Load step 3.

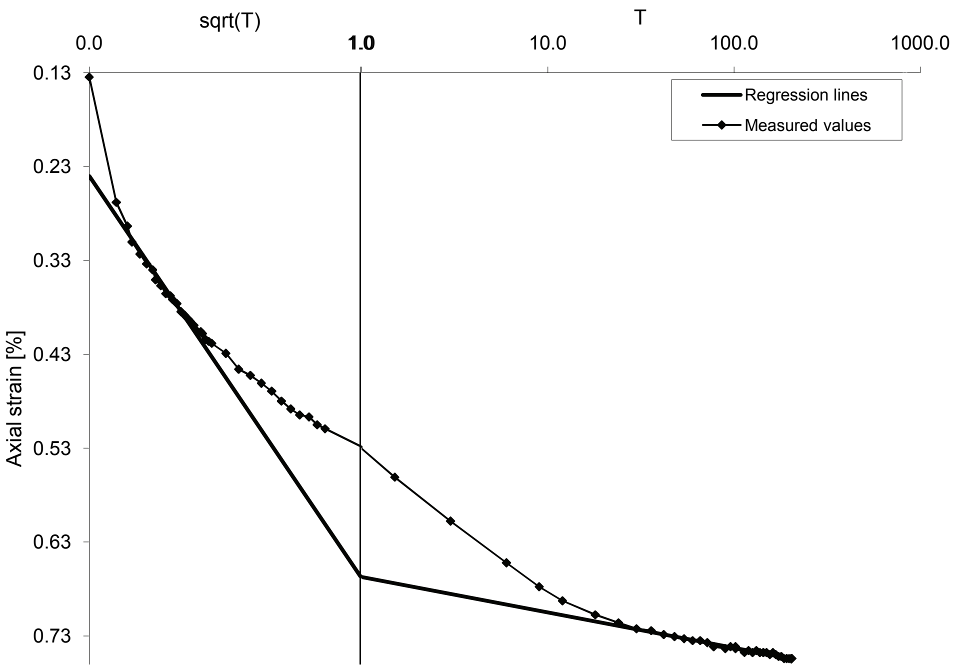

Figure B.4: Load step 4.

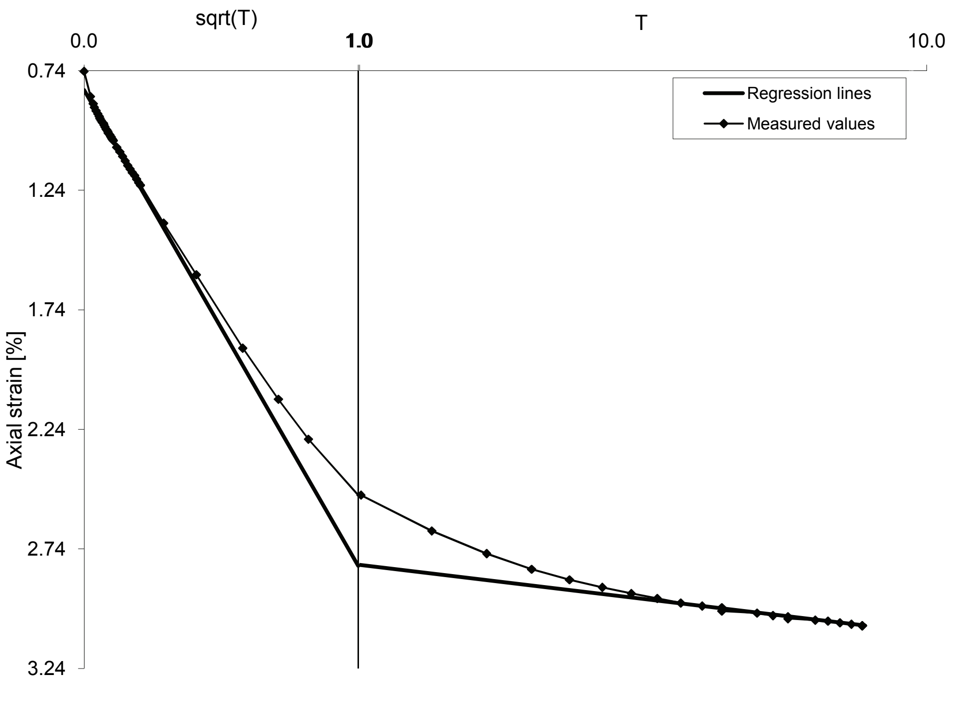

Figure B.5: Load step 5.

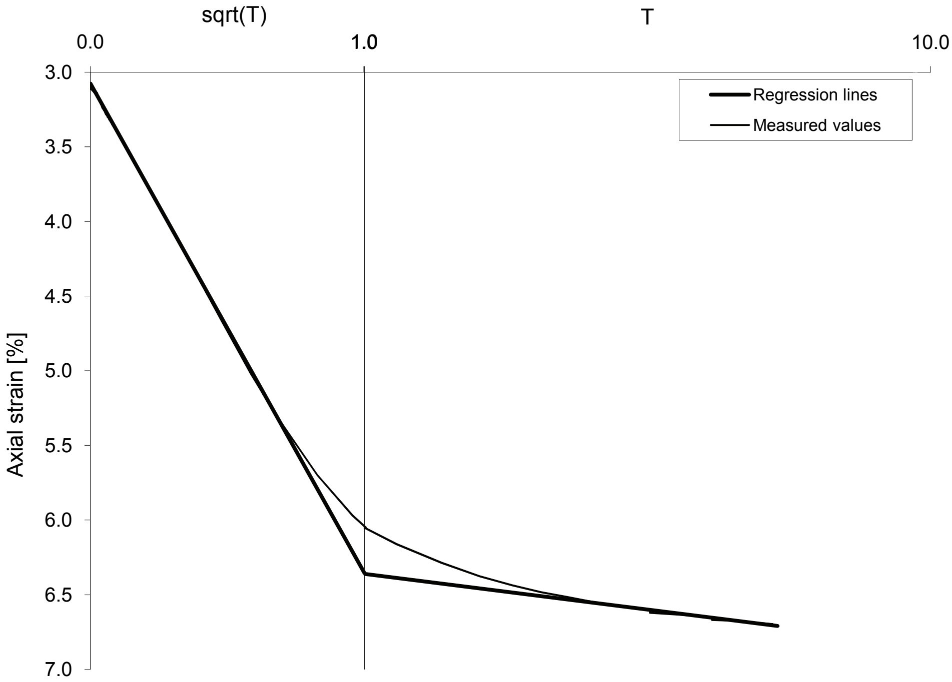

Figure B.6: Load step 6.

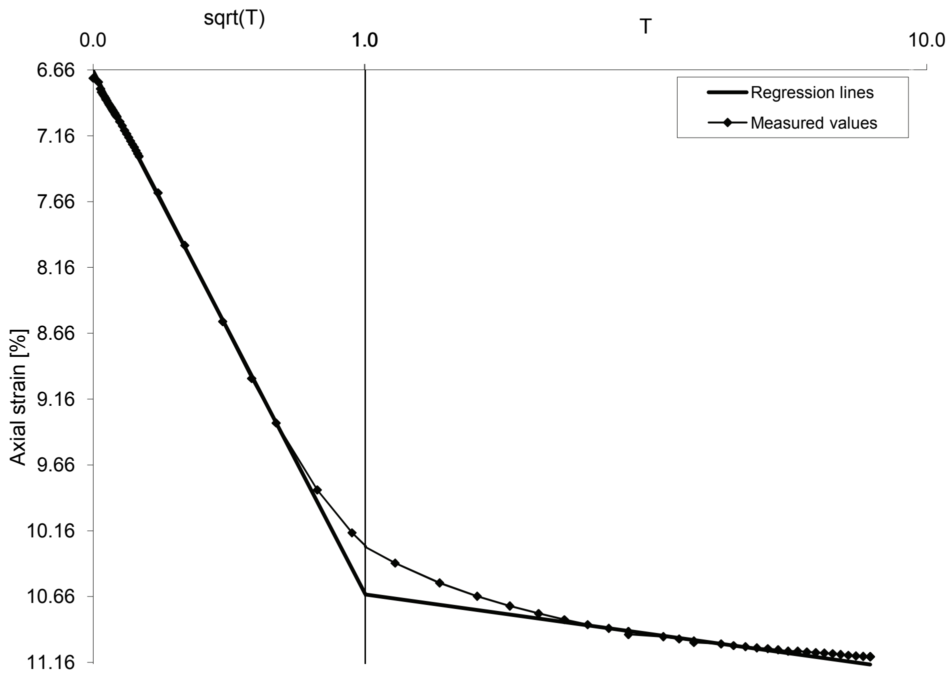

Figure B.7: Load step 7.

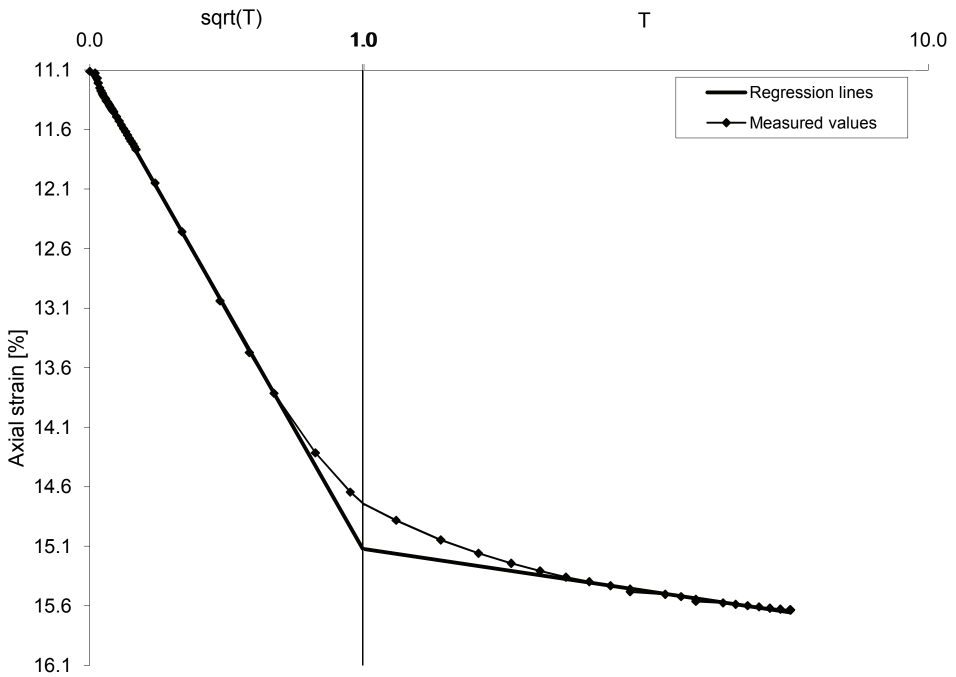

Figure B.8: Load step 8.

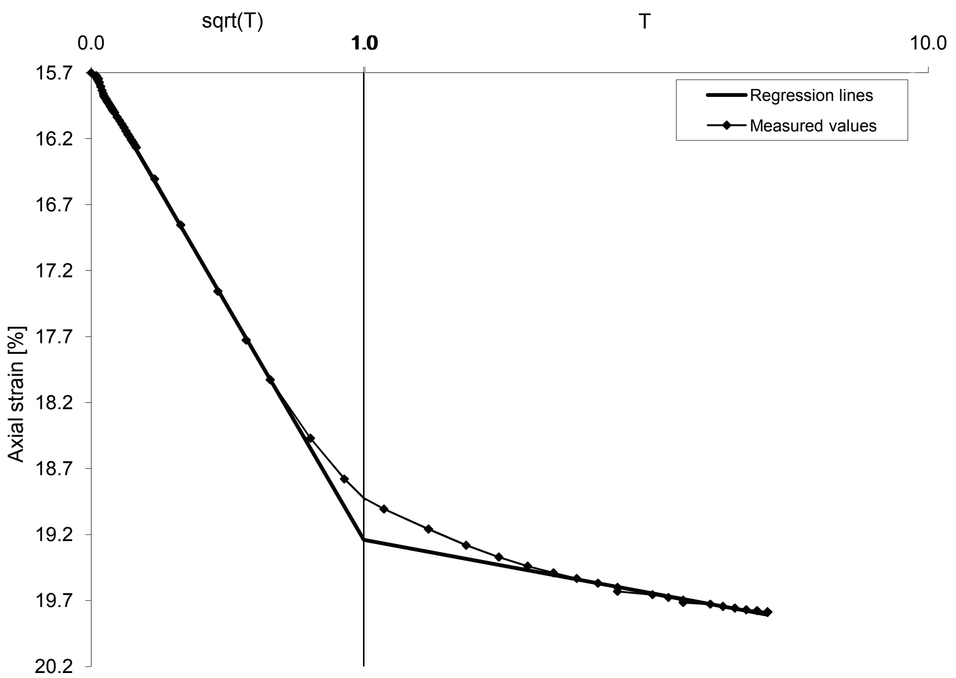

Figure B.9: Load step 9.

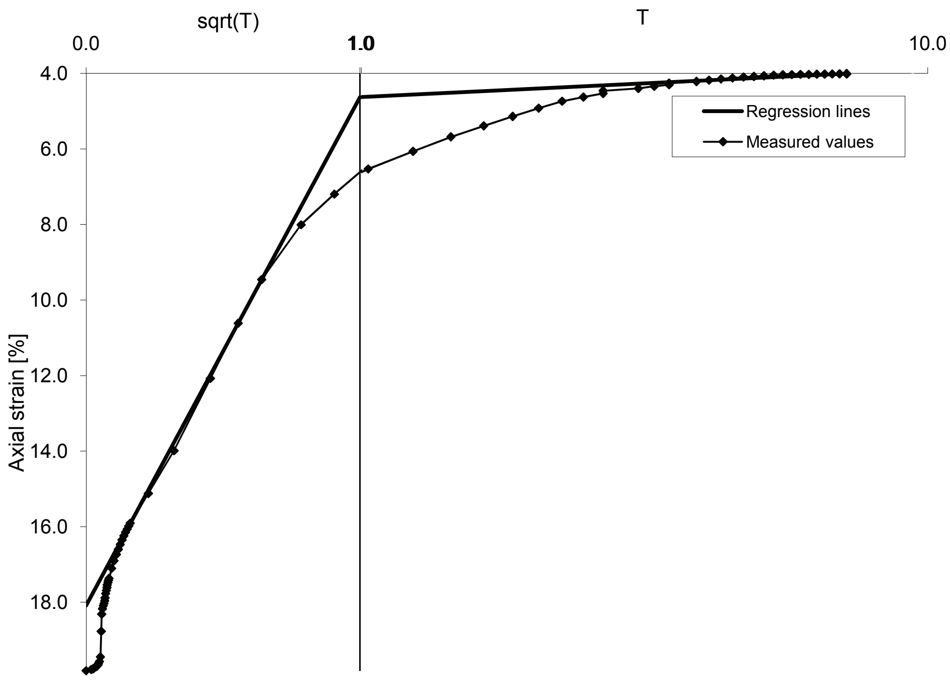

Figure B.10: Load step 10.

APPENDIX C

STRAIN–TIME CURVES FOR THE SECOND CONSOLIDATION TEST

In this appendix, the strain–time curves for each load step of the second consolidation test are presented.

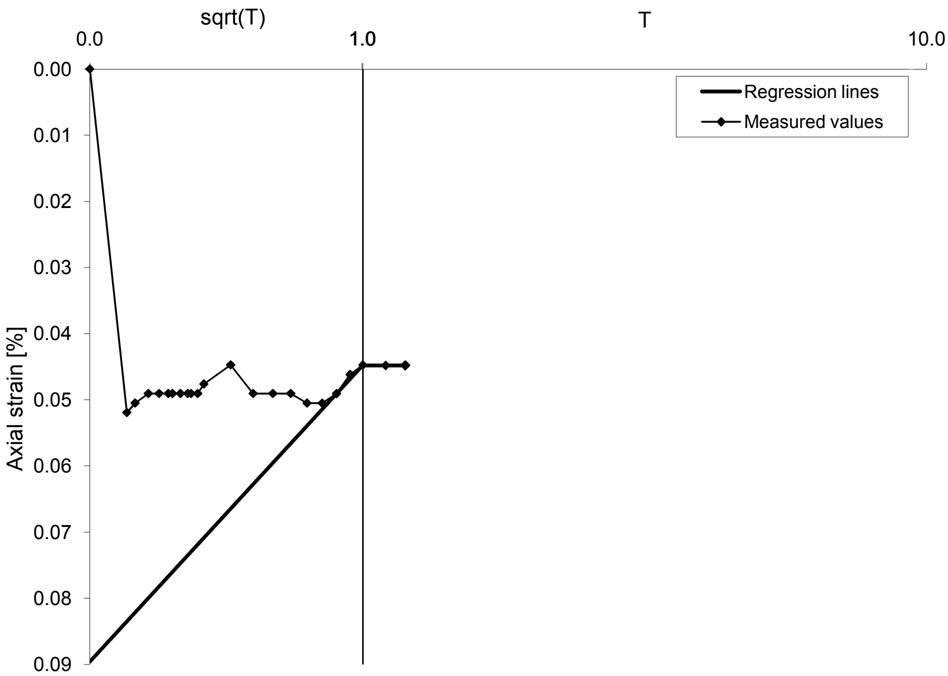

Figure C.1: Load step 1.

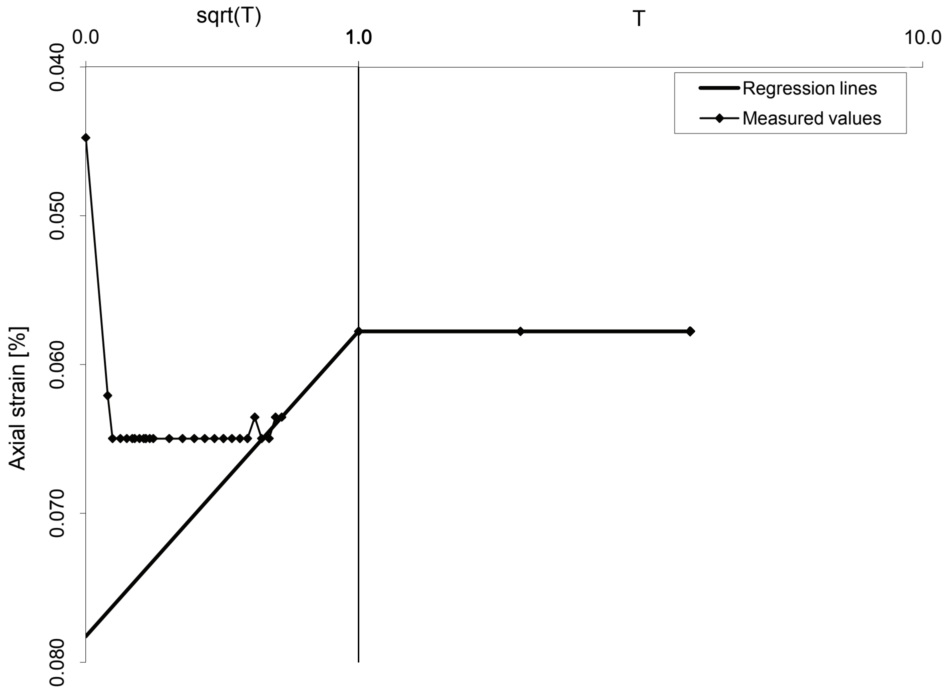

Figure C.2: Load step 2.

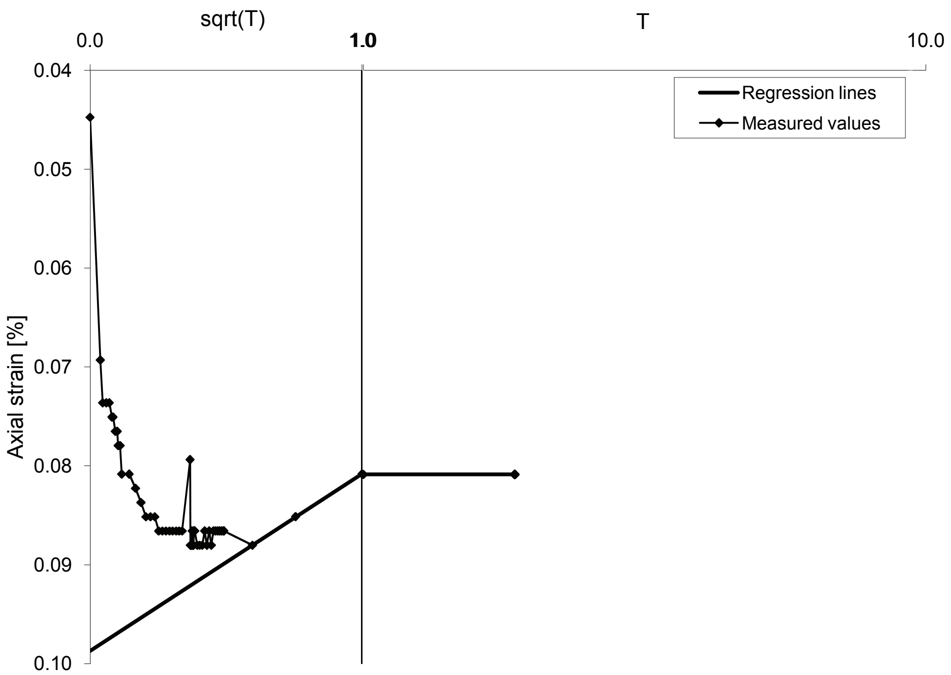

Figure C.3: Load step 3.

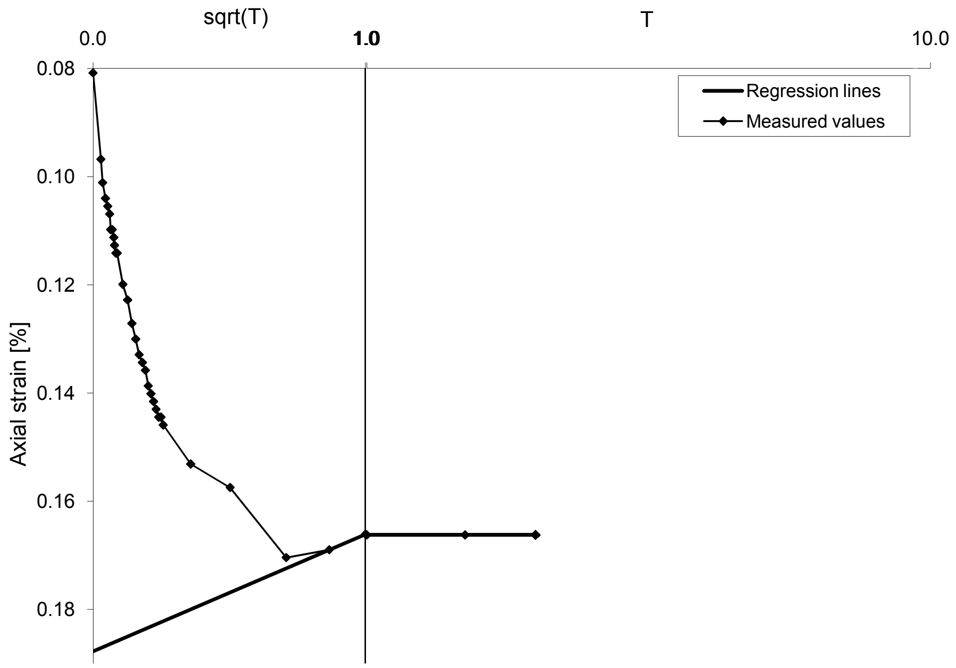

Figure C.4: Load step 4.

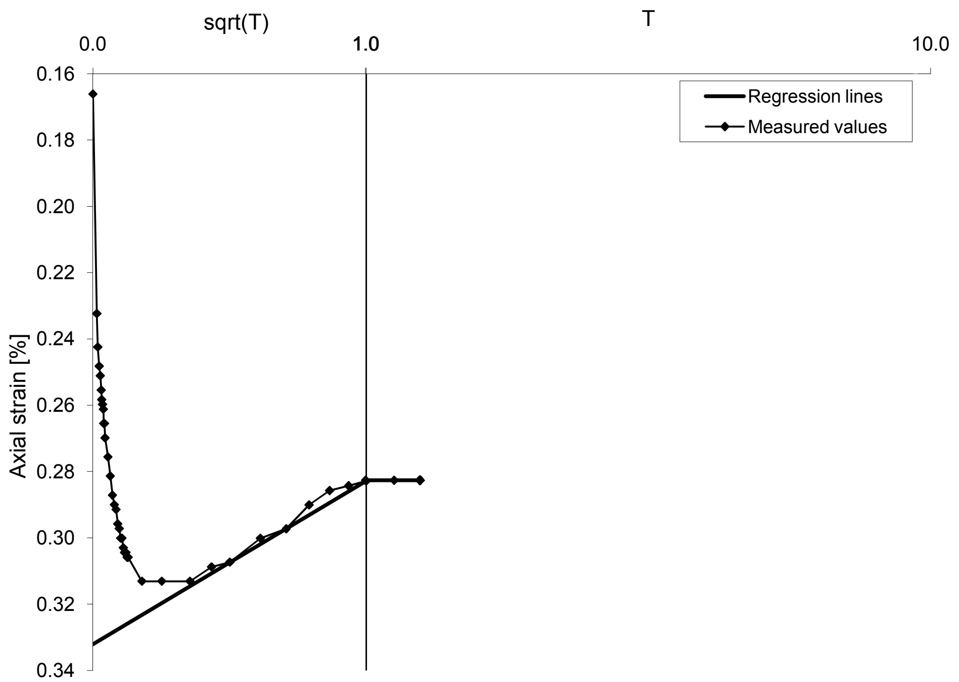

Figure C.5: Load step 5.

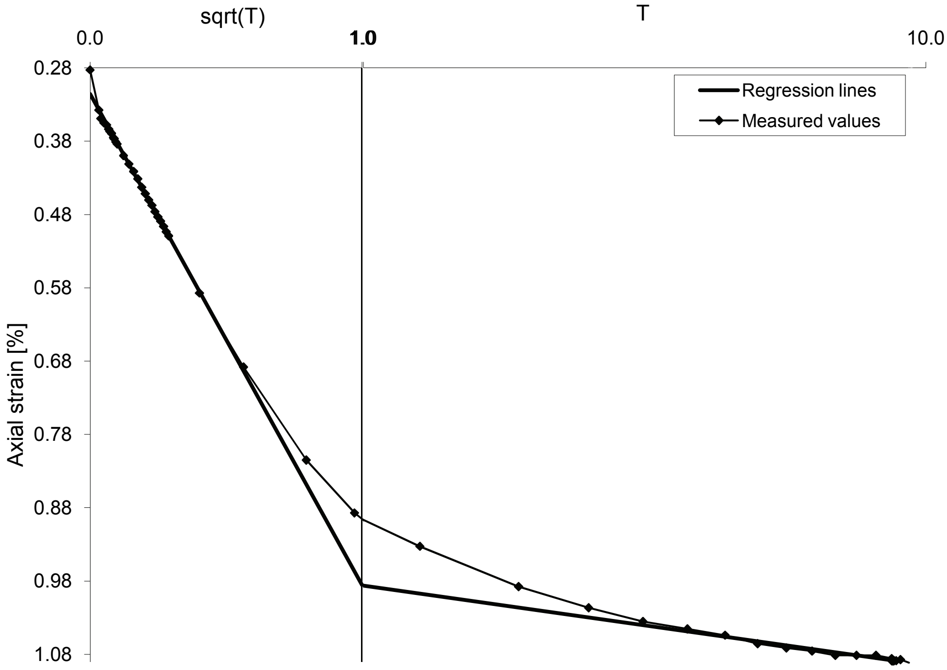

Figure C.6: Load step 6.

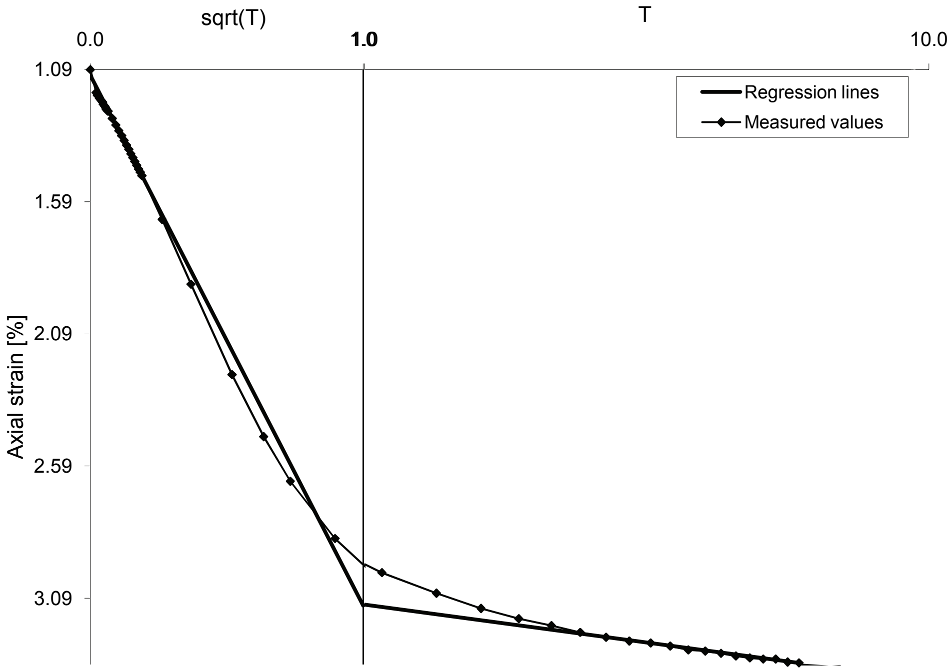

Figure C.7: Load step 7.

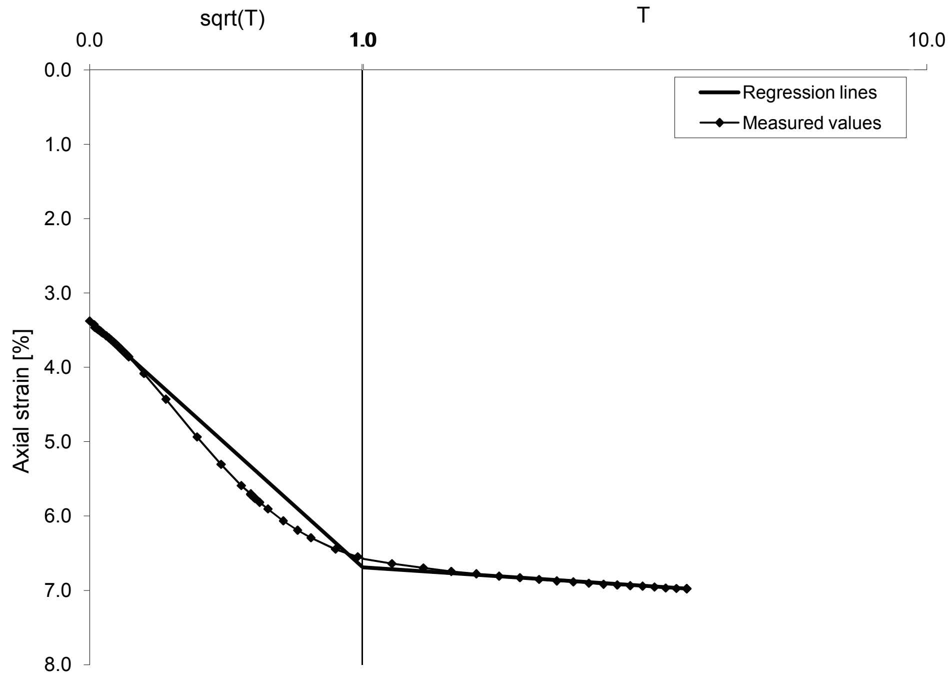

Figure C.8: Load step 8.

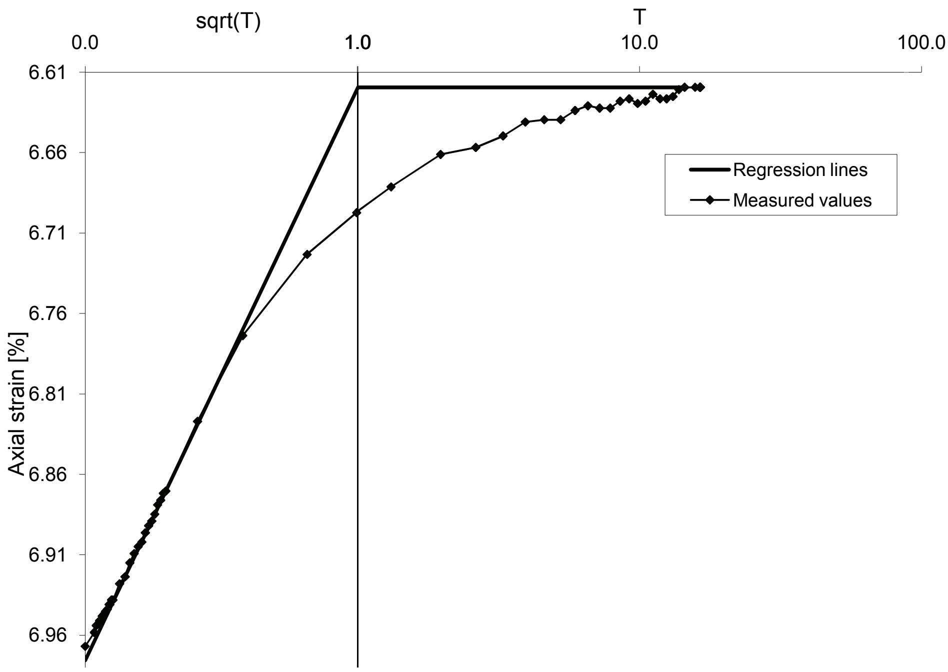

Figure C.9: Load step 9.

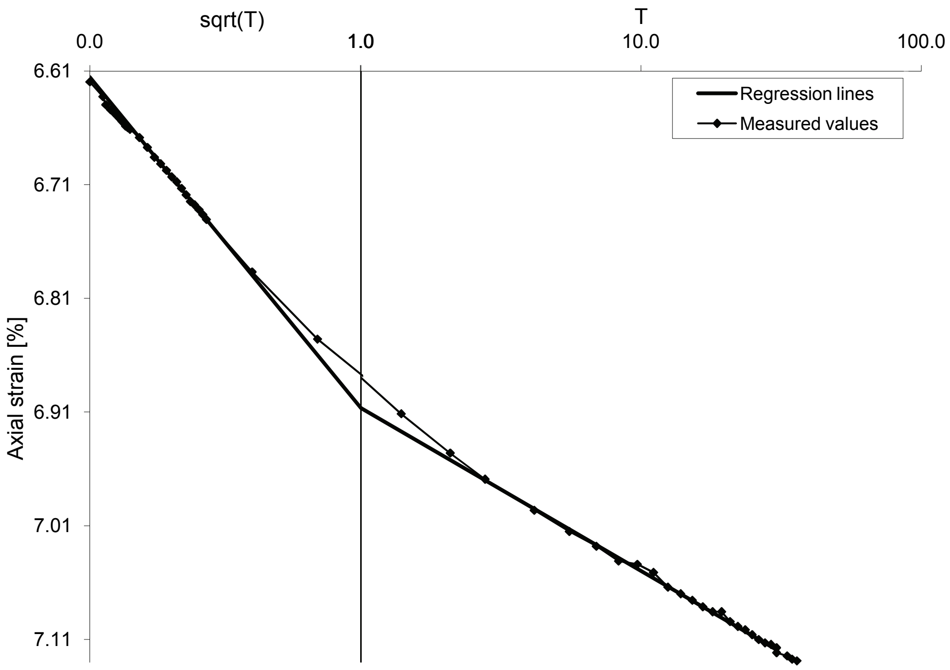

Figure C.10: Load step 10.

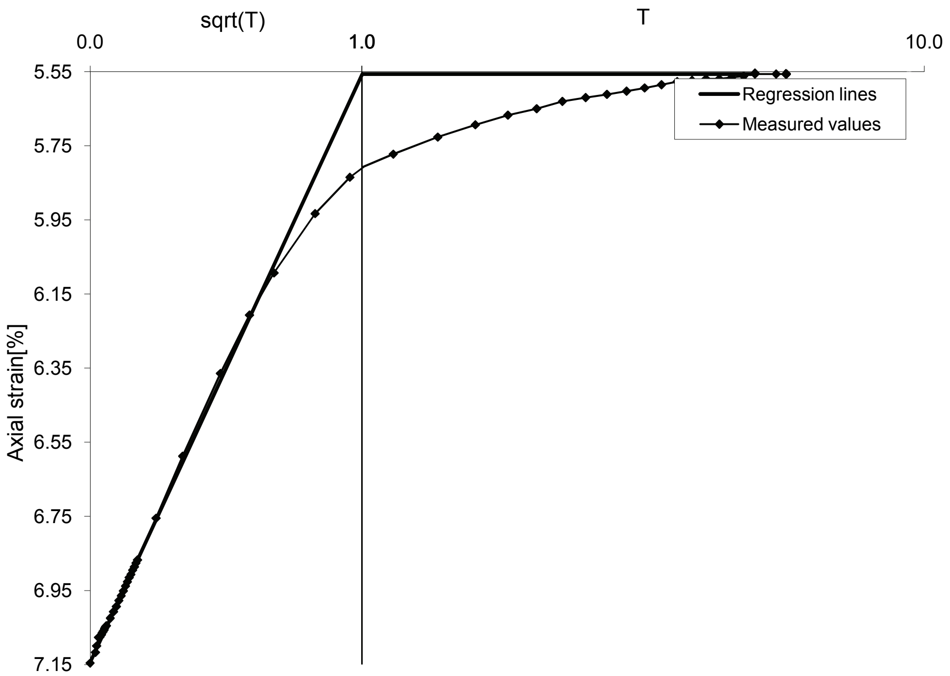

Figure C.11: Load step 11.

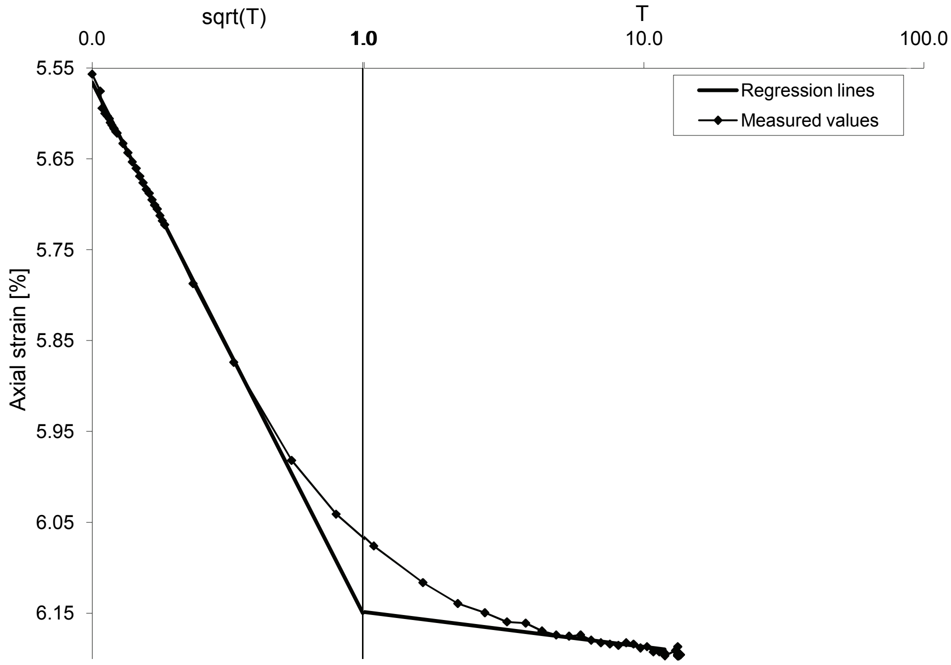

Figure C.12: Load step 12.

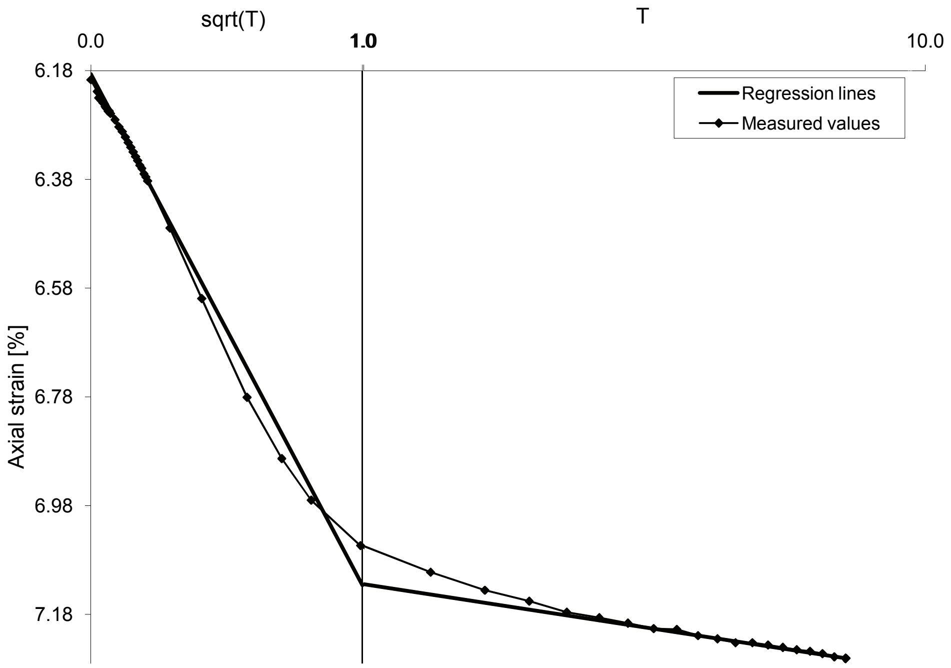

Figure C.13: Load step 13.

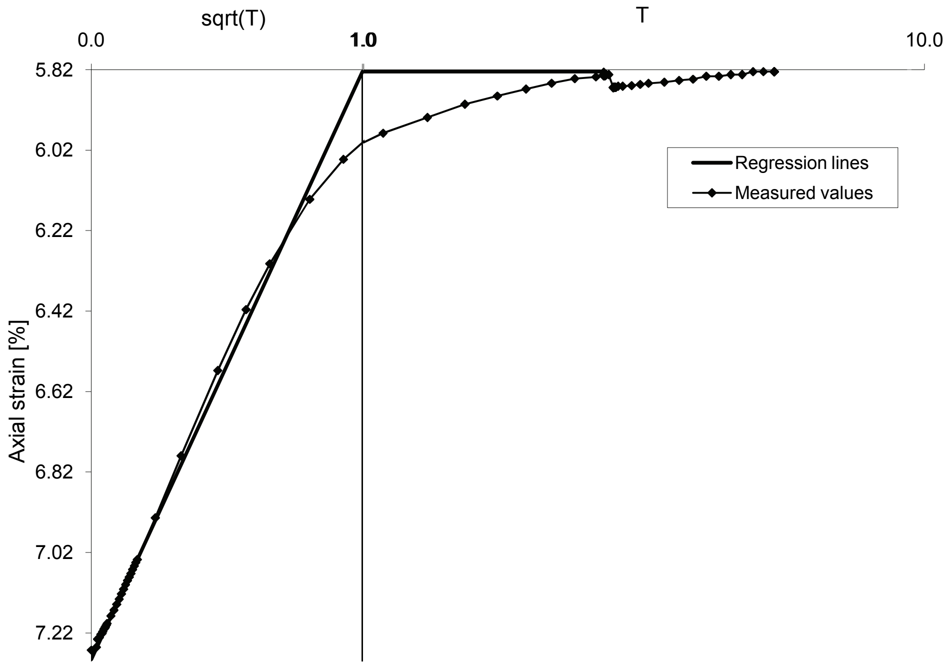

Figure C.14: Load step 14.

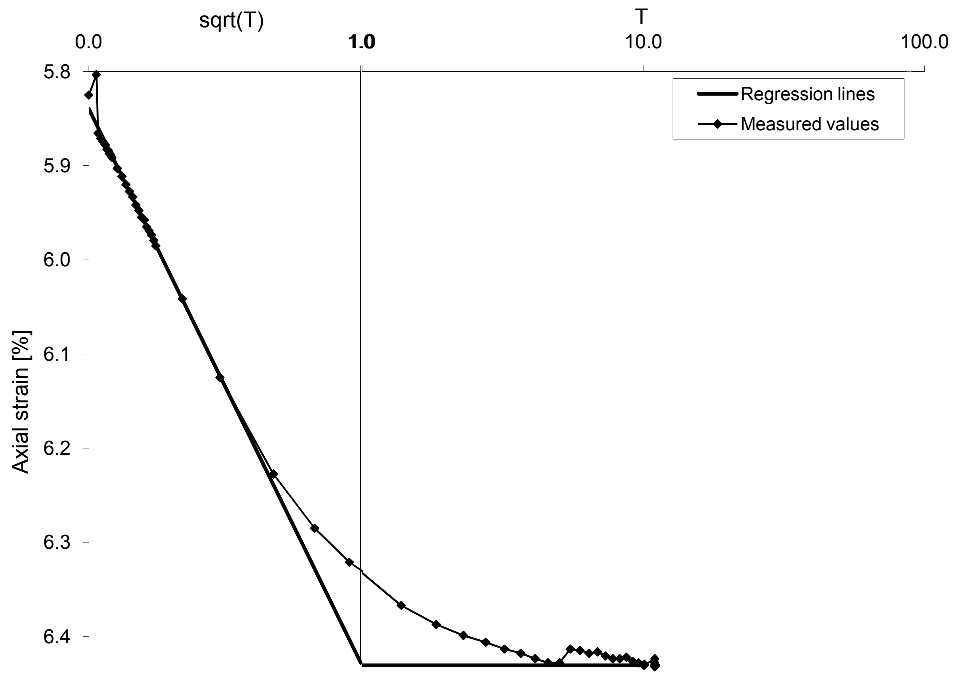

Figure C.15: Load step 15.

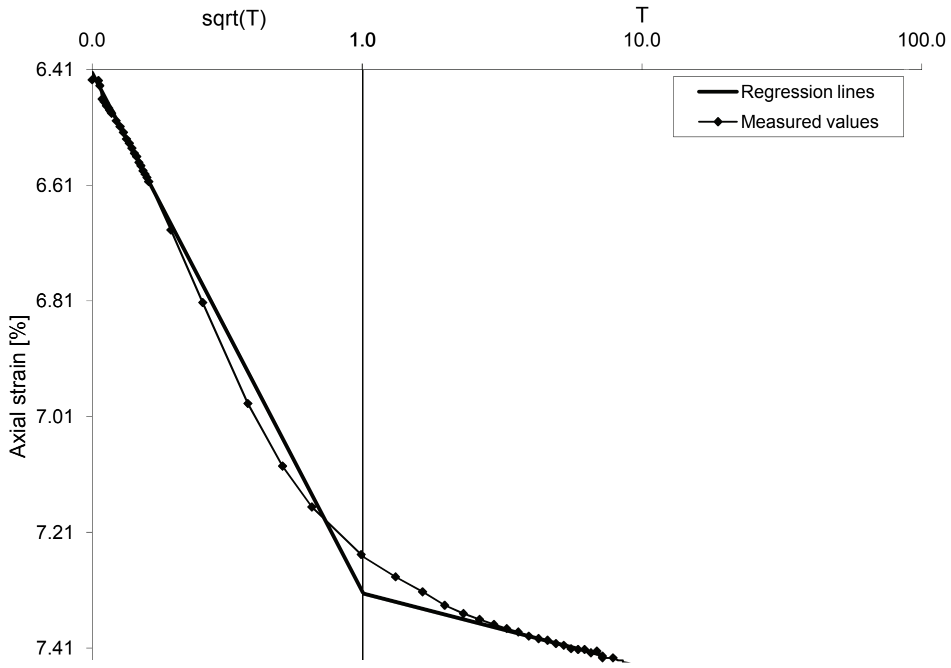

Figure C.16: Load step 16.

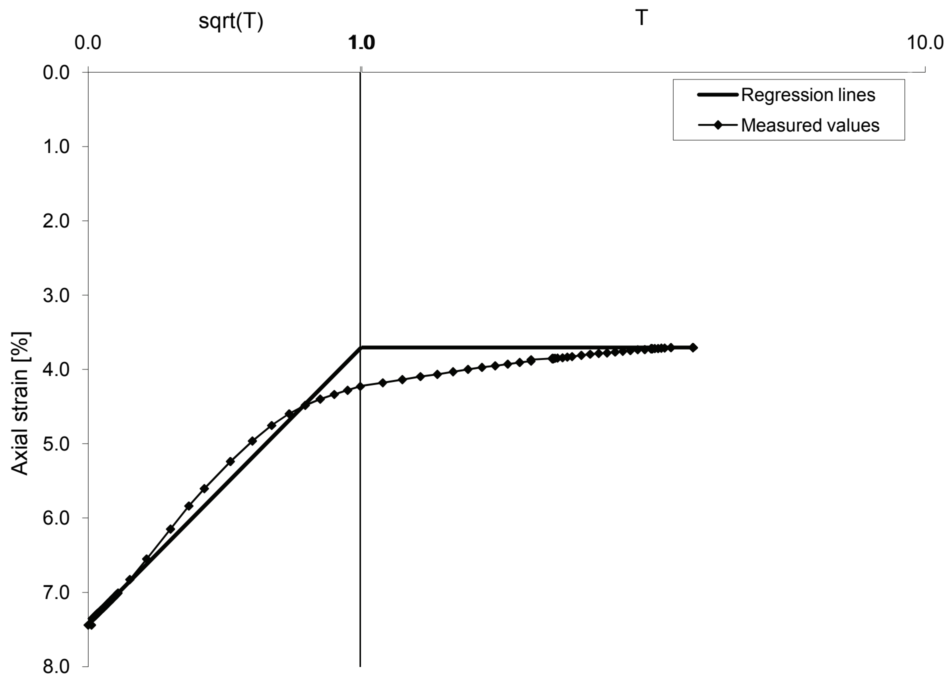

Figure C.17: Load step 17.

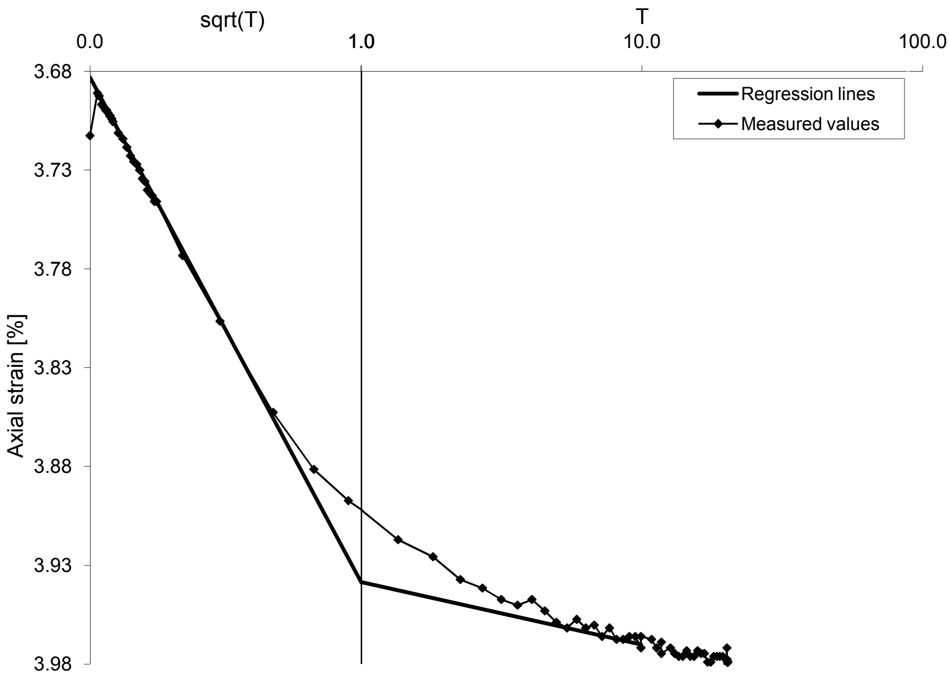

Figure C.18: Load step 18.

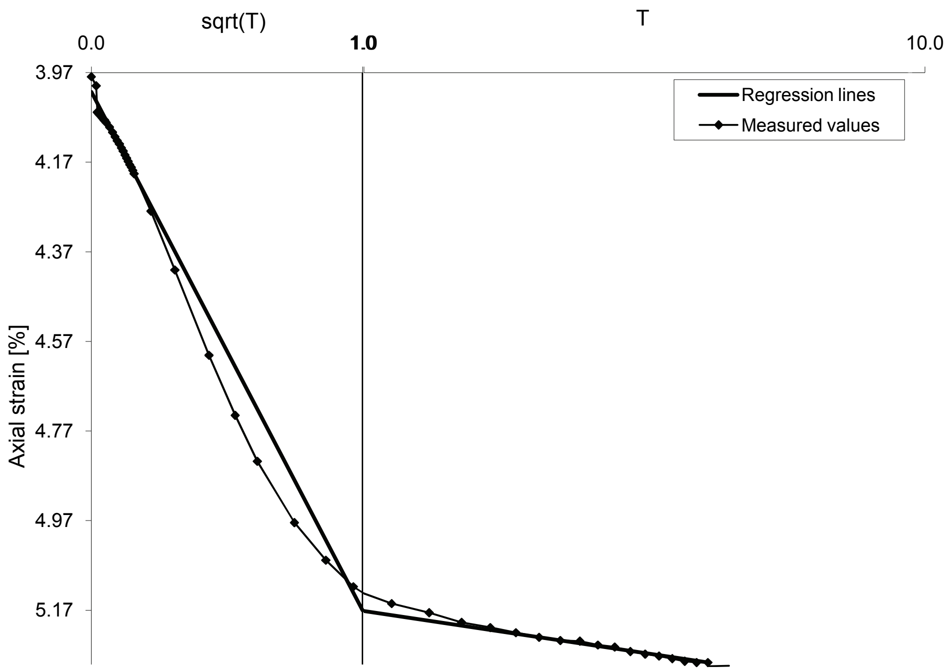

Figure C.19: Load step 19.

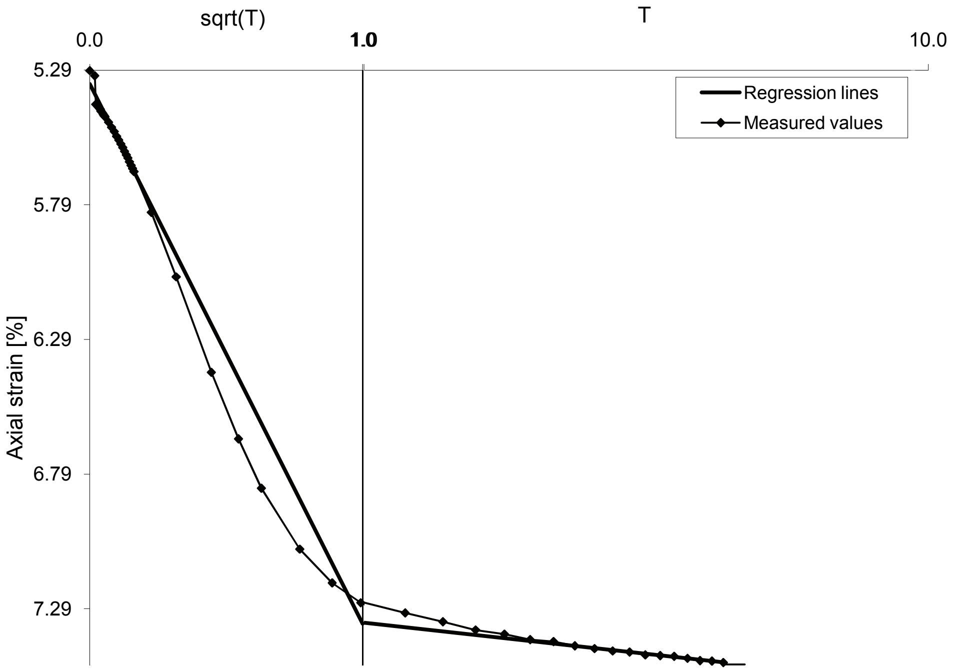

Figure C.20: Load step 20.

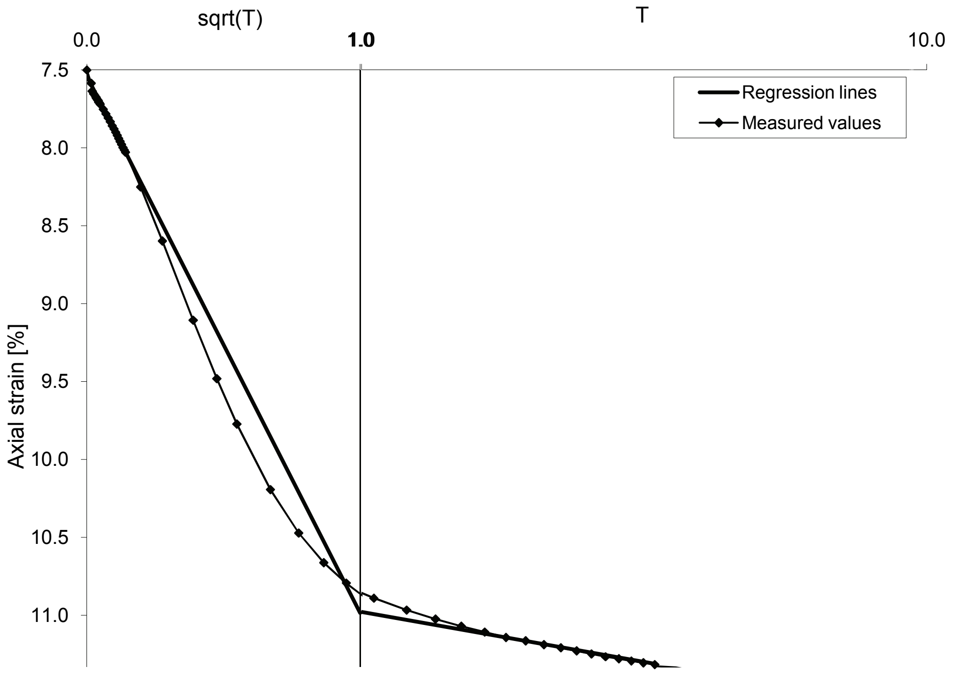

Figure C.21: Load step 21.

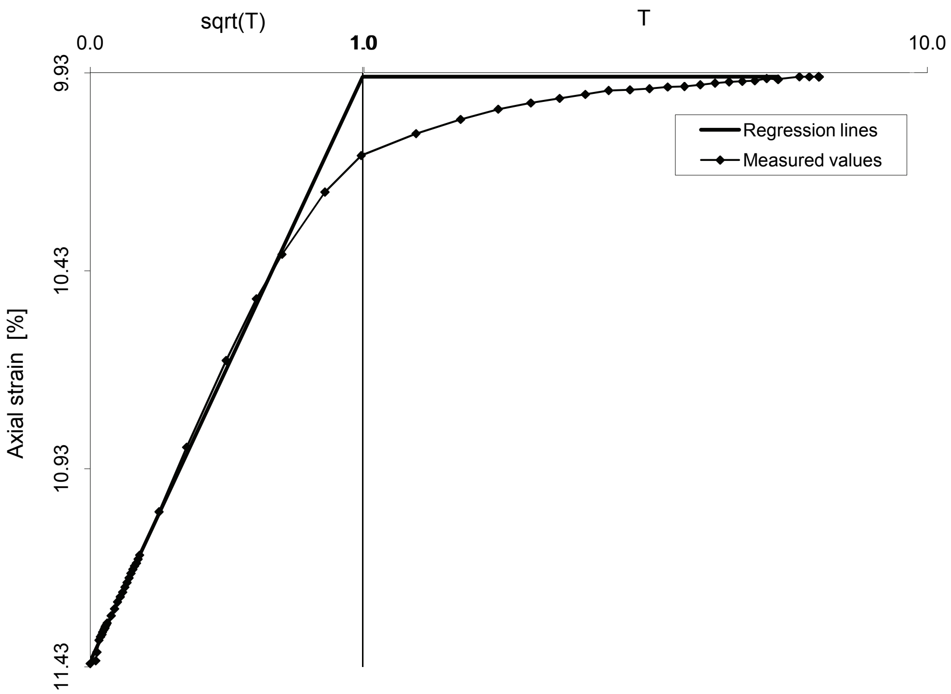

Figure C.22: Load step 22.

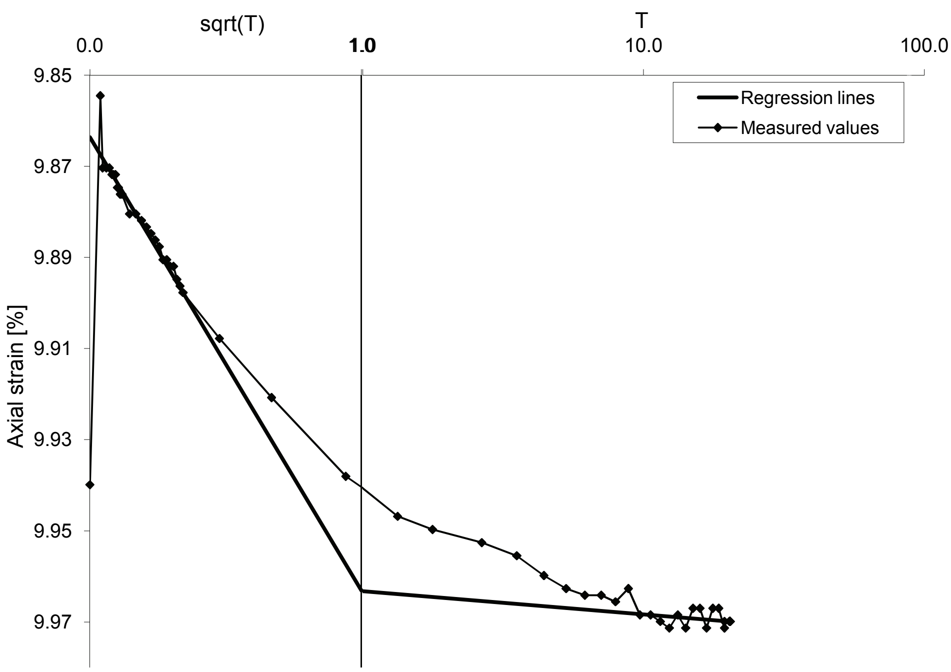

Figure C.23: Load step 23.

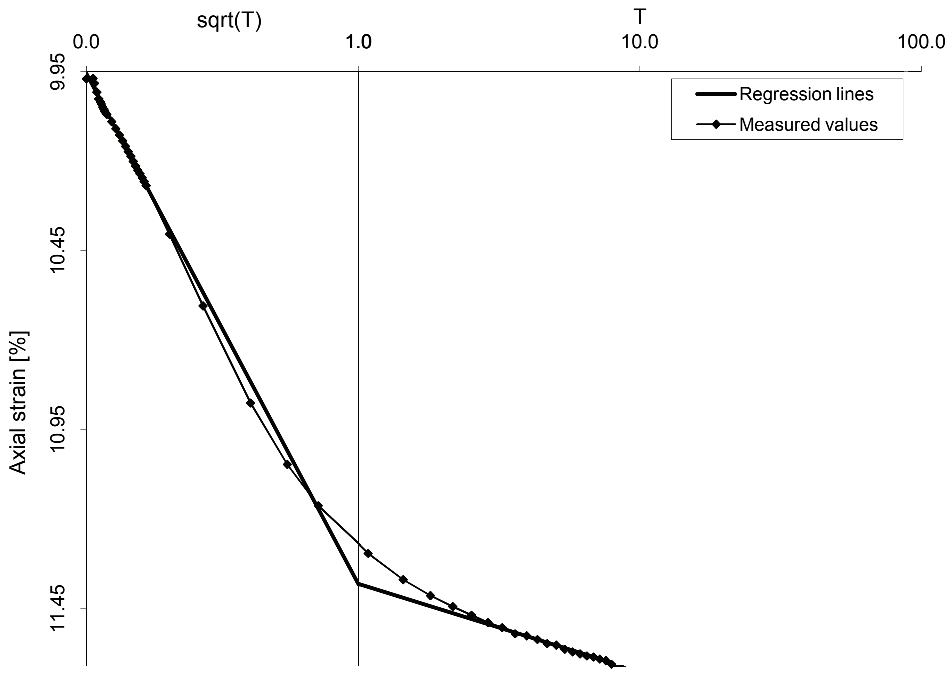

Figure C.24: Load step 24.

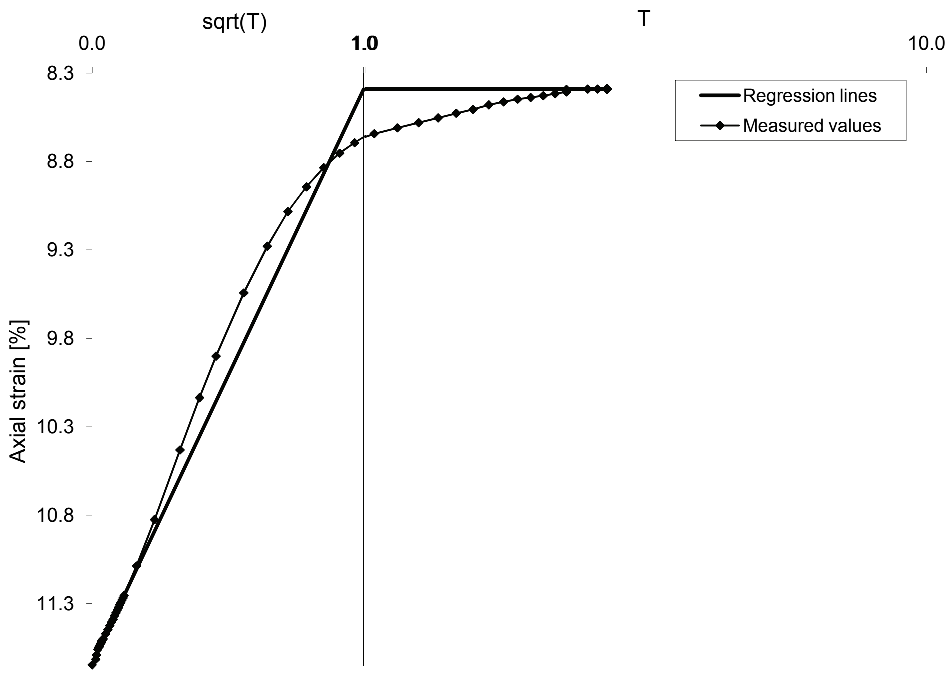

Figure C.25: Load step 25.

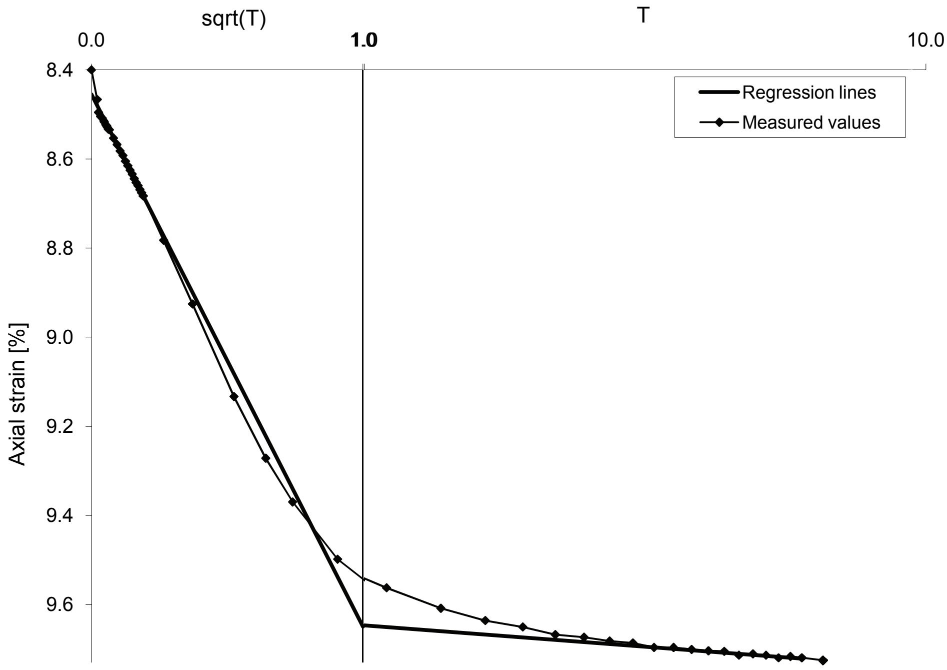

Figure C.26: Load step 26.

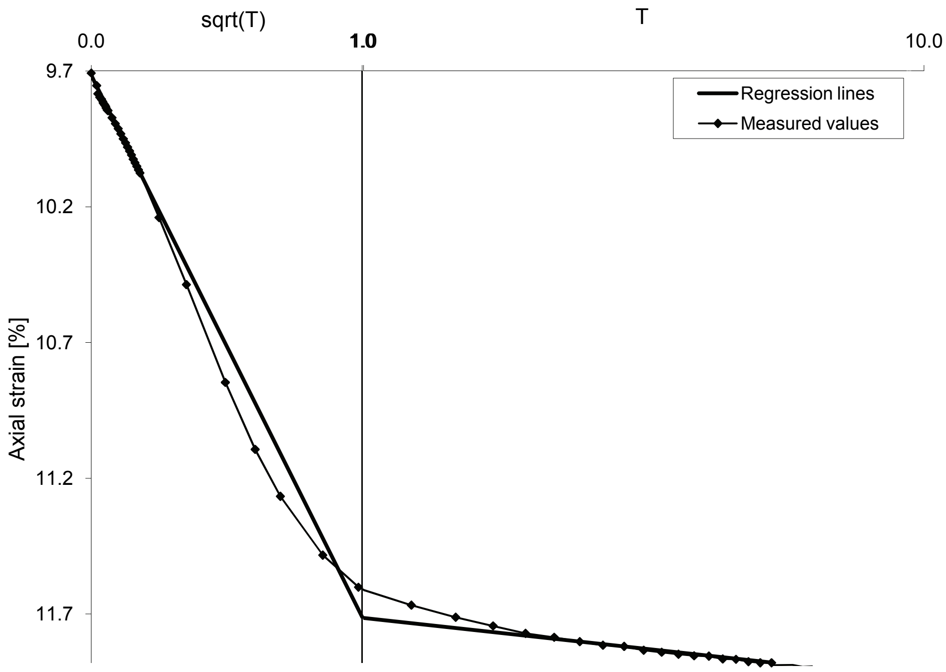

Figure C.27: Load step 27.

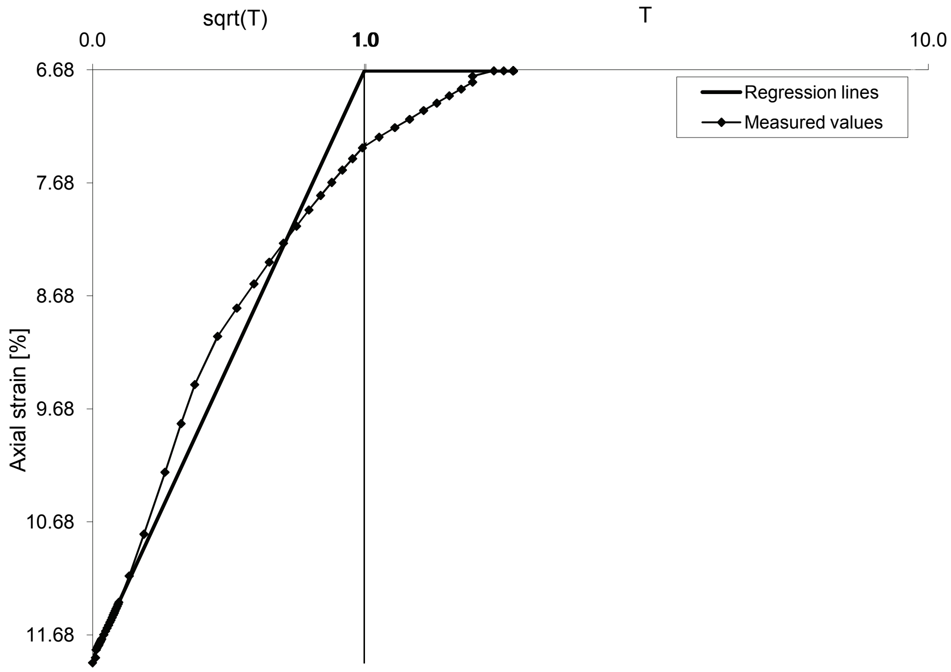

Figure C.28: Load step 28.

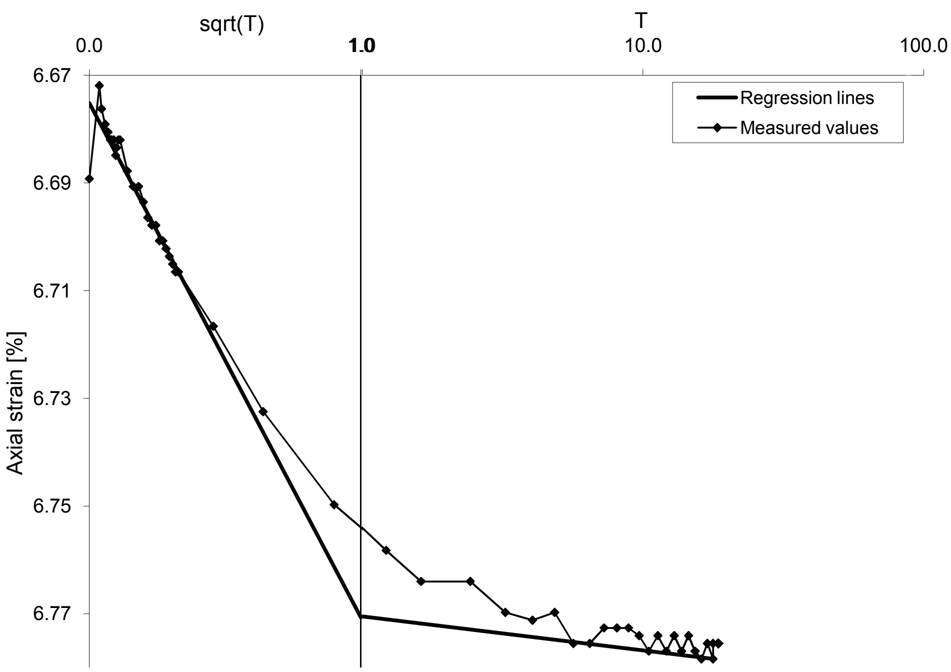

Figure C.29: Load step 29.

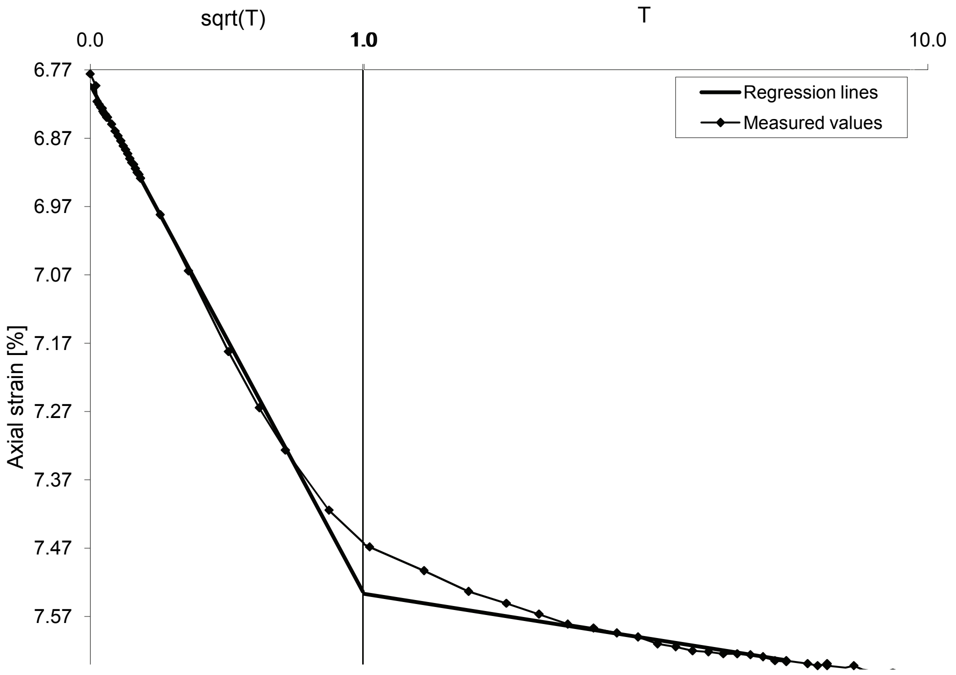

Figure C.30: Load step 30.

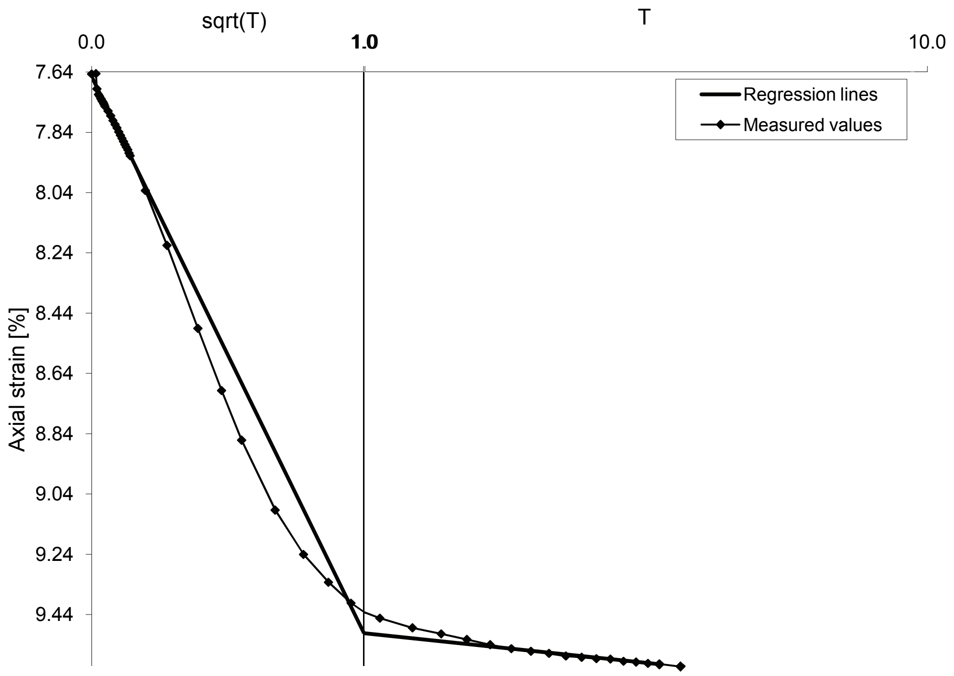

Figure C.31: Load step 31.

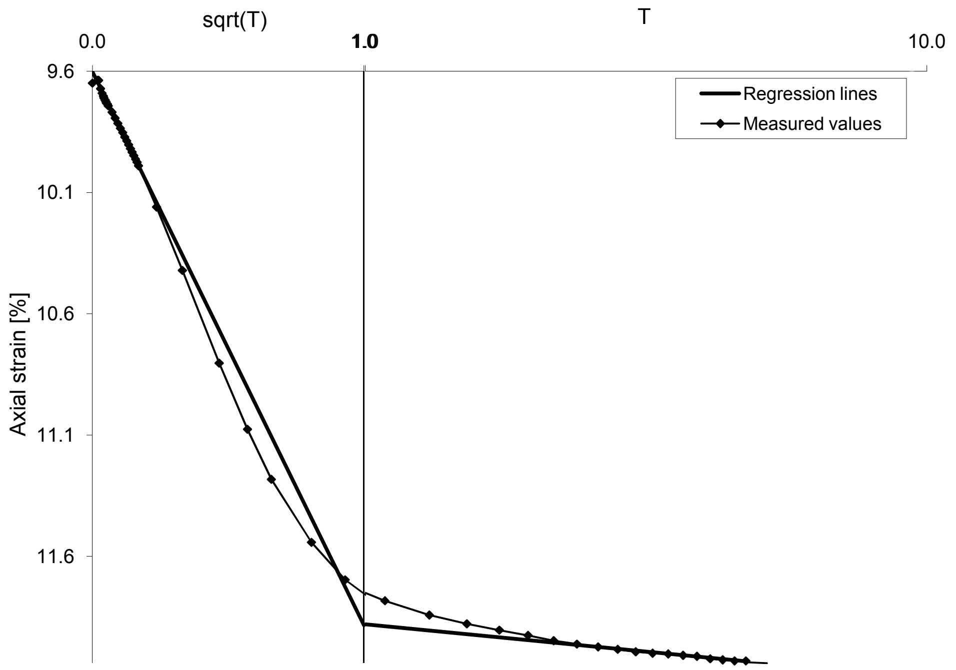

Figure C.32: Load step 32.

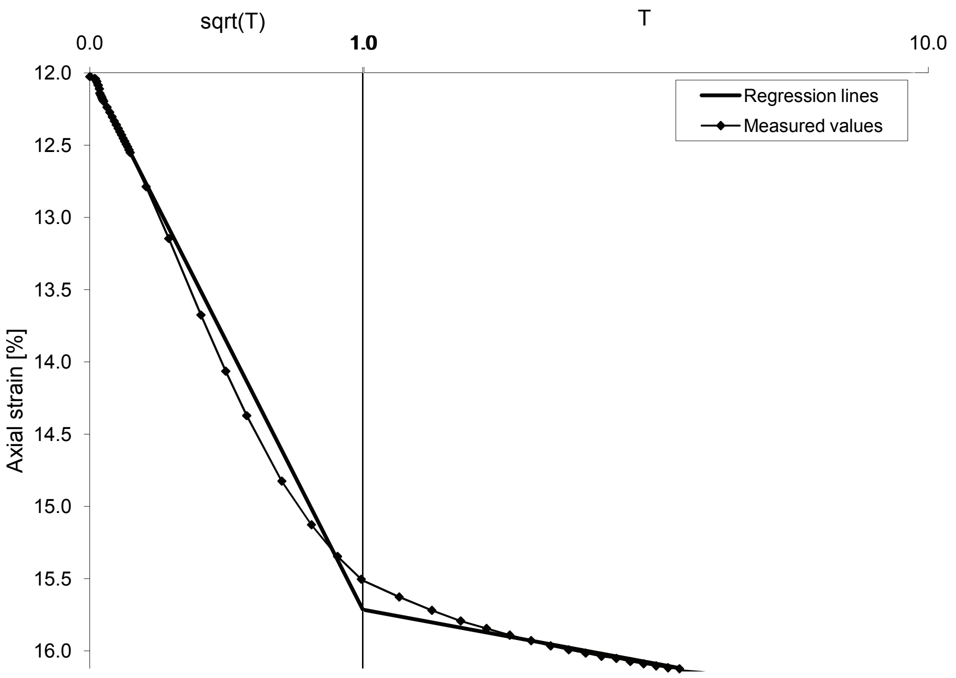

Figure C.33: Load step 33.

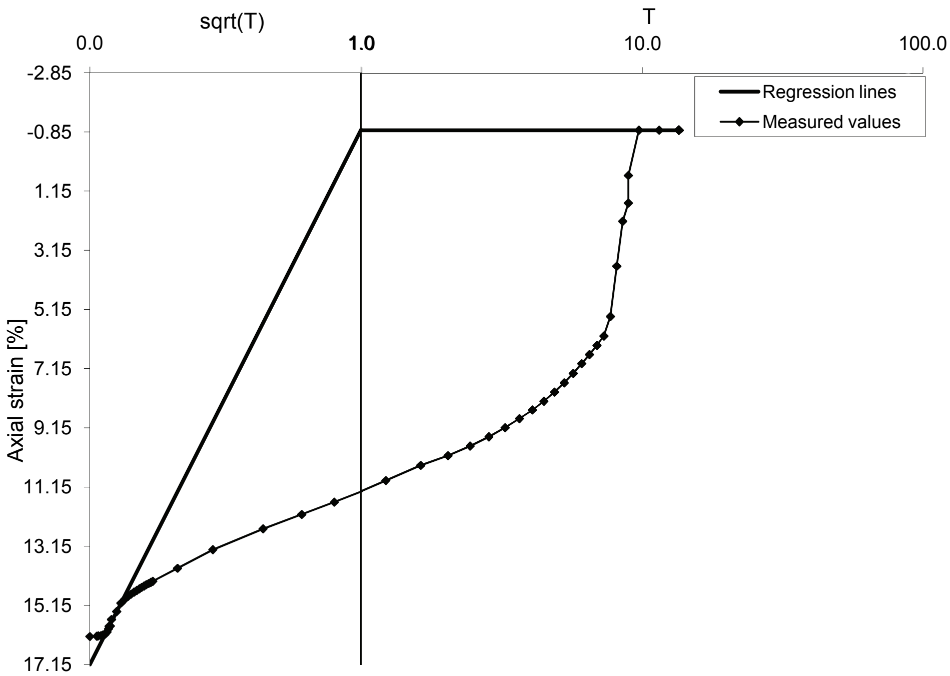

Figure C.34: Load step 34.

APPENDIX D

LITERATURE REVIEW

In the present appendix, a brief review of the considered literature concerning methods of analysing the effects of swelling is presented.

D.1 Okkels and Bødker, 2008

In Okkels and Bødker (2008), the first order theory of one-dimensional consolidation by Terzaghi is used to determine the penetration depth of the swelling zone and the magnitude and time frame of the consequently heave. As an approximation, the one-sided drainage is assumed to be linearly distributed.

The height of the swelling zone n is determined by equalising the incoming volume of water and the heave at a specific time calculated as consolidation settlements of preconsolidated clay. The progress of the height of the swelling zone with time for a coefficient of consolidation of $c_k = 10^{-8}$ m^2/s can be seen in Figure D.1.

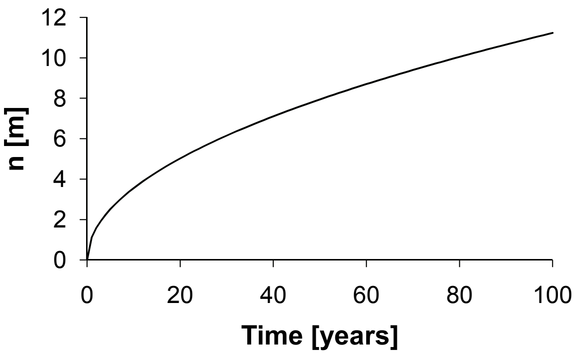

Figure D.1: Progress of the height of the swelling zone of the swelling zone with time for $c_k = 10^{-8}$ m^2/s.

The pore pressure is determined by the height of the swelling zone by which the total heave is calculated similar to settlements of a thin normally consolidated clay by the conventional theory of consolidation. For this calculation the compression index for the unloading path C_{cu} is applied. Whether this index or the compression index for the primary path $C_{c\varepsilon}$ should be applied is debatable.

D.2 Moust Jacobsen and Gwizdala, 1992

A combination of the one-dimensional theory of consolidation and the numerical method of calculation of settlements by Moust Jacobsen and Gwizdala (1992) is applied for determining the vertical displacements of the pile toe and the ground surface without influence of the pile. The displacements are determined by comparison of displacements of soil without influence of the pile and pile deformations including linear elastic–perfectly plastic soil–pile interaction.

The soil displacements are determined for a preconsolidated clay loaded by a rectangular foundation by the one-dimensional theory of consolidation. The pressure is assumed to be distributed 1:2. The soil layer is divided into a number of thin sublayers. Thus, the vertical displacement of each sublayer can be determined as the deformation of a thin layer.

The pile toe displacements including the soil–pile interaction are determined by the method described in Moust Jacobsen and Gwizdala (1992). The method is to calculate the shaft resistance and toe resistance separately for different displacements, plot the two load–displacement curves and combine them in a numerical calculation of the total displacements. This method is applied because the load–displacement curve for the shaft resistance differ significantly from the curve for the toe resistance.

D.3 Poulos and Davis, 1980

In Poulos and Davis (1980), the pile displacements in a swelling soil are determined by elastic calculations. The basic analysis includes the assumptions of linear elastic soil, no slip in the soil–pile interface and and incompressible pile.

The soil displacements along the pile are determined as a reduction of the movements of a soil profile without influence of the pile due to soil–pile interaction. The pile is divided into a number of elements and by vertical equilibrium, an expression for the imposed pile load is given. For a given soil movement without influence of the pile, the pile displacements can be calculated.

The basic theory is modified to account for slip in the pile-soil interface, compressive and tensile failure of the pile, layered soil and variation in time. Slip is taken into account by introducing a limit for the shear stresses of the pile shaft. The limit, i.e. the strength of the interface, is equalised to the Coulomb failure criterion.

D.4 Overview of Existing Theory

An overview of the existing theory can be seen in Table D.1.

Table D.1: Overview of the existing theory. O&B is Okkels and Bødker (2008), MJ&G is Moust Jacobsen and Gwizdala (1992) and P&D is Poulos and Davis (1980). Index s is for soil, p for pile and i for interface.

	O&B	Modified MJ&G	P&D
Output	δ_s	δ_p, δ_p	δ_p, δ_p
Basic theory	Theory of consolidation	Theory of consolidation	Theory of linear–elasticity
Controlling parameters	n	n	n
	γ_s	γ_s	Swelling profile (linearly decreasing, etc.)
	Surface load	Surface load	
	c_k	Pile material	E_s
	Time	Factor of regeneration	ν_s
	C_{cu}	c_u	Distribution of τ_i
		D_p	D_p
			L_p/D_p
			Axial load on pile
			Tensile failure of pile
			If slip in pile-soil interface: shear strength of interface

As seen in Table D.1, the number of parameters with influence on the soil and pile displacements differ for the three methods.

APPENDIX E

CONSOLIDATION TEST OF TERTIARY CLAY AT MOESGAARD MUSEUM

In connection with the understanding of swelling soils, consolidation tests can be used to physically comprehend some of the mechanisms of these types of soils. A case study of tertiary clay near Aarhus is used to determine the swelling pressure σ'_S, the normal consolidation path of the stress–strain curve and the preconsolidation stress σ'_{pc} by a consolidation test with incremental loading up to about 8700 kPa without un- or reloading. Furthermore, a consolidation test with incremental loading and a number of un- and reloading paths are analysed to determine the compression index for the unloading path C_{cu} and the constrained modulus E_{oed}.

E.1 Determination of Preconsolidation Stress

Several different methods can be applied to estimate the preconsolidation stress σ'_{pc}. In the following, some of the methods are described.

E.1.1 Casagrande's Method

The preconsolidation stress is determined by use of the load–displacement curve if the primary path is observed, cf. Figure E.1.

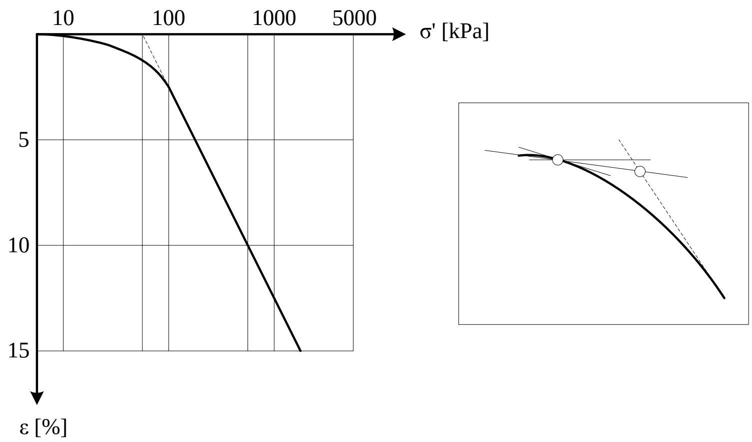

Figure E.1: Casagrande's method of determining σ'_{pc}. According to Harremoës et al. (1997, Fig. 6.12).

σ'_{pc} is estimated as the intersection of the primary path and the bisector of the tangent to the curve at the point of largest curvature and a horizontal line through this point. This method cannot be used for highly overconsolidated clays where the primary path is not reached.

(Harremoës et al., 1997)

E.1.2 Terzaghi's Method

In Terzaghi's method, the curved line of the primary loading curve, in the following named the primary path, is used to determine σ'_{pc}. According to Terzaghi, the primary path can be described by Equation E.1.

$$\varepsilon = C_{c\varepsilon} \cdot \log\left(1 + \frac{\sigma'}{\sigma'_{\kappa}}\right) + \varepsilon_0 \tag{E.1}$$

Where:
- $C_{c\varepsilon}$ is the compression index of the primary loading curve,
- σ'_{κ} is a reference stress,
- ε_0 is the start value of the consolidation strain (not equal to the initial strain ε_i).

The reference stress σ'_{κ} is the addition to σ' by which the primary path gets linear in a semi-logarithmic depiction, named the virgin curve, cf. Figure E.2.

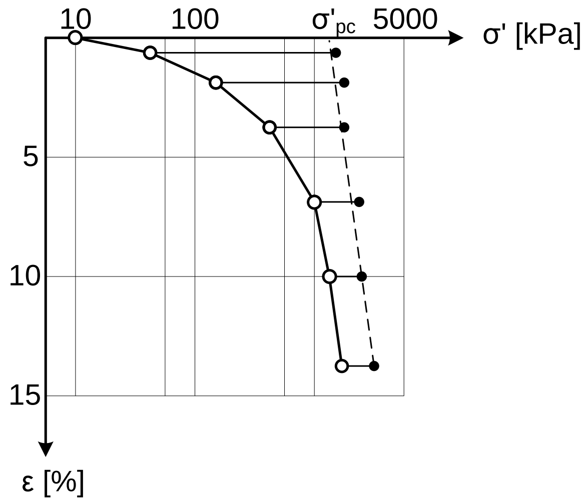

Figure E.2: Determination of the virgin curve used for Terzaghi's method.

σ'_{pc} is then estimated by Equation E.2 by use of the Casagrande method.

$$\sigma'_{pc} \approx 2.0 \cdot \sigma'_{\kappa} \tag{E.2}$$

(Moust Jacobsen, 1993; Thøgersen, 2001)

E.1.3 Akai's Method

Akai's method makes use of the fact that the creep strain ε_s increases precipitously when $\sigma' \to \sigma'_{pc}$. Akai discovered that ε_s increases proportionally with σ' for $\sigma' < \sigma'_{pc}$ and with $\log \sigma'$ for $\sigma' > \sigma'_{pc}$. Hence, σ'_{pc} can be estimated to lie in the interval at which a change in inclination occurs for a $(\log \sigma', \varepsilon_s)$-depiction, cf. Figure E.3. (Moust Jacobsen, 1993).

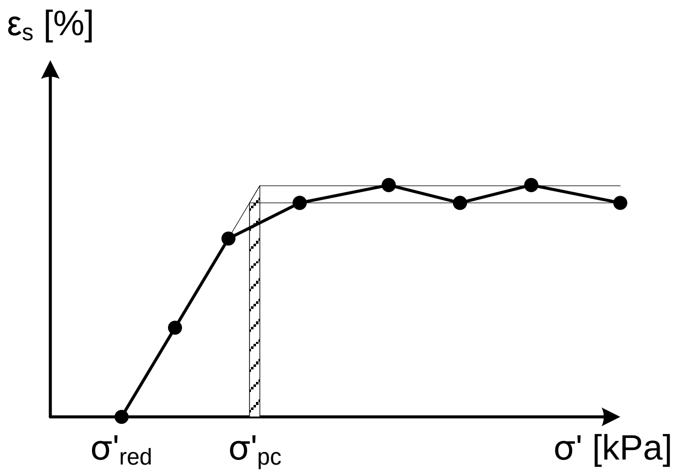

Figure E.3: Akai's method of determining σ'_{pc}. According to Moust Jacobsen (1993, Fig. 5.13).

E.1.4 Janbu's Method

By Janbu's method the preconsolidation stress is estimated as the effective stress at the point where the secant modulus E_{50} becomes linear plotted as a function of σ', cf. Figure E.4.

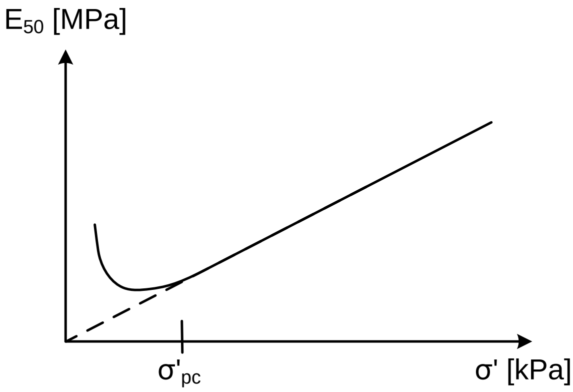

Figure E.4: Janbu's method of determining σ'_{pc} based on the secant modulus E_{50}.

E.1.5 Determination by the Coefficient of Consolidation

Lotte Thøgersen defined in her Ph.D. thesis a method to determine the preconsolidation stress by the coefficient of consolidation c_k defined in Equation E.3.

$$c_k = \frac{k \cdot E_{eod}}{\gamma_w} \tag{E.3}$$

c_k is determined for each load step and can be plotted as a function of the effective stress σ' after ended test, cf. Figure E.5.

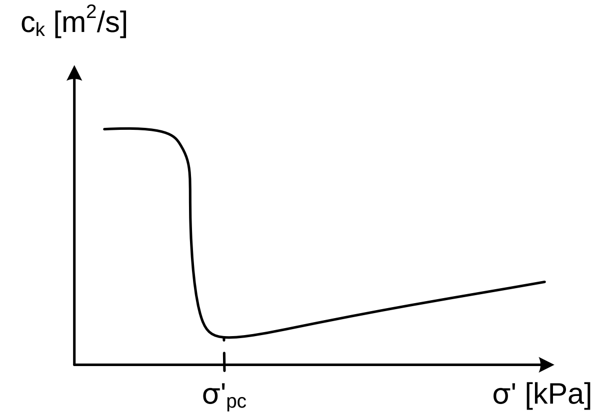

Figure E.5: Lotte Thøgersen's method of determining σ'_{pc}. According to Thøgersen (2001, Fig. 5.9).

When the effective stresses exceed the preconsolidation stress σ_{pc}, the clay becomes normally consolidated as the overconsolidation ratio is smaller than 1. In this area larger deformations occur leading to decreasing permeability. Simultaneously, the oedometer modulus E_{oed} is increasing according to Equation E.4 leading to an almost constant or slightly increasing product of k and E_{oed}. σ'_{pc} is estimated as the value where c_k becomes almost constant or slightly increasing with increasing σ'.

$$E_{oed} = \frac{\ln 10}{C_{c\varepsilon}} \cdot \sigma' \tag{E.4}$$

(Thøgersen, 2001)

E.2 The Consolidation Tests

An addition to the existing Danish Moesgaard Museum 10 km south of Aarhus is to be accomplished during the next three years. Unfortunately, problems have been experienced concerning upward movement of the structure; these problems are partly analysed by laboratory tests. Two consolidation tests are conducted on the tertiary clay formation to determine the one-dimensional deformation. For the laboratory tests, two test tubes consisting of A-tube specimens are available as described below.

- Boring B105, test specimen 29, drawn at 14.0-14.7 m below ground surface
- Boring B106, test specimen 21, drawn at 10.0-10.8 m below ground surface

Test specimen 21 from boring B106 might be sandy and test specimen 29 from boring B106 is used in the laboratory test since it is expected to represent the very plastic clay without glacial sand or gravel. (COWI A/S, 2010) The location of Moesgaard Museum can be seen in Figure E.6.

Figure E.6: The location of Moesgaard Museum near Aarhus.

In the following, the first consolidation test is described in detail.

E.3 Soil Conditions

The geological description of the area of Moesgaard Museum is based on boring records of the two borings and soil description in connection with the laboratory tests.

The soil conditions are as follows: Uppermost, about 0.5 m of late glacial solifluction deposits consisting of sandy clay is encountered. Subsequently, about 11 m of glacial clay till with a few layers of melt water clay, silt and sand of about 0.5-1.0 m extent is encountered. This is underlain by 18 m of glacially disturbed, tertiary sheets of Viborg Clay from Lower Oligocene and the plastic clay Røsnæs Clay from Eocene. The clay is characterised as very plastic, greyish olive green, the upper part with a few pyrite concretions, the lower part slightly micaceous with a few sand strias and gravel grains. The layer is not penetrated by the boring. The water level is situated 5.0 m below ground surface.

The test specimen used in the consolidation test was found to be very homogeneous with only a few sand grains, cf. Figures E.7 and E.8.

Figure E.7: *Homogenised soil used for classification tests.*

Figure E.8: *Traversed dried soil specimen used in the consolidation test.*

The natural water content of the glacial clay is varying between 19.0 % and 35.5 % with an arithmetic mean of 30.1 %. The natural water content is determined in connection with the laboratory tests to be in the range $w = 32.8 - 34.1$ % with an arithmetic mean of 33.2 %.

The saturated unit weight is varying between 18.8 kN/m^3 and 21.4 kN/m^3 with an arithmetic mean of γ_{sat} = 19.6 kN/m^3. In the laboratory the saturated unit weight is measured to be in the range $\gamma_{sat} = 18.1 - 18.7$ kN/m^3 with an arithmetic mean of γ_{sat} = 18.4 kN/m^3.

The plasticity and liquidity limits are in the ranges $w_P = 28.0 - 39.0$ % and $w_L = 91.0 - 92.0$ %, respectively, leading to a plasticity index in the range $I_P = w_L - w_P = 53.0 - 63.0$ % with an arithmetic mean of 58.0 %. In the laboratory, the plasticity and liquidity limits are found to be in the ranges $w_P = 34.5 - 35.0$ % and $w_L = 95.0 - 105.6$ %, respectively, leading to a plasticity index in the range $I_P = 60.0 - 71.1$ % with an arithmetic mean of 65.5 % By these values of w_L and I_P the soil is characterised as a clay with very high plasticity by the Casagrande chart in agreement with the geological description (Krebs Ovesen et al., 2007).

E.4 Test Preparation

To ensure that no additional swelling caused by osmotic pressure is produced by adding de-ionised water to the test specimen, the chloride concentration and pH value of the pore water of the soil is determined for mixing the correct water used in the test.

The chloride concentration of the pore water is measured by the procedure described by Grønbech (2010). To obtain equivalent concentration in the test water, it is found that 5.13 g/l must be added to the water.

The pH value of the water used in the test is chosen as 9.20 and measured as 9.19.

E.5 Test Procedure

The applied test setup is the Danish Consolidation Apparatus developed by Moust Jacobsen, cf. Figure E.9.

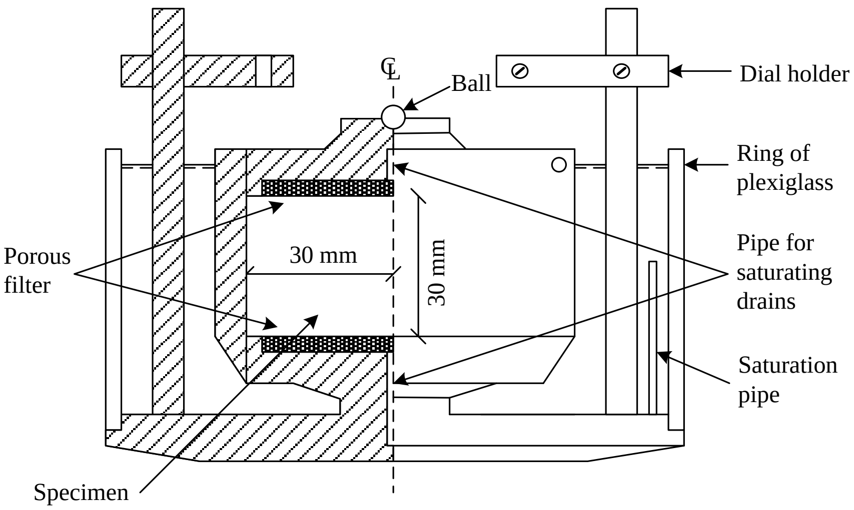

Figure E.9: The Danish Consolidation Apparatus. After Thøgersen (2001, Fig. 5.1).

The specimen is carefully pressed out of the A-tube with a diameter of 70 mm until it is possible to place the transition tube, cf. Figure E.10, of a diameter of 60 mm in continuation of the A-tube, which is after a few centimetres. A 60 mm specimen is used because the magnitude of the preconsolidation stress σ'_{pc} is expected to be very high. After placing the transition tube, the specimen is pressed out of the A-tube until the transition tube is filled and the specimen is cut off. Subsequently, the specimen is installed in the oedometer ring, trimmed to a height of 30 mm and placed in the cell. A double-sided drain with porous filter in top and bottom is used, where the filter areal approximately equals the specimen area for faster drainage.

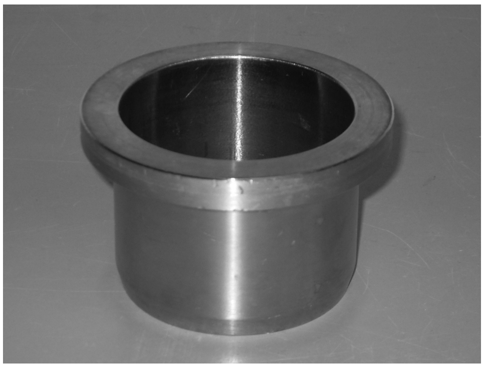

Figure E.10: Transition tube with a diameter of 60 mm.

After the installation of the specimen, the two displacement transducers are positioned and adjusted and the cell is filled with the salt water mentioned in Section E.4 to ensure full saturation of the specimen during the test, cf. Figure E.11. If the specimen is not fully saturated, negative pore pressure is generated in the pore water leading to effective stresses of such an amount that the void ratio changes significantly (Harremoës et al., 1997).

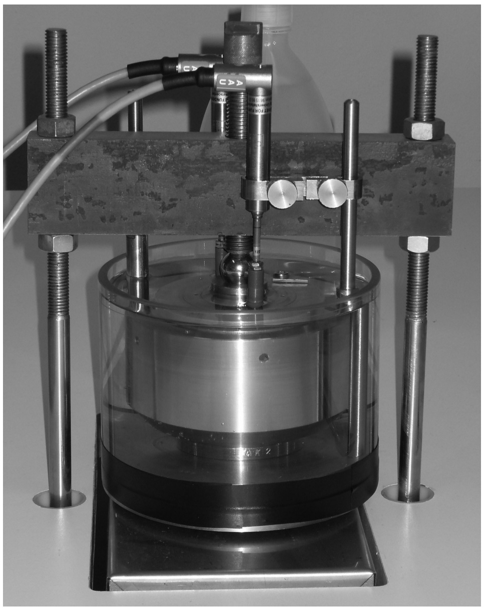

Figure E.11: Oedometer cell installed on the test table.

The loading program is listed in Table E.1 where the load is applied in a distance to the apparatus so that the load acting on the cell is ten times the applied load, cf. Figure E.12. The load on the soil specimen consists of both the load on pressure head, cf. Table E.1, and the pressure as a result of the weight of pressure head and ball. The weight of pressure head and ball is measured as 441 g resulting in an additional pressure of 1.5 kPa.

Table E.1: Loading program of the consolidation test.

Step	Applied load [kg]	Load on pressure head [kg]	Load on pressure head [kPa]
1	0.3	3	10.4
2	0.6	6	20.8
3	1.2	12	41.7
4	2.3	23	79.9
5	4.3	43	149.3
6	8.7	87	302.2
7	17.3	173	600.8
8	34.6	346	1201.7
9	69.1	691	2399.9
10	138.2	1382	4799.8
11	250.5	2505	8700.2

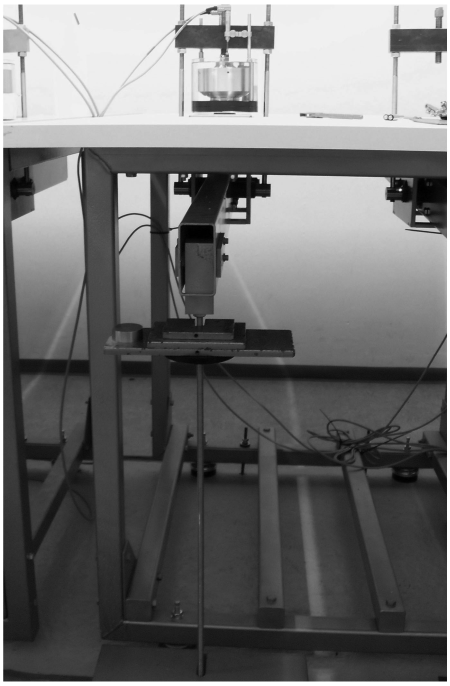

Figure E.12: Test setup of the oedometer apparatus and loading system.

The test proceeds in the following manner:

1. The data collecting program is started,
2. Loading according to load step 1 is applied,
3. When swelling occurs, i.e. when both transducers are measuring upwards movement, loading according to load step 2 is applied,
4. The above is repeated until no swelling is observed,
5. The remaining load steps are applied every other day if secondary consolidation has occurred. This is observed by nearly zero compression measured by the transducers corresponding to fully drainage of pore water (Harremoës et al., 1997). A visual inspection of the time curves also reveals the occurrence of secondary consolidation by an S-shaped development.

During the test, interrelated measurements of time and displacement are stored.

E.6 Test Results

In the following the results of the first consolidation test are outlined.

E.6.1 Swelling Pressure

Swelling of the soil specimen stopped during load step 5 leading to a swelling pressure in the range $\sigma'_S = 150.8$-303.7 kPa when the pressure originating from the pressure head and ball is taken into account. The total in situ stress determined about 14.2 m below ground surface for the saturated unit weight $\gamma_{sat} = 18.5$ kN/m^3 is $\sigma'_0 = 120.7$ kPa which is close to the interval of the swelling pressure. The pressure 303.7 kPa was applied 1 hour and 10 minutes after starting the consolidation test.

E.6.2 Deformation Parameters Determined by Consolidation and Creep Progress for Each Load Step

The consolidation and creep, also known as secondary consolidation, progress are determined for each load step by use of the calculation spreadsheet provided by Aalborg University. In the following, the traditional interpretation method using $(\sqrt{t},\varepsilon)$- and $(\log t,\varepsilon)$-depictions of the strains is applied to load step 9.

The total load, i.e. the load on the pressure head and the pressure originating from the pressure head and ball, for load step 8 is $\sigma' = 1203.2$ kPa and for load step 9 $\sigma' = 2401.4$ kPa, thus a load increase after full consolidation of $\Delta\sigma' = 1198.2$ kPa.

In the spreadsheet provided Aalborg University, two points on the linear part of the time curve in $(\sqrt{t},\varepsilon)$-depiction is marked for fitting a linear regression line to the primary consolidation. In the same way, two points are marked on the approximately linear part of the $(\log t,\varepsilon)$-depiction in the end of the S-curve for fitting a linear regression line to the secondary consolidation. The constant t' is adjusted so that the two linear regression lines intersect at the dimensionless time factor $T = t/t' = 1$. For load step 9 the constant t' is found to be $t' = 529.2$ min leading to the time curve shown in Figure E.13.

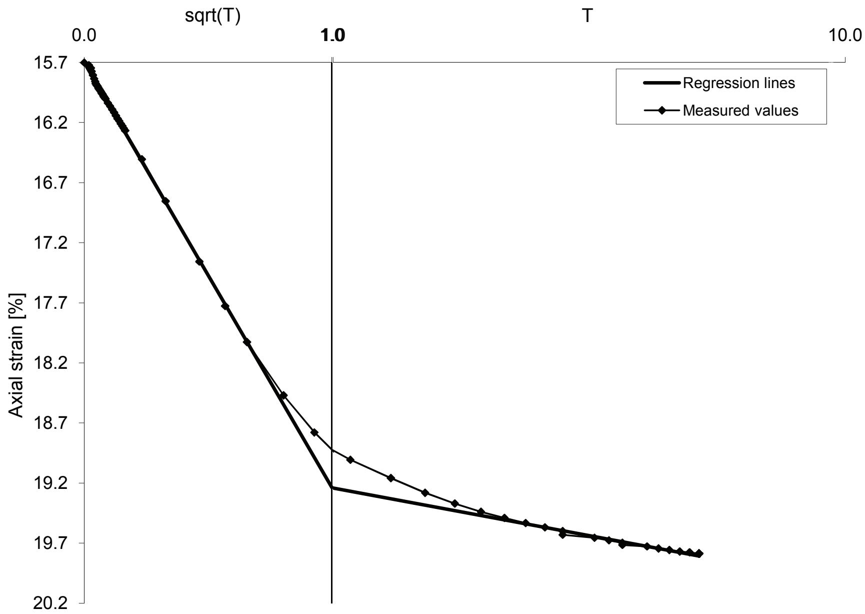

Figure E.13: Consolidation and creep progress for load step 9 determined by traditional consolidation analysis.

The linear regression lines are defined by Equation E.5.

$$\varepsilon(t) = \begin{cases} a_1\sqrt{T} + b_1 & \text{for } T \leq 1 \\ a_2 \log T + b_2 & \text{for } T \geq 1 \end{cases} \tag{E.5}$$

Where:

a_1,a_2 are the slopes of the linear regression lines, cf. Table E.2

b_1,b_2 are the points of intersection between the regression lines and the ε-axis, i.e. the starting strain of the consolidation ε_0, cf. Table E.2.

Table E.2: Parameters for the expressions for the the linear regression lines. The numbers 1 and 2 represent indices for a and b indicating consolidation and creep, respectively.

	a [%]	b [%]
1	3.970	6.668
2	0.590	10.638

The factor a_2 equals the creep strain ε_s.

The secant modulus E_{50} for load step 9 is determined by Equation E.6.

$$E_{50} = \frac{\Delta\sigma'}{\varepsilon_{100,9} - \varepsilon_{100,8}} = \frac{1198.2\, kPa}{10.638\ \% - 6.356\ \%} \cdot 100 = 27.98\, MPa \tag{E.6}$$

Where:
$\varepsilon_{100,8}$ is the strain at full consolidation for load step 8,
$\varepsilon_{100,9}$ is the strain at full consolidation for load step 9.

The local constrained modulus for load step 9 $E_{oed,l}$ is determined by Equation E.7.

$$E_{oed,l} = \frac{\Delta\sigma'}{\varepsilon_{100,9} - \varepsilon_{0,9}} = \frac{1198.2\,kPa}{10.638\,\% - 6.668\,\%} \cdot 100 = 30.18\,MPa \tag{E.7}$$

The consolidation coefficient c_k is determined by Equation E.8.

$$c_k = \frac{H_{D,25}^2}{t'} = \frac{0.0138\,m}{529.2\,min \cdot 60} = 6.0 \cdot 10^{-9}\,m^2/s \tag{E.8}$$

Where:
$H_{D,25}$ is the distance of drainage at $U = 25\,\%$.

The coefficient of permeability k is determined by Equation E.9.

$$k = \frac{c_k \cdot \gamma_w}{E_{oed,l}} = \frac{6.0 \cdot 10^{-9}\,m^2/s \cdot 10\,kN/m^3}{30.18\,MPa \cdot 10^3} = 2.0 \cdot 10^{-12}\,m/s \tag{E.9}$$

E.6.3 Determination of Preconsolidation Stress

The preconsolidation stress σ'_{pc} is estimated by the Terzaghi method where the primary path and the virgin curve of the load-displacement curve can be seen in Figure E.14.

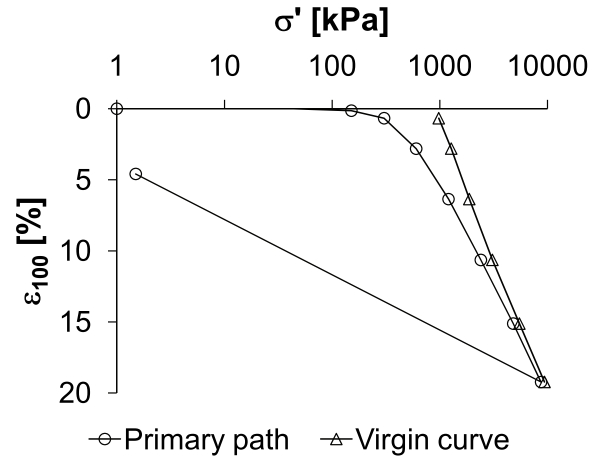

Figure E.14: Primary path and virgin curve for the consolidation test.

The reference stress is found to be $\sigma'_\kappa = 674$ kPa leading to a preconsolidation stress of $\sigma'_{pc} \approx 1350$ kPa.

Estimated by Akai's method, the preconsolidation stress is in the range $\sigma'_{pc} \approx 1200 - 2400$ kPa, cf. Figure E.15.

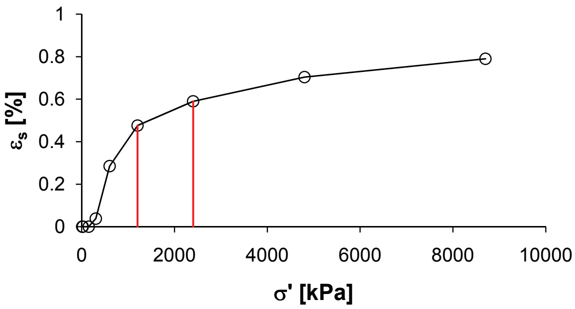

Figure E.15: Plot of the creep strain ε_s and the effective stress σ' where the range of σ'_{pc} is indicated by the vertical red lines.

Estimated by Janbu's method, the preconsolidation stress is approximately $\sigma'_{pc} \approx 1800$ kPa, cf. Figure E.16.

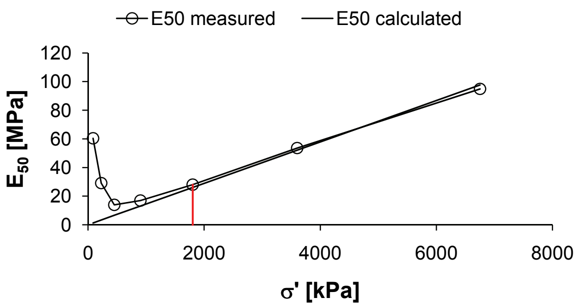

Figure E.16: Plot of the secant modulus E_{50} and the effective stress σ' where the approximate value of σ'_{pc} is indicated by the vertical red line.

Estimated by the coefficient of consolidation c_k, the preconsolidation stress is approximately $\sigma'_{pc} \approx 1200$ kPa, cf. Figure E.16.

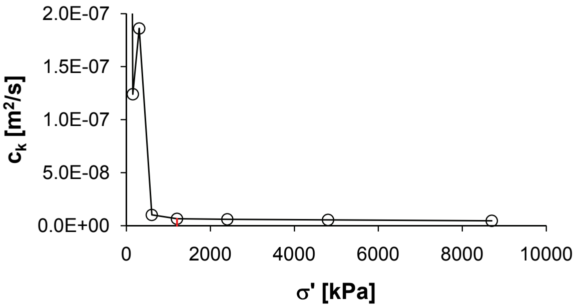

Figure E.17: Plot of the coefficient of consolidation c_k and the effective stress σ' where the approximate value of σ'_{pc} is indicated by the vertical red line.

The estimations of σ'_{pc} are listed in Table E.3.

Table E.3: Estimations of the preconsolidation stress σ'_{pc} by different methods.

Method	σ'_{pc} [kPa]
Terzaghi	1350
Akai	1200-1400
Janbu	1800
c_k	1200

E.6.4 Determination of Compression Index of the Primary Loading Path

The compression index is determined as the slope of the linear part of the primary loading path as $C_{c\varepsilon} = 15.9$ %.

APPENDIX F

TRIAXIAL TEST OF TERTIARY CLAY AT MOESGAARD MUSEUM

In addition to the consolidation tests, a triaxial test is conducted to determine the undrained shear strength c_u and the effective strength parameters c' and φ'. This appendix describes the procedure of the test and the deformation of the test specimen after the test.

F.1 Soil Conditions

The geological description of the soil can be seen in Appendix E. The natural water content of test specimen 29 from boring B105 is determined before the triaxial test as w =32.4 %. In the laboratory the saturated unit weight is measured before the triaxial test as $\gamma_{sat} = 18.3$ kN/m^3 which is used in the calibration of the numerical model. The void ratio is determined before the triaxial test as $e = 0.95$.

F.2 Test Procedure

The first phase of the triaxial test is the trimming of the specimen to a cylinder with the dimensions $H = D = 70$ mm. After installation of the specimen in the triaxial cell, a negative pressure of 20 kPa is added. After filling of the cell, the specimen and the drains in top and bottom are saturated and the backpressure of 200 kPa is established. Backpressure is applied to the pore water to obtain maximum saturation.

After the trimming of the test specimen, the loading phase with open drains is initiated to recreate the stress history. This is conducted two days after the end of the test trimming phase to ensure that all pore pressure has drained away. The loading phase is conducted as an anisotropic loading controlled by K_0. This procedure is selected rather than an area controlled loading to minimise time consumption. At first, the specimen is loaded to $0.9{\cdot}\sigma'_{pc}$ which for the preconsolidation stress determined by the consolidation test as σ'_{pc} = 1300-1400 kPa, cf. Appendix E, leads to the range 1170-1260 kPa. The value of $0.9{\cdot}\sigma'_{pc}$ 1200 kPa is used. The effective internal angle of friction is estimated as $\varphi' = 16°$ by which K_0 is determined as 0.72 by Equation F.1.

$$K_0 = 1 - \sin\varphi' = 1 - \sin 16° = 0.72 \tag{F.1}$$

Hence, the radial stress is determined as $\sigma'_3 = K_0 \cdot \sigma'_{pc} = 865$ kPa.

Secondly, after two days at this stress state, the specimen is unloaded with constant K_0 to the effective vertical in situ stress determined about 14.2 m below ground surface for the submerged unit weight $\gamma' = 18.5\ kN/m^3 - 10\ kN/m^3 = 8.5\ kN/m^3$ as $\sigma'_0 = 120.7$ kPa. This leads to an overconsolidation ratio of $OCR = \frac{\sigma'_{pc}}{\sigma'_0} = 9.9$ by which $K_{0,OC}$ is determined as 3.76 by Equation F.2.

$$K_{0,OC} = K_0 \cdot OCR^{K_0} = 0.72 \cdot 9.9^{0.72} = 3.76 \tag{F.2}$$

Hence, the radial stress is determined as $\sigma'_3 = 454$ kPa. Unfortunately, something went wrong with the unloading equipment, and the specimen was only unloaded to $\sigma'_1 = 544$ kPa and $\sigma'_3 = 610$ kPa.

The test is conducted with a backpressure of 200 kPa to minimise the effect of air inside the cell, if any. The stress steps can be seen in Table F.1.

Table F.1: Stress steps for the consolidation phase of the triaxial test. The values in parentheses are the desired values which were not reached.

Description	Axial stress σ'_1 [kPa]	Radial stress σ'_3 [kPa]	Backpressure [kPa]
Loading to $0.9 \cdot \sigma'_{pc}$	1200	865	200
Unloading to σ'_0	544 (120)	610 (454)	200

The third phase is the failure test where the specimen is loaded to failure with a strain rate of 0.5 %/h. The loading happens undrained with open drains but constant volume and $\Delta u = 0$ for constant u = the backpressure. The failure test is conducted two days after the end of the loading phase.

F.3 Deformation of Test Specimen

After the completion of the triaxial test, some deformation of the test specimen is observed. The shape of the specimen is no longer completely cylindrical as seen in Figure F.1a.

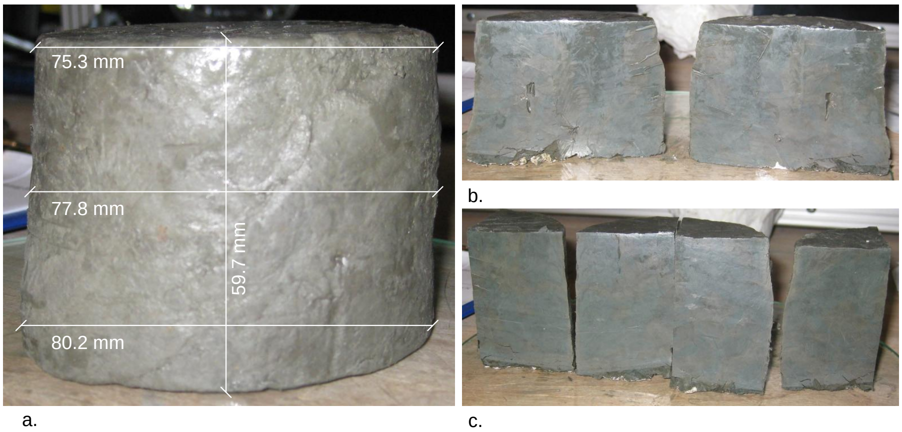

Figure F.1: Deformed test specimen after the completion of the triaxial test.

Additionally, Figures F.1b and F.1c show that no large stones are present in the test specimen. The presence of stones in the specimen implies an increase in the strength of the soil which does not reflect the true strength properties.

As seen in Figures F.1b and F.1c, the bottom of the specimen, which corresponds to the top of specimen when installed in the triaxial cell, is corrected with plaster. This should not have any influence on the results.

APPENDIX G

ABOUT PLAXIS 2D

In this appendix, the concept of modelling in PLAXIS is briefly described, followed by a listing of several issues which are important to be aware of in PLAXIS. This is followed by a description of initial stresses, applied material models and interfaces.

G.1 About Modelling in PLAXIS

The geometry model is based on the components points, lines and clusters, whereas the finite element mesh is based on elements, nodes and stress points. Clusters are divided into either 15- or 6-node triangular elements to model the soil where the former provides accurate calculation of stresses and failure loads, and the latter a quick calculation. (Brinkgreve et al., 2008c)

The 15-node triangular element provides a fourth order interpolation for displacements using 12 Gaussian integration points, called stress points in PLAXIS, for numerical integration. Gauss points are the positions of integration points determined by the Gauss-Legrendre integration (Ottosen and Petersson, 1992). The 6-node triangular element provides a second order interpolation for displacements using three Gauss points for numerical integration. The 6-node triangular element generally overpredicts failure loads and safety factors and should be used with care in axisymmetric models. In the analyses of present project, an axisymmetric model is used to model the axisymmetric pile, and, thus, it is chosen to built the model by 15-node elements. (Brinkgreve et al., 2008b)

Structural model behaviour and soil–structure interaction are modelled by plate, geogrid and interface elements. Displacements (u_x and u_y) are calculated at the nodes, whereas stresses and strains are calculated at individual Gauss points. An element contains "number of nodes"-3 stress points. (Brinkgreve et al., 2008c)

G.2 Important when Modelling in PLAXIS

It is important to chose a horizontal extent of the model which enables a possible failure mechanism and ensures that the outer boundary has no effect on the results (Brinkgreve et al., 2008c).

K_0 for normally consolidated clays is based on Jaky's formula defined in Equation G.1 (Brinkgreve et al., 2008c).

$$K_{0,NC} = 1 - \sin\varphi \tag{G.1}$$

When entering a new value of φ, K_0 is not automatically changed and should be done manually.

When deactivating a soil cluster, e.g. in connection with an excavation stage, the pore pressures are not automatically deactivated, thus, the water remains in the excavation area leading to a submerged excavation (Brinkgreve et al., 2008c).

In PLAXIS, tensile forces and stresses are defined positive in contrast to common geotechnical practice (Brinkgreve et al., 2008b).

G.3 Initial Stresses

Initial stresses, where the geometry contains a horizontal soil surface, layering or phreatic level, are generated by the K_0-procedure, which only considers soil weight and not external loads or weight of structural elements, and only calculates effective stresses and pore pressures in soil elements and interfaces. If the plot of plastic points from the *Stresses* menu includes many red plastic points (Coulomb points), this indicates a violation of Coulomb's criterion by the initial stress state, and the K_0-value should be chosen closer to 1.0. (Brinkgreve et al., 2008b)

When the soil surface, the layering or the phreatic level is non-horizontal, the initial stress field is calculated by the method *Gravity loading*. By this method, the initial stresses are calculated plastic by increase of the multiplier for the soil weight from 0.0 to 1.0. (Brinkgreve et al., 2008c)

G.4 Applied Material Models

Instead of using Hooke's law involving only the two parameters Young's modulus E and Poisson's ratio ν to model soil behaviour, which is too simple for this purpose, more advanced material models can be applied. The models used in present analyses are described in the proceeding sections. Following models for the soil behaviour have not been applied in the analyses:

- Mohr-Coulomb model

  Is not applied because it does not include the increase of stiffness during unloading and reloading in compare to primary loading. Since the present analyses concern an unloading situation, the Mohr-Coulomb model would not lead to satisfactory results because of the incorrect soil stiffness. Additionally, the Mohr-Coulomb model does not account for the stress dependency of Young's moduli of elasticity, which is a property of real soils.

- Joint Rock model

  Is mainly used for modelling of rock layers involving a stratification and predefined failure lines, which are not present in these analyses. Hence, the model is not used in the analyses of plastic unfissured clays. (Brinkgreve et al., 2008a)

- Soft Soil Creep model

  Is not applied because it does not model unloading satisfactory. (Brinkgreve et al., 2008a)

- Soft Soil model

  The same argument as for the Soft Soil Creep model. (Brinkgreve et al., 2008a)

- Hardening Soil model with small-strain stiffness

  The Hardening Soil model is applied rather than the advanced Hardening Soil model with small-strain stiffness for simplicity.

- Modified Cam Clay model

  Is mainly used for almost normally consolidated clays, which is not the case for the analysed soil type. (Brinkgreve et al., 2008a)

G.4.1 Hardening Soil Model

For modelling of the soil, the Hardening Soil model (HS) is applied. The HS is an advanced version of the Mohr-Coulomb model where three different stiffnesses replace the average Young's modulus of elasticity E. The stiffnesses are: the secant stiffness determined by drained triaxial test E_{50}, the unloading–reloading stiffness E_{ur} and the tangent stiffness determined for primarily oedometer loading E_{oed}, also known as the constrained modulus. If no information about E_{ur} and E_{oed} is available, approximate average values for different soil types may be used, cf. Equation G.2. (Brinkgreve et al., 2008a)

$$E_{ur} \approx 3 \cdot E_{50} \qquad E_{oed} \approx E_{50} \tag{G.2}$$

Additionally, the stiffness moduli used in the Hardening Soil model are stress-dependent, i.e. the stiffness is increasing with depth. (Brinkgreve et al., 2008a)

The Hardening Soil model includes hardening, the theory of plasticity, soil dilatancy and a cap yield surface controlled by the constrained modulus E_{oed}. Two types of hardening are applied in the model: shear hardening, which models the irreversible strains due to primary loading, and compression hardening, which models the irreversible strains due to primary compression in constrained loading and isotropic loading. The compression hardening is controlled by the cap yield surface, which is introduced to limit the elastic region so that plastic behaviour is registered during isotropic compression. The shear yield surface along with the yield cap can be seen in Figure G.1.

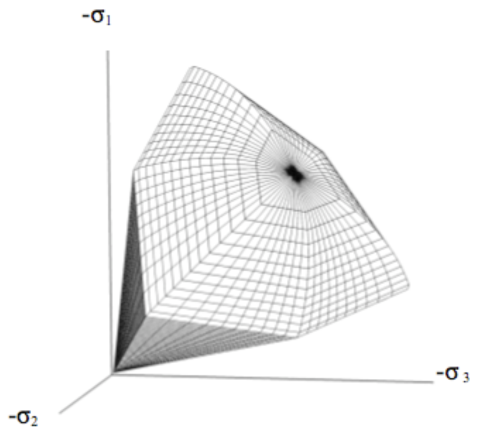

Figure G.1: The shear yield surface and cap yield surface of the Hardening Soil model in principle stress space (Brinkgreve et al., 2008a, Fig. 5.9). Note that compressive stresses are negative in PLAXIS.

An advantage of the Hardening Soil model is that the stress–strain relationship is, more realistically, hyperbolic instead of bilinear, which applies for the linear elastic–perfectly plastic Mohr-Coulomb model in compare. In addition, the hardening of the soil is included by stress level dependent material parameters, which implies that plastic strains during primary loading are accounted for along with the elastic strains developed in both primary loading and unloading/reloading.

In the Hardening Soil model, a limit of dilatancy, i.e. the maximum porosity, after extensive shearing can be applied by the dilatancy cut-off. The limit is based on the initial void ratio e_{init}.

(Brinkgreve et al., 2008a)

Limitations of the Model

The known and observed limitations of the Hardening Soil model are listed in the following.

- The model does not account for softening due to soil dilatancy.
- The model only models isotropic hardening, hence, neither hysteretic and cyclic loading nor cyclic mobility is considered.
- It is necessary that the user chose stiffness parameters in accordance with the dominant strain levels.

(Brinkgreve et al., 2008a, p. 1-4)

G.4.2 Linear Elastic Material Model

The linear elastic material model is used to model the pile material as concrete. The model makes use of Hooke's law of isotropic linear elasticity where only Young's modulus of elasticity E and Poisson's ratio ν are applied parameters.

G.5 Interfaces

A strength reduction factor R_{inter} is used to relate the strength of the soil to the strength in the interfaces according to Equations G.3 and G.4.
(Brinkgreve et al., 2008c)

$$\tan\varphi_{interface} = R_{inter}\tan\varphi_{soil} \tag{G.3}$$

$$c_{interface} = R_{inter}c_{soil} \tag{G.4}$$

The stiffness matrix for the interface elements is determined by Newton Cotes integration where the numerical integration points are chosen in advance (Ottosen and Petersson, 1992; Brinkgreve et al., 2008b). If no detailed information about the magnitude of R_{inter} is available, the parameter is estimated as $R_{inter} = 2/3$ (Brinkgreve et al., 2008b).

(Brinkgreve et al., 2008a)

APPENDIX H

NUMERICAL MODELLING IN PLAXIS

In this appendix, the numerical modelling of the interaction between a circular pile and a swelling soil in PLAXIS is considered where the results of different models are outlined. Both models excluding and including the pile are constructed. Swelling is a soil characteristic which is complex to include in numerical modelling. For simplicity, the swelling behaviour is modelled as unloading by an excavation where the interaction on the pile due to soil heave illustrates the pile-soil interaction due to swelling.

H.1 Case Study

For the investigations, a case study is analysed. This involves a circular concrete pile with the dimensions $L = 20$ m and $D = 0.34$ m placed in clay immediately after a 10 m excavation. The outer width of the soil mass, which equals the diameter of the model, is chosen as $B = 20$ m. This complies with the recommendation by Abbas et al. (2008) of $B = 40D \approx 14$ m. The height of the model is chosen as the height of the excavation added to the height of the swelling zone $n = 11$ m. The model can be seen in Figure H.1.

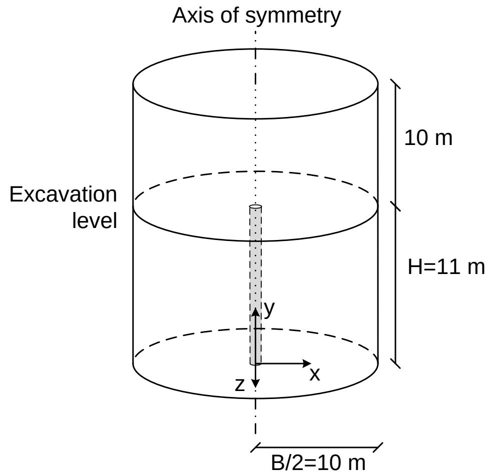

Figure H.1: Dimensions of the soil model and pile for the analysed case study. The diameter of the pile is $D = 0.34$ m.

H.1.1 Material Parameters of the Clay

The clay is modelled as an undrained Hardening Soil material. The undrained behaviour is applied so that the development of excess pore pressures, or in the case of unloading, negative pore pressures, as a function of time can be observed.

Little Belt clay is a tertiary clay with a high content of the clay mineral smectite, which is very expansive in combination with water, thus, a swelling soil. A combination of values is used in the preliminary studies of swelling in PLAXIS. This includes the sample called “Felt” with a natural water content of $w = 33.3$ % and the plasticity index $I_P = 183.8$ % defined in Thøgersen (2001) and the example of effective and undrained strength parameters of Little Belt clay given in Harremoës et al. (1997).

Unit Weight

The saturated unit weight of the clay is determined in connection with a consolidation test to $\gamma_{sat} = 18.49$ kN/m^3 (Thøgersen, 2001). The unsaturated unit weight is estimated to $\gamma_{unsat} = 16.49$ kN/m^3.

Coefficient of Permeability

The coefficient of permeability k is chosen as 10^{-11} m/s. Based on Kulhawy and Mayne (1990), this value seems plausible. The soil is assumed to be homogeneous in both horizontal and vertical direction by which the horizontal and vertical coefficients of permeability can be set equal. In nature, however, this assumption is probably not valid. In intact clay, the mineralogy and particle orientation leads to differences in the size of the horizontal and vertical coefficients of permeability. If the clay is fissured as for the considered Little Belt Clay, the flow of the pore water is significantly increased through the fissures leading to unequal coefficients of permeability. During swelling, the fissures expand which implies even more flow of the pore water. (Barnes, 2000)

Poisson's Ratio

Poisson's ratio is chosen as $\nu = 0.3$.

Cohesion

Both the effective cohesion c' and the undrained shear strength c_u are applied as reference values of cohesion c_{ref} for the case study of swelling in PLAXIS together with the effective angle of internal friction φ' and $\varphi_u = 0$, respectively. This is chosen because both the drained and undrained parameters give rise to problems when implemented in undrained materials.

In PLAXIS, the undrained behaviour is analysed by the effective stresses. This implies that the undrained strength parameters are interpreted as drained strength parameters instead. Simultaneously, the effective stresses during loading decrease leading to larger excess pore pressures than in nature.

When using the effective strength parameters combined with the undrained soil behaviour, the mean effective stress p' is constant up to failure. In nature, the development of p' is somewhat different. During loading, normally consolidated clay tends to compress. However, since the soil behaviour is undrained, the volume is constant leading to increasing excess pore pressures. Hence, the mean effective stress is decreasing and not constant as in PLAXIS. Preconsolidated clay tends to both compress and dilate during loading. The dilatation, i.e. the increase in volume, cannot take place for undrained behaviour leading to negative excess pore pressures. This implies an increase of p'. Hence, the deviatoric stress q' is overestimated by PLAXIS as seen in Figure H.2 leading to an overestimation of $c_u = 0.5 \cdot q'$. (Brinkgreve et al., 2008a)

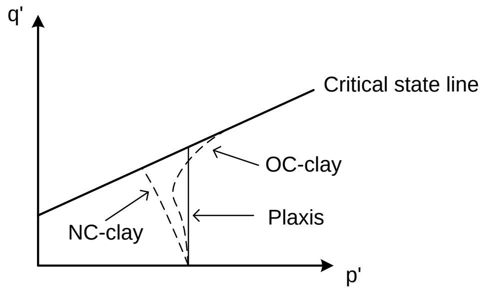

Figure H.2: Effective stress paths for normally consolidated clay (NC-clay), over consolidated clay (OC-clay) and for an undrained Hardening Soil material with drained strength parameters defined in PLAXIS (Plaxis).

The advantage of applying effective strength parameters to undrained behaviour instead of undrained is that the increase in shear stresses during consolidation are automatically obtained (Brinkgreve et al., 2008a).

An effective cohesion of $c' = 40$ kPa and the undrained shear strength chosen as $c_u = 225$ kPa are applied, cf. Harremoës et al. (1997) for Little Belt Clay.

Angle of Internal Friction

The effective angle of internal friction is estimated as $\varphi' = 16°$ for Little Belt Clay, cf. Harremoës et al. (1997). For undrained strength parameters, the angle of friction is set to zero.

Young's Modulus of Elasticity

For the Mohr-Coulomb material model, the constrained modulus E_{oed} is used as the reference value of Young's modulus of elasticity E_{ref}. The constrained modulus is estimated to $E_{oed} = 10$ MPa.

Angle of Dilatancy

The angle of dilatancy is chosen as $\psi = 0$ as for most clays (Brinkgreve et al., 2008b).

H.1.2 Interfaces Applied to the Pile

The applied interfaces are elongated 1 m under the pile toe, in continuation of the toe but still following the surface of the pile toe and in continuation of the horizontal side of the pile head, cf. Figure H.3.

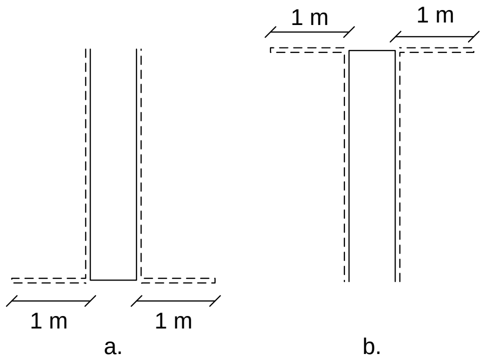

Figure H.3: The applied type of interfaces at a. the pile toe and b. pile head.

A virtual thickness is applied to the interface elements by multiplying a virtual thickness factor of 0.1 to the average element size. The virtual thickness is a fictive dimension used for obtaining adequate stiffness of the interface. The average element size is determined by the global coarseness (Brinkgreve et al., 2008b).

The interface is assigned the properties of the surrounding soil cluster with a strength reduction factor R_{inter} determined by the surface resistance of the pile t_{max}. It is yet unknown whether a possible failure of soil–pile interface due to swelling occurs as a drained or undrained failure. In the following, it is assumed that the failure is undrained. Thus, the surface resistance t_{max} of the pile is determined by Equation H.1 where the factor 1.5 is a factor of correlation to determine the characteristic value of t_{max} by the Danish National Annex to Eurocode 7 (European Committee for Standardisation, 2008).

$$t_{max} = \frac{m \cdot r \cdot c_u}{1.5} = \frac{1 \cdot 0.4 \cdot 225\ kPa}{1.5} = 60\ kPa \tag{H.1}$$

The strength reduction factor R_{inter} is defined in Equation H.2.

$$R_{inter} = \frac{t_{max}}{c_u} = \frac{60\ kPa}{225\ kPa} = 0.267 \tag{H.2}$$

H.1.3 Material Parameters of the Concrete

The concrete is modelled as a non-porous linear elastic material with following material parameters.

Unit Weight

The unsaturated unit weight of the concrete is estimated as $\gamma_{unsat} = 24.0\,\mathrm{kN/m^3}$.

Poisson's Ratio

Poisson's ratio is chosen as $\nu = 0.15$ for concrete, cf. Brinkgreve et al. (2008b).

Young's Modulus of Elasticity

The reference value of Young's modulus of elasticity E_{ref} is chosen as $E_{ref} = 34.8 \cdot 10^6$ kPa.

H.1.4 Summation of Material Parameters

The properties of the applied materials are listed in Table H.1.

Table H.1: Material properties of the applied materials.

Parameter	Name	Clay	Concrete
Material model	Model	Mohr-Coulomb	Mohr Coulomb
Material behaviour	Type	Undrained	Non-porous
Saturated unit weight	γ_{sat}	18.49 kN/m^3	-
Unsaturated unit weight	γ_{unsat}	16.49 kN/m^3	24 kN/m^3
Horizontal coefficient of permeability	k_x	10^{-11} m/s	-
Vertical coefficient of permeability	k_y	10^{-11} m/s	-
Poisson's ratio	ν	0.3	0.15
Cohesion	c_{ref} (c'/c_u)	40 kPa/225 kPa	-
Constrained modulus	E_{oed}	$10 \cdot 10^3$ kPa	$34.8 \cdot 10^6$ kPa
Secant modulus	E_{50}	$10 \cdot 10^3$ kPa	$34.8 \cdot 10^6$ kPa
Un-/reloading modulus	E_{ur}	$30 \cdot 10^3$ kPa	$34.8 \cdot 10^6$ kPa
Angle of internal friction	φ'/φ_u	16°/0°	-
Angle of dilatancy	ψ	0°	-
Interface strength	R_{inter}	0.267	-

BIBLIOGRAPHY

Abbas, J. M., Z. H. Chika, and M. R. Taha (2008). Single pile simulation and analysis subjected to lateral load. *Electronic Journal of Geotechnical Engineering 13*(E), 1–15.

API (2000). *Recommended Practice for Planning, Designing and Constructing Fixed Offshore Platforms - Working Stress Design*. American Petroleum Institute.

Augustesen, A. H. (2006). *The Effects of Time on Soil Behaviour and Pile Capacity*. Ph. D. thesis, Department of Civil Engineering, Water and Soil, Aalborg University.

Barnes, G. E. (2000). *Soil Mechanics: Principles and Practice* (2nd ed.). Hampshire, UK: Palgrave Macmillan.

Brinkgreve, R. B. J., W. Broere, and D. Waterman (2008a). *PLAXIS 2D Material Models Manual - Version 9.0*. PLAXIS bv.

Brinkgreve, R. B. J., W. Broere, and D. Waterman (2008b). *PLAXIS 2D Reference Manual - Version 9.0*. PLAXIS bv.

Brinkgreve, R. B. J., W. Broere, and D. Waterman (2008c). *PLAXIS 2D Tutorial Manual - Version 9.0*. PLAXIS bv.

COWI A/S (2009). Case 71433-G-1 Moesgaard Museum, Moesgård Allé 20, Højbjerg. Boring records, COWI A/S.

COWI A/S (2010, 26 February). Moesgaard Museum, Moesgård Allé 20, Højbjerg - Forslag til program for udførelse af konsoliderings- og triaxialforsøg. Intern report. Document no. 71433.

DGF's Laboratoriekomité (2001). *DGF-Bulletin 15: Laboratoriehåndbogen*. Aalborg, Denmark: Dansk Geoteknisk Forening.

European Committee for Standardisation (2008). *EN 1997-1 DK NA:2008 National Annex to Eurocode 7: Geotechnical design - Part 1: General rules*. Dansk Standard.

Grønbech, G. L. (2010, January). Manual for measurement of Chloride in clays. Aalborg University.

Harremoës, P., H. Moust Jacobsen, and N. Krebs Ovesen (1997). *Lærebog i GEOTEKNIK 1* (5th ed.). Århus, Denmark: Polyteknisk Forlag.

Holtz, W. G. (1983). The influence of vegetation on the swelling and shrinking of clays in the united states of america. *Géotechnique 33*(2), 159–163.

Jardine, R., F. Chow, R. Overy, and J. Standing (2005). *ICP design methods for driven piles in sands and clays* (1st ed.). Thomas Telford.

Jensen, B. C. (2007). *Betonkonstruktioner efter DS 411* (3rd ed.). Nyt Teknisk Forlag.

Johannesen, C. L., J. V. Madsen, and K. T. Vestergaard (2008, June). Geoteknikniske egenskaber for tertiært ler ved Light*house - forsøg med og numerisk modellering af søvindmergel. Aalborg University.

Krebs Ovesen, N., L. D. Fuglsang, and G. Bagge (2007). *Lærebog i Geoteknik* (1st ed.). Lyngby, Denmark: Polyteknisk Forlag.

Kulhawy, F. H. and P. W. Mayne (1990). *Manual on Estimating Soil Properties for Foundation Design*. Cornell University.

Moust Jacobsen, H. (1993). *Lærebog i videregående geoteknik 2 - Sætninger i jord*. Aalborg, Denmark: Aalborg Universitet.

Moust Jacobsen, H. and K. Gwizdala (1992). *Bearing capacity and settlements of piles*. Aalborg, Denmark: Centertrykkeriet, Aalborg University.

Okkels, N. and K. Bødker (2008). Beregning af hævninger under antagelse af retlinjet dræning. In *Nordisk Geoteknikermøde no. 15*, Sandefjord, Norway, pp. 383–389.

Ottosen, N. S. and H. Petersson (1992). *Introduction to the Finite Element Method*. University of Lund, Sweden: Prentice Hall.

Poulos, H. G. and E. H. Davis (1980). *Pile foundation analysis and design* (1st ed.). John Wiley and sons.

Sazhin, V. S. (1968). Method of determining the magnitude of rise of piles following flooding of swelling soils. *Soil Mechanics and Foundation Engineering 5*(1), 49–52.

Steenfelt, J. S., C. S. Sørensen, and W. Bai (2007). *Teknisk Ståbi - Fundering*, Chapter 10. Nyt Teknisk Forlag.

Thøgersen, L. (2001). *Effects of Experimental Techniques and Osmotic Pressure on the Measured Behaviour of Tertiary Expansive Clay, Volume 1*. Ph. D. thesis, Soil Mechanics Laboratory, Aalborg University.

Tomlinson, M. and J. Woodward (2008). *Pile Design and Construction Practice* (5th ed.). Taylor & Fancis.